MIT/WHOI 2002-08

Massachusetts Institute of Technology

Woods Hole Oceanographic Institution

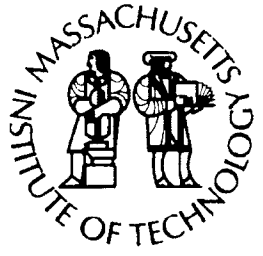

Joint Program in Oceanography/ Applied Ocean Science and Engineering

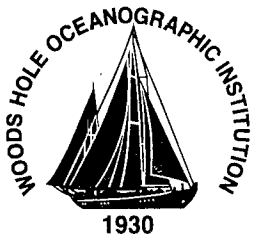

DOCTORAL DISSERTATION

Mark-Recapture Statistics and Demographic Analysis

by

Masami Fujiwara

June 2002

MIT/WHOI

2002-08

Mark-Recapture Statistics and Demographic Analysis

by

Masami Fujiwara

Massachusetts Institute of Technology
Cambridge, Massachusetts 02139

and

Woods Hole Oceanographic Institution
Woods Hole, Massachusetts 02543

June 2002

DOCTORAL DISSERTATION

Funding was provided by The David and Lucile Packard Foundation, the Rinehart Coastal Research Center, the Woods Hole Oceanographic Institution Sea Grant Program (NOAA NA86RG0075), and a Graduate Research Fellowship.

This thesis should be cited as: Masami Fujiwara, 2002. Mark-Recapture Statistics and Demographic Analysis. Ph.D. Thesis. MIT/WHOI, 2002-08.

Approved for publication; distribution unlimited.

Approved for Distribution:

John J. Stegeman, Chair
Department of Biology

Paola Malanotte-Rizzoli
MIT Director of Joint Program

John W. Farrington
WHOI Dean of Graduate Studies

Mark-Recapture Statistics and Demographic Analysis

by

Masami Fujiwara

B.S., University of Alaska Fairbanks (1993)
M.S., University of Alaska Fairbanks (1997)

Submitted in partial fulfillment
of the requirements of the degree of

Doctor of Philosophy

at the

MASSACHUSETTS INSTITUTE of TECHNOLOGY

and the

WOODS HOLE OCEANOGRAPHIC INSTITUTION

June 2002

Signature of Author 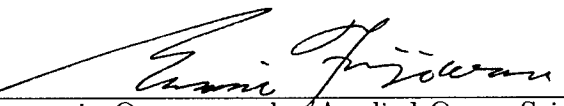

Joint Program in Oceanography/Applied Ocean Science and Engineering
Massachusetts Institute of Technology
and Woods Hole Oceanographic Institution
June 2002

Certified by 

Hal Caswell
Thesis Supervisor

Accepted by 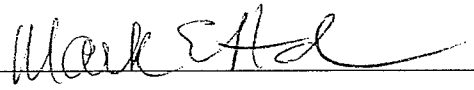

Mark Hahn
Chair, Joint Committee for Biology
Woods Hole Oceanographic Institution

Mark-Recapture Statistics and Demographic Analysis

by
Masami Fujiwara

Submitted in partial fulfillment of the requirements of the degree of
Doctor of Philosophy
at the
MASSACHUSETTS INSTITUTE of TECHNOLOGY
and the
WOODS HOLE OCEANOGRAPHIC INSTITUTION
June 2002

Abstract

Mark-recapture analysis of populations is becoming an important tool in population biology. Mark-recapture methods can be used to estimate transition probabilities among life-stages from capture histories of marked individuals for which stages can be determined at each sampling occasion. This method is called a multi-stage mark-recapture (MSMR) method. In this thesis, I describe advances I made in the MSMR method and present analyses that apply this method to actual data.

The advances I made in the MSMR method are motivated by a need to provide a link between mark-recapture data and demographic models such as matrix population models and integrodifference models. I resolve some issues that are commonly encountered during sampling, such as the fact that the sex or life-stage of some individuals is unknown during some sampling occasions and that individuals become unobservable during some life-stages. I introduce a stage-structure that permits simple conversion of estimated transition probabilities into a matrix population model. I describe an algorithm to simplify programming for parameter estimation. I also introduce a method to estimate the distribution of dispersal displacements (a dispersal kernel) from mark-recapture data.

I apply some of the methods described above to data of the North Atlantic right whale (*Eubalaena glacialis*). The right whales are considered one of the most endangered mammals. The current population size is about 300 in the northwestern Atlantic, and the number is declining. I applied the multi-stage mark-recapture statistics to the 17-year individual sighting history data. Using the estimated transition probabilities, I constructed a population projection matrix, which was used for further demographic analyses. I found that the population was slowly increasing in 1980, but it started to decline slowly around 1992. I show that (1) this change was caused by increased mortality of females that have just given birth, (2) protecting two females a year from the deaths is enough to prevent the declining trend, and (3) demographic stochasticity is a more important factor influencing their long-term viability than environmental stochasticity.

Dissertation Advisor: Hal Caswell, Senior Scientist, Woods Hole Oceanographic Institution

Acknowledgments

I am very grateful to my advisor Hal Caswell for accepting me as his student and even more grateful for his guidance and patience to tolerate me for almost five years. If I achieve any success in the future, a significant part of it will owe to the training I received from him. I am also grateful to other members of my thesis committee, Glenn Flierl, James Nichols, Michael Neubert, and Andrew Solow, for their insights and constructive advice. I especially thank Michael Neubert for his mathematical assistance.

I thank Scott Kraus, Amy Knowlton, Phillip Hamilton, and New England Aquarium for photographic identification data of the North Atlantic right whale. The data are used in Chapter 2, 3, 5, and 6. I thank Solange Brault, Jean-Dominique Lebreton, James Nichols, and other participants of the first Woods Hole Workshop on the Demography of Marine Mammals for discussions and suggestions. I also thank Joel Cohen and Roger Nisbet for participating in annual Nantucket laboratory retreats as special guests and helping me with some of my problems. I also thank Takenori Takada for useful information and many helpful suggestions.

This thesis is a collection of manuscripts that were published, accepted, or to be submitted to various journals. All the manuscripts were co-authored with my advisor Hal Caswell except the manuscript on the dispersal kernel estimation method (Chapter 4). The latter is co-authored with Michael Neubert and Hal Caswell. I thank James Bence, Evan Cooch, and an anonymous reviewer for their comments on Chapter 2, James Bence, Jean-Dominique Lebreton, and Gary White for their comments on Chapter 3, and Peter Kareiva, James Nichols, and an anonymous reviewer for their comments on Chapter 4 during the review processes for journals. I also thank Heidi Fuchs for commenting on abstract and Chapter 1.

The David and Lucile Packard Foundation, the Rinehart Coastal Research Center, and the Woods Hole Oceanographic Institution Sea Grant Program (NOAA NA86RG0075) supported this work through grants to Hal Caswell. Graduate Research Fellowship from Woods Hole Oceanographic Institution also supported the first year of my study.

I am very grateful to Lauren Mullineaux for her assistance as the education coordinator for the Joint Program in Biology. My smooth ride through the Ph.D. program owes a great deal to her. I am also grateful to Judy McDowell for acting as a chair person of my thesis defense. I also thank Marsha Bissonette, Stella Callagee, Marcey Simon, Susan Tomeo, Mary Jane Tucci, Julia Westwater, and other staff at Education Office and Biology Department for their help in business matters.

My life at Woods Hole Oceanographic Institution was significantly improved ($p < 0.001$) by my friends. I thank Karin Harding, Mark Hill, Tin Klanjscek, Petra Krepac, and Amanda McDonald for their help with miscellaneous matters. I only hope that I did not annoy them too much as their office mate. I am also very grateful to John and Ofelia Tolli for occasional invitations to their dinner.

Last but not least, I would like to thank my wife Yumi and son Takuma. Without their support, this thesis could have not been completed. I would like to dedicate this thesis to them.

Contents

List of Figures

List of Tables

Chapter 1

Introduction

Mark-recapture (capture-recapture) methods have become an important tool in population biology. The methods are used to estimate population size (e.g. Petersen, 1896; Lincoln, 1930; Jackson, 1933), survival probability (e.g. Burnham et al., 1987; Lebreton et al., 1992; Caswell et al., 1999), and transition probabilities among spatial locations (e.g. Arnason, 1972, 1973) and life stages (e.g. Nichols et al., 1992b). In a mark-recapture study, a population consisting of previously marked (or identified) individuals is resampled in subsequent sampling occasions. By resampling the population, information on the capturability of individuals is obtained. This information allows better estimates of population parameters than methods where the parameters are calculated directly from count data under the assumption that probability of capturing individuals is 1.

1.1 Brief History of Mark-Recapture Methodology

Mark-recapture sampling was originally developed as an alternative approach to a census for estimating population size. In the original method, the resampling was only done once to obtain the numbers of individuals that were marked and unmarked at the resampling occasion, from which capture probability was estimated. By dividing the number of originally marked individuals by the capture probability, the abundance of individuals in a population was estimated. Let x, y, and z be the number of individuals marked at time 1, the number of individuals caught at time 2, and the number of recaptured marked individuals at time

2, respectively. Then the population size N can be estimated as

$$\widehat{N} = \frac{y}{z}x, \tag{1.1}$$

where $\frac{z}{y}$ is an estimated capture probability assuming it was the same at the two sampling occasions. Equation (1.1) is often called the Lincoln-Petersen estimator in mark-recapture literature. This estimator implicitly assumes that the population is closed to immigration, emigration, birth, and death, and also assumes that capturability of marked and unmarked individuals are the same. This method was first used by Laplace in the $18th$ century to estimate the human population in France (Cormack, 1968). It was rediscovered later by Petersen (1896) and Lincoln (1930) and used to estimate population size of fish and waterfowl, respectively.

The method to estimate survival probability from mark-recapture data was developed by Cormack (1964), Jolly (1965), and Seber (1965). This method is often called the Cormack-Jolly-Seber (CJS) method. While the only data required for the Lincoln-Petersen estimator are number of individuals marked, number of marked individuals recaptured, and the total number of individuals recaptured, the CJS method requires additional information on whether or not each uniquely marked individual was recaptured at each sampling occasion (i.e. individual capture history data). In the CJS method, the individual capture histories are modeled assuming all marked individuals have the same capture probability; however, it does not make any assumption on the capturability of unmarked individuals. In reality, the capture probability may be different among individuals (i.e. heterogeneous), and ones with lower capture probability may be more likely to be unmarked than others. Because the CJS method does not make any assumption on the capturability of unmarked individuals, it is more robust to the heterogeneity in capture probability than the Lincoln-Petersen estimator. Extensive reviews of the CJS method can be found in Burnham et al. (1987) and Lebreton et al. (1992).

As an extension of the CJS method, Arnason (1972) and Arnason (1973) developed

a method to estimate movement rates of individuals among discrete spaces, along with their survival and capture probabilities. This method is called multi-type mark-recapture method. The multi-type mark-recapture method requires information on where individuals were marked and recaptured, in addition to the individual capture histories that are required for the CJS method. The data are modeled with capture probability, survival probability, and transition probabilities among spatial locations. This method was later generalized by Nichols et al. (1992b) to be used with multi-stage mark-recapture data, in which "stage" can be defined in terms of the life cycle (age classes, size classes, developmental stages), or any other property that divides individuals into subgroups.

1.2 Overview of Thesis

The focus of my thesis work is on advancing the mark-recapture analysis method to extract useful information for demographic analyses from the data. The thesis consists of five main chapters following this introduction. The first three chapters are primarily on new mark-recapture methodology, and the last two chapters are application of the methods to actual data of the North Atlantic right whale.

In Chapter 2, I present four major improvements in the multi-stage mark-recapture method. (1) I use a Markov chain formulation of the life cycle to express the likelihood functions in matrix form, which makes numerical calculations simpler. (2) I introduce a method to incorporate capture histories with uncertain stage and sex identifications, which allows the use of capture history data with incomplete information. (3) I introduce a simple function that allows multinomial transition probabilities to be written as functions of covariates (time or environmental factors). (4) Finally, I show how to convert transition probabilities estimated by the MSMR method into a matrix population model.

In Chapter 3, I present a new method to estimate survival probability from the capture histories of marked individuals that become unobservable during some life stages. During mark-recapture studies of open populations, animals often temporarily emigrate from study

areas. Such temporary emigration can cause biased estimates of survival probabilities and other parameters. The new method uses stage-structured models that include one or more stages representing the individuals that have temporarily emigrated. Although not all parameters can be estimated in such stage structures, some important parameters are still estimable. The estimability of parameter values is determined from the rank of the Jacobian of the likelihood function. I apply the temporary-emigration mark-recapture method to artificial data, representing various life histories, and demonstrate consistency between actual and estimated values. The method presented in this chapter will be especially useful for studies of seabird, sea turtle, and marine mammal populations where breeding is delayed and where individuals are sampled only on their breeding grounds.

In Chapter 4, I present a new method for estimating a distribution of dispersal displacements (a dispersal kernel) from mark-recapture data. One conventional method of calculating the dispersal kernel assumes that displacements are normally distributed (e.g. resulting from a diffusion process), and that individuals remain within sampled areas. The first assumption prohibits an analysis of dispersal data that are not normally distributed (a common situation); the second assumption leads to underestimation of dispersal distance because individuals that disperse outside of sampling areas are never recaptured. The new method eliminates these two assumptions. This method uses integrodifference equations to express the probability of spatial mark-recapture data; associated dispersal and recapture parameters are then estimated using a maximum likelihood method. The accuracy of model selection was examined using Akaike Information Criteria (AIC). The method presented in this chapter will allow re-examination of existing data sets and suggests designs for future mark-recapture experiments.

In Chapter 5, I apply the method presented in Chapter 2 to the data of the North Atlantic right whale. The North Atlantic right whale (*Eubalaena glacialis*) is considered the most endangered large whale species. The current population size is about 300 in the northwestern Atlantic, and the number is declining. I applied the multi-stage mark-recapture statistics to the 17-year individual sighting history data collected by New England

Aquarium, MA. Using the estimated transition probabilities, I constructed a population projection matrix. In this chapter, I also present various demographic analyses based on the projection matrix.

In Chapter 6, I extend the analysis in Chapter 5. In particular, I analyze the importance of demographic and environmental stochasticity to the population viability. I apply the branching process calculations (e.g. Caswell, 2001), calculations based on a diffusion approximation to the changes in log of population size (e.g. Tuljapurkar, 1990; Dennis et al., 1991), and simulation (e.g. Caswell, 2001) to calculate the expected time to extinction from the estimated parameters.

At the time of writing this thesis, Chapter 2 and 3 have been accepted to *Ecology*. Chapter 4 is to be submitted to *Biometrics*. Chapter 5 has been published in *Nature*. Chapter 6 is to be submitted to a journal that is to be determined.

Chapter 2

Estimating population projection matrices from multi-stage mark-recapture data

2.1 Introduction

Mark-recapture estimates of survival probability have been applied to many animal populations (e.g., Lebreton et al., 1992; Forsman et al., 1996; Weimerskirch et al., 1997; Hastings & Testa, 1998; Caswell et al., 1999; Pease & Mattson, 1999), and this method has become an important tool in population management. Mark-recapture estimates are based on capture histories of individually identified animals, which contain information on whether or not each individual was captured at each sampling occasion. For example, capture history data may be obtained by annual observations of banded birds or photographically identified whales. When such data are available, mark-recapture statistics are considered one of the best approaches for estimation of survival probability.

Modern demographic analysis goes beyond calculating survival, by breaking the life cycle into stages (which may be based on age, size, developmental or behavioral states, physiological condition, spatial location, or any other property that divides individuals into subgroups). The fate of individuals is described in terms of transition probabilities among these stages, and those transition probabilities form the basis for matrix population models (Caswell, 2001). Nichols et al. (1992b) introduced a method to estimate transition probabil-

ities among stages from mark-recapture data, which we call the multi-stage mark-recapture (MSMR) method. This method extends the method originally developed to estimate probabilities of movement among spatial locations (Arnason, 1972, 1973; Brownie et al., 1993; Lebreton, 1995). For the MSMR method, in addition to information on whether or not each individual was captured, the capture history data must also include the stage of captured individuals at each capture occasion. MSMR models account for inter-group heterogeneity in survival and capture probability by grouping similar individuals into stages. The development from single-stage to multi-stage mark-recapture statistics parallels the development from unstructured to structured population models. In fact, one motivation for the statistical development was the need to estimate parameters in stage-structured matrix population models from mark-recapture data (Nichols et al., 1992b).

The analysis is based on maximization of a likelihood function that depends on all the possible sequences of stage transitions compatible with an observed capture history. There can be very many of these sequences, and one of the most complicated parts of the method of Nichols et al. (1992b) is writing them all down with their associated probabilities. In this paper, we describe the life cycle as a Markov chain, and take advantage of this description to write the likelihood in a simple matrix notation. A sketch of this method was given in Caswell (2001, Section 6.1.2.2). Here we give a complete presentation, and extend the method to incorporate uncertainty in stage and sex identifications, which allows the use of capture histories containing incomplete information. We also introduce a simple function that allows multinomial transition probabilities to be written as a functions of covariates (e.g., environmental variables or time). Finally, we show how to convert the estimated transition probabilities into a matrix population model.

2.2 MSMR Statistics

The MSMR method involves three main steps: (1) constructing an appropriate stage structure, (2) expressing the likelihood function in terms of parameters, based on available cap-

ture histories, and (3) finding the best parameter estimates using maximum likelihood theory. The parameters in the MSMR model are those that define the capture probabilities of each stage at each sampling occasion and the transition probabilities among stages between consecutive sampling occasions. The method assumes that individuals in the same stage are identical and independent, but that individuals in different stages may differ in their transition and capture probabilities. The MSMR method is very flexible and can be applied to almost any stage structure. Constructing a useful stage structure that is compatible with the life cycle of populations requires experience in addition to sufficient mathematical and biological knowledge, and different stage structures are extensively reviewed in Caswell (2001). In this paper, methods for expressing the likelihood function and estimating parameters are described assuming an appropriate stage structure has been constructed.

To make our discussion more concrete, we will demonstrate the method using a stage structure (Fig. 2.1) developed to describe the life history of the North Atlantic right whale (*Eubalaena glacialis*). This is a two-sex, multi-stage model that distinguishes calves (stage 1), immature individuals (stage 2), and mature individuals (stage 3). In addition to these three stages, females also have a stage for individuals nursing a calf (stage 4); we call the individuals in this stage "mothers." Stage 0 corresponds to death, and the probabilities ϕ_{0i} associated with the arrows going to stage 0 are stage-specific mortality rates. As usual, "mortality" includes both death and permanent emigration.

The objective of the MSMR approach is to estimate the transition probabilities associated with each arrow and the capture probabilities of each stage. In the next section, we show how to construct matrices containing the transition and capture probabilities, and to account for uncertainty in the assignment of individuals to stages. Then we will show how to calculate the likelihood in terms of these matrices.

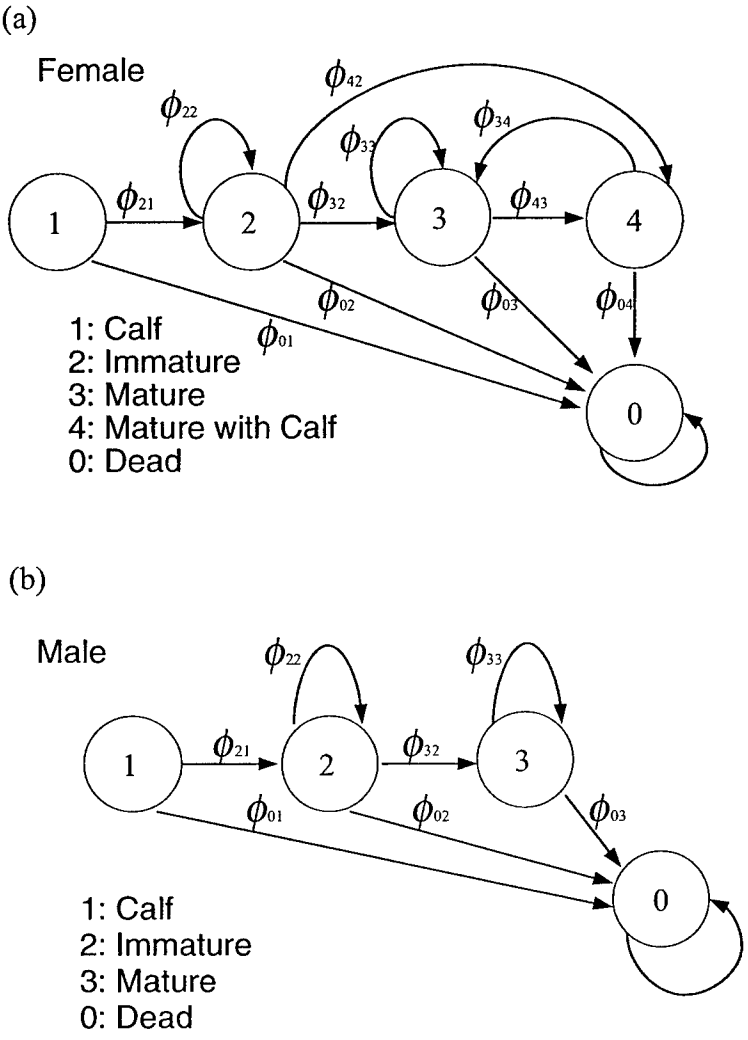

Figure 2.1: A stage structure for female (a) and male (b) right whales. This structure is used as an example for the MSMR statistics.

2.2.1 Transition and Capture Probability Matrices

The transition matrix is constructed by first putting the transition probability ϕ_{ji} from (living) stage i to (living) stage j in the (j,i) position. To this matrix is appended a row containing the probabilities of transition from each stage to stage 0 (death) and a column containing the probabilities of transition from stage 0 to each stage. Because we treat death as a stage, the result is the transition matrix of an absorbing Markov chain, with death as an absorbing state. The matrix is column stochastic. The ability to treat transitions as a Markov chain is critical to our analysis. The transition matrix for females, corresponding to the stage structure in Fig. 2.1 is

$$\mathbf{\Phi}_t^{(f)}(\boldsymbol{\theta}) = \left(\begin{array}{cccc|c} 0 & 0 & 0 & 0 & 0 \\ \phi_{21}(t) & \phi_{22}(t) & 0 & 0 & 0 \\ 0 & \phi_{32}(t) & \phi_{33}(t) & \phi_{34}(t) & 0 \\ 0 & \phi_{42}(t) & \phi_{43}(t) & 0 & 0 \\ \hline \phi_{01}(t) & \phi_{02}(t) & \phi_{03}(t) & \phi_{04}(t) & 1 \end{array}\right), \tag{2.1}$$

where $\phi_{ji}(t)$ is the probability of females making transition from stage i to j between time t and $t+1$. The upper left block of the matrix describes the transition among live stages, and lower left block of the matrix contains stage specific probabilities of death. The 1 in the (5,5) entry is the probability of dead individuals remaining dead in the following year. The notation $\phi_{ji}(t)$ in this paper corresponds to ϕ_{tij} in Nichols et al. (1992b).

Similarly, the transition matrix for males, corresponding to the stage structure in Fig. 2.1, is

$$\mathbf{\Phi}_t^{(m)}(\boldsymbol{\theta}) = \left(\begin{array}{ccc|c} 0 & 0 & 0 & 0 \\ \phi_{21}(t) & \phi_{22}(t) & 0 & 0 \\ 0 & \phi_{32}(t) & \phi_{33}(t) & 0 \\ \hline \phi_{01}(t) & \phi_{02}(t) & \phi_{03}(t) & 1 \end{array}\right). \tag{2.2}$$

We have written $\mathbf{\Phi}_t^{(f)}$ and $\mathbf{\Phi}_t^{(m)}$ as a function of a vector of parameters $\boldsymbol{\theta}$. Then parameters could be the ϕ_{ji} themselves, or lower level parameters from which the ϕ_{ji} can be calculated. The objective is to estimate $\boldsymbol{\theta}$.

Capture probability matrices $\mathbf{P}_t$, defined for females and males separately, contain stage-specific capture probabilities on the diagonal and zeros elsewhere:

$$\mathbf{P}_t^{(f)}(\boldsymbol{\theta}) = \begin{pmatrix} p_1(t) & 0 & 0 & 0 & 0 \\ 0 & p_2(t) & 0 & 0 & 0 \\ 0 & 0 & p_3(t) & 0 & 0 \\ 0 & 0 & 0 & p_4(t) & 0 \\ 0 & 0 & 0 & 0 & 0 \end{pmatrix}, \tag{2.3}$$

$$\mathbf{P}_t^{(m)}(\boldsymbol{\theta}) = \begin{pmatrix} p_1(t) & 0 & 0 & 0 \\ 0 & p_2(t) & 0 & 0 \\ 0 & 0 & p_3(t) & 0 \\ 0 & 0 & 0 & 0 \end{pmatrix}. \tag{2.4}$$

where $p_j(t)$ is the probability of capturing individuals in stage j at time t. This notation corresponds to p_{jt} in Nichols et al. (1992b). As written here, $\mathbf{P}_t^{(f)}$ and $\mathbf{P}_t^{(m)}$ assume that dead individuals are never captured ($p_0^{(f)} = p_0^{(m)} = 0$), but such captures could be included.

Transition and capture probability matrices can be defined separately for females and males when information on sex identification is available, as in our example, but it is not always possible or necessary to have a two-sex model. In such cases, only a single transition and capture probability matrix is needed.

2.2.2 Stage-Assignment Matrices

A stage-assignment matrix is defined for each individual each time it is captured. The diagonal elements of the matrix are proportional to the certainty of stage identification at time t (i.e., to the probability that the individual is in a given stage when it is captured).

This probability should be known prior to estimating transition and capture probabilities. In our example, individual k is a female; its stage-assignment matrix is

$$\mathbf{U}_t^{(k)} = \begin{pmatrix} u_1^{(k)}(t) & 0 & 0 & 0 & 0 \\ 0 & u_2^{(k)}(t) & 0 & 0 & 0 \\ 0 & 0 & u_3^{(k)}(t) & 0 & 0 \\ 0 & 0 & 0 & u_4^{(k)}(t) & 0 \\ 0 & 0 & 0 & 0 & u_0^{(k)}(t) \end{pmatrix}, \tag{2.5}$$

where $u_j^{(k)}(t)$ is the probability that individual k at time t is in stage j ($j = 1, 2, 3, 4$). Similarly, if individual k is male, its stage-assignment matrix is

$$\mathbf{U}_t^{(k)} = \begin{pmatrix} u_1^{(k)}(t) & 0 & 0 & 0 \\ 0 & u_2^{(k)}(t) & 0 & 0 \\ 0 & 0 & u_3^{(k)}(t) & 0 \\ 0 & 0 & 0 & u_0^{(k)}(t) \end{pmatrix}. \tag{2.6}$$

Because we assume that the capture probability of dead individuals is zero, the value for $u_0^{(k)}(t)$ will not enter into the likelihood calculations. Multiplication of $\mathbf{U}_t^{(k)}$ by a scalar has no effect on the maximum likelihood estimates.

If the stage of the individual is known with certainty, its stage-assignment matrix contains a 1 in the corresponding diagonal entry and zeros elsewhere. On the other hand, if the stage of an individual is completely unknown, the identity matrix can be used for $\mathbf{U}_t^{(k)}$. This specifies a uniform probability distribution over the possible stages. Alternatively, if an independent assessment of the probability is available, it can be entered into the matrix. For example, in an age-structured model of fish, age of fish is sometimes determined from their length using age-length keys (e.g. Fournier & Archibald, 1982; Deriso et al., 1985; Quinn & Deriso, 1999). Such a key could provide the probability distribution of age of the fish, which can be entered into the stage assignment matrices, for an age-structured model.

2.2.3 Likelihood

The likelihood of the parameter vector $\boldsymbol{\theta}$ contains contributions from the capture history of each individual. We denote by $l_k(\boldsymbol{\theta})$ the contribution to the likelihood from individual k; it is proportional to the probability of the capture history. That probability is the sum of the probabilities of all possible sequences of transitions that could have been taken by the individual k. There may be many such possibilities. Their sum, however, can be calculated using the transition, capture probability, and stage-assignment matrices by the following algorithm. We assume the individual is first captured at time t_1.

1. Categorize individual k by its stage at its first capture, taking uncertainty in stage assignment into account,

$$\mathbf{U}_{t_1}^{(k)}\mathbf{e}. \tag{2.7}$$

   where $\mathbf{e}$ is a vector of ones. This product is a vector whose entries are proportional to the probabilities of the initial stage of the individual at t.

2. Calculate the probability distribution of the stage at t_2 by multiplying this vector by the transition matrix $\boldsymbol{\Phi}_{t_1}$.

$$\boldsymbol{\Phi}_{t_1}\mathbf{U}_{t_1}^{(k)}\mathbf{e}. \tag{2.8}$$

3. Calculate the probabilities of observation outcomes at t_2:

   if individual k was captured at t_2, multiply by the sighting matrix $\mathbf{P}_{t_2}$:

$$\mathbf{P}_{t_2}\boldsymbol{\Phi}_{t_1}\mathbf{U}_{t_1}^{(k)}\mathbf{e}, \tag{2.9}$$

   if individual k was not captured at t_2, multiply by $(\mathbf{I}-\mathbf{P}_{t_2})$:

$$(\mathbf{I}-\mathbf{P}_{t_2})\boldsymbol{\Phi}_{t_1}\mathbf{U}_{t_1}^{(k)}\mathbf{e}, \tag{2.10}$$

   where $\mathbf{I}$ is the identity matrix,

4. Account for stage identification at t_2 by multiplying by the stage assignment matrix; if individual k was captured at t_2

$$\mathbf{U}_{t_2}^{(k)}\mathbf{P}_{t_2}\mathbf{\Phi}_{t_1}\mathbf{U}_{t_1}^{(k)}\mathbf{e}, \tag{2.11}$$

if individual k was not captured at t_2

$$\mathbf{I}(\mathbf{I}-\mathbf{P}_{t_2})\mathbf{\Phi}_{t_1}\mathbf{U}_{t_1}^{(k)}\mathbf{e}. \tag{2.12}$$

5. Repeat steps 2-4 until the end of the capture history for individual k. The result is a vector whose ith entry is proportional to the probability of all the pathways by which individual k could have moved from its initial stage at t_1 to stage i at t_h and that are compatible with its capture history.

6. The final step is to sum the resulting vector of probabilities to obtain,

$$l_k(\boldsymbol{\theta})_k = \mathbf{e}^{\mathsf{T}}\mathbf{U}_{t_h}^{(k)}\cdots\mathbf{\Phi}_{t_1}\mathbf{U}_{t_1}^{(k)}\mathbf{e}, \tag{2.13}$$

In this algorithm, the probability distribution of the individual's stage is updated sequentially over time taking into account the new data available at each time step and possible stage transitions determined by the stage structure. Therefore, the right-hand side of equation (2.13) is the probability of the capture history for individual k, taking into account all possible transition sequences compatible with that history.

The likelihood $l_k(\boldsymbol{\theta})$ is calculated using only female or male matrices if the sex of individual k is known. If the sex of individual k is uncertain, the above algorithm is repeated to get likelihoods $l_k^{(f)}(\boldsymbol{\theta})$ and $l_k^{(m)}(\boldsymbol{\theta})$ using the female- and male-specific matrices, respectively. Then, the likelihood $l_k(\boldsymbol{\theta})$ is

$$l_k(\boldsymbol{\theta}) = p_f l_k^{(f)}(\boldsymbol{\theta}) + (1-p_f) l_k^{(m)}(\boldsymbol{\theta}), \tag{2.14}$$

where p_f is the probability that the individual k is female. The probability p_f is 1 or 0 when the sex of the individual is known to be female or male, respectively. If the sex of the individual is unknown, a probability must be provided to calculate the likelihood.

Some examples of probabilities of the capture histories of individuals with four capture periods are shown in Table 2.1. Because our example contains multiple stages, many possible capture histories exist, of which only a few are shown in Table 2.1. For simplicity, we assume that sex of all individuals is known to be female. None of the likelihoods in Table 2.1 contains $\mathbf{P}_1$, because the probability of a capture history is always conditional on the first capture; therefore, capture probability at the first sampling time cannot be estimated. For the same reason, the likelihoods of individuals 5, 7, 8, 11, 12, and 13 do not begin at time $t = 1$, because capture histories prior to the first capture of an individual do not enter into probability calculations.

Given the likelihood functions $l_k(\boldsymbol{\theta})$ for all individuals, the likelihood associated with the data consisting of n capture histories is proportional to the product of the n likelihood functions

$$L(\boldsymbol{\theta}) \propto \prod_{k=1}^{n} l_k(\boldsymbol{\theta}). \tag{2.15}$$

Here, we assume that individuals are captured and make stage transitions independently, but based on identical probability distributions (i.e. we assume the number of outcomes falling into the possible capture history sequences is multinomial).

Maximum likelihood estimates $\widehat{\boldsymbol{\theta}}$ are found by maximizing $L(\boldsymbol{\theta})$. The likelihood function can be maximized numerically using software such as MATLAB. For example, the MATLAB routine `fminu` can be used to find the maximum likelihood by minimizing $-\log L(\boldsymbol{\theta})$.

2.3 Transition Probabilities as Functions of Covariates

Transition probabilities $\phi_{ji}(t)$ may change over the course of a study, and the changes may be correlated with various factors. We would like to model the probabilities as functions of covariates measuring those factors. For example, population density and sampling effort

Table 2.1: Some possible capture histories corresponding to the example stage structure in Fig. 2.1 and their likelihood.

ID (k)	Capture History*	Likelihood $l_k(\boldsymbol{\theta})$
1	3433	$\mathbf{e}^\intercal \mathbf{U}_4^{(1)} \mathbf{P}_4 \mathbf{\Phi}_3 \mathbf{U}_3^{(1)} \mathbf{P}_3 \mathbf{\Phi}_2 \mathbf{U}_2^{(1)} \mathbf{P}_2 \mathbf{\Phi}_1 \mathbf{U}_1^{(1)} \mathbf{e}$
2	122X	$\mathbf{e}^\intercal (\mathbf{I} - \mathbf{P}_4) \mathbf{\Phi}_3 \mathbf{U}_3^{(2)} \mathbf{P}_3 \mathbf{\Phi}_2 \mathbf{U}_2^{(2)} \mathbf{P}_2 \mathbf{\Phi}_1 \mathbf{U}_1^{(2)} e$
3	22X3	$\mathbf{e}^\intercal \mathbf{U}_4^{(3)} \mathbf{P}_4 \mathbf{\Phi}_3 (\mathbf{I} - \mathbf{P}_3) \mathbf{\Phi}_2 \mathbf{U}_2^{(3)} \mathbf{P}_2 \mathbf{\Phi}_1 \mathbf{U}_1^{(3)} e$
4	1X22	$\mathbf{e}^\intercal \mathbf{U}_4^{(4)} \mathbf{P}_4 \mathbf{\Phi}_3 \mathbf{U}_3^{(4)} \mathbf{P}_3 \mathbf{\Phi}_2 (\mathbf{I} - \mathbf{P}_2) \mathbf{\Phi}_1 \mathbf{U}_1^{(4)} e$
5	X343	$\mathbf{e}^\intercal \mathbf{U}_4^{(5)} \mathbf{P}_4 \mathbf{\Phi}_3 \mathbf{U}_3^{(5)} \mathbf{P}_3 \mathbf{\Phi}_2 \mathbf{U}_2^{(5)} e$
6	12XX	$\mathbf{e}^\intercal (\mathbf{I} - \mathbf{P}_4) \mathbf{\Phi}_3 (\mathbf{I} - \mathbf{P}_3) \mathbf{\Phi}_2 \mathbf{U}_2^{(6)} \mathbf{P}_2 \mathbf{\Phi}_1 \mathbf{U}_1^{(6)} e$
7	XX33	$\mathbf{e}^\intercal \mathbf{U}_4^{(7)} \mathbf{P}_4 \mathbf{\Phi}_3 \mathbf{U}_2^{(7)} e$
8	X43X	$\mathbf{e}^\intercal (\mathbf{I} - \mathbf{P}_4) \mathbf{\Phi}_3 \mathbf{U}_3^{(8)} \mathbf{P}_3 \mathbf{\Phi}_2 \mathbf{U}_2^{(8)} e$
9	4XX3	$\mathbf{e}^\intercal \mathbf{U}_4^{(9)} \mathbf{P}_4 \mathbf{\Phi}_3 (\mathbf{I} - \mathbf{P}_3) \mathbf{\Phi}_2 (\mathbf{I} - \mathbf{P}_2) \mathbf{\Phi}_1 \mathbf{U}_1^{(9)} e$
10	2X2X	$\mathbf{e}^\intercal (\mathbf{I} - \mathbf{P}_4) \mathbf{\Phi}_3 \mathbf{U}_3^{(10)} \mathbf{P}_3 \mathbf{\Phi}_2 (\mathbf{I} - \mathbf{P}_2) \mathbf{\Phi}_1 \mathbf{U}_1^{(10)} e$
11	X3X4	$\mathbf{e}^\intercal \mathbf{U}_4^{(11)} \mathbf{P}_4 \mathbf{\Phi}_3 (\mathbf{I} - \mathbf{P}_3) \mathbf{\Phi}_2 \mathbf{U}_2^{(11)} e$
12	XX1X	$\mathbf{e}^\intercal (\mathbf{I} - \mathbf{P}_4) \mathbf{\Phi}_3 \mathbf{U}_3^{(12)} e$
13	X3XX	$\mathbf{e}^\intercal (\mathbf{I} - \mathbf{P}_4) \mathbf{\Phi}_3 (\mathbf{I} - \mathbf{P}_3) \mathbf{\Phi}_2 \mathbf{U}_2^{(13)} e$
14	2XXX	$\mathbf{e}^\intercal (\mathbf{I} - \mathbf{P}_4) \mathbf{\Phi}_3 (\mathbf{I} - \mathbf{P}_3) \mathbf{\Phi}_2 (\mathbf{I} - \mathbf{P}_2) \mathbf{\Phi}_1 \mathbf{U}_1^{(14)} e$

Note: When stage of captured individual is i, $\mathbf{U}_t^{(k)}$ is a matrix with 1 in the ith row of the ith column and 0 elsewhere.

* X indicates the individual was not captured; numbers indicate the stage of captured individuals.

were used to model the survival and capture probabilities in studies of the roe deer (*Capreolus capreolus*) and the common lizard (*Lacerta vivipara*), respectively (Lebreton et al., 1992), and time has been used to model the survival probability of the northern spotted owl (*Strix occidentalis caurina*)(Forsman et al., 1996) and the North Atlantic right whale (Caswell et al., 1999).

Covariates are incorporated in the transition probability using a link function. The link function must satisfy the constraint that each column of the transition matrix sums to 1, and each entry of the matrix must lie between 0 and 1. A flexible function that satisfies these properties is the polychotomous logistic function, which is derived by expressing the log of the odds ratio as a linear function of the covariates (Hosmer & Lemeshow, 1989). Let $x_t^{(d)}$ be the value of dth covariate at time t. The polychotomous logistic function is

$$\phi_{ji}(t) = \frac{\exp\left(\alpha_{ji} + \sum_d \beta_{ji}^{(d)} x_t^{(d)}\right)}{1 + \sum_j \exp\left(\alpha_{ji} + \sum_d \beta_{ji}^{(d)} x_t^{(d)}\right)}, \tag{2.16}$$

where α_{ji} is an intercept parameter, and $\beta_{ji}^{(d)}$ is a slope parameter associated with the dth covariate. When all the slope parameters are zero for all d, i, and j, the transition matrix is constant over time. The simple logistic function that is often used in mark-recapture literatures (e.g. Burnham et al., 1987; Lebreton et al., 1992) is a special case of the polychotomous logistic function for a binary outcome.

2.4 Matrix Population Models

Population projection matrices contain both transition probabilities and fertilities (see Caswell, 2001). Because the transition probabilities are estimated by the MSMR method, we can construct the projection matrix if we know the fertility terms. In this section, we show an example of how those terms might be obtained, and how to compute confidence intervals for population growth rate calculated from the population matrix.

2.4.1 Conversion from a Transition Matrix to a Population Projection Matrix

The right whale example provides enough information to write a 2-sex model. To do so, we renumber the male stages in Figure 2.1 as 5, 6, 7. Letting $\phi_{ji}(t)$ denote the transition probability as before, the projection matrix is

$$\mathbf{A}_t = \left(\begin{array}{cccc|ccc} 0 & F_2(t) & F_3(t) & 0 & 0 & 0 & 0 \\ \phi_{21}(t) & \phi_{22}(t) & 0 & 0 & 0 & 0 & 0 \\ 0 & \phi_{32}(t) & \phi_{33}(t) & \phi_{34}(t) & 0 & 0 & 0 \\ 0 & \phi_{42}(t) & \phi_{43}(t) & 0 & 0 & 0 & 0 \\ \hline 0 & F_6(t) & F_7(t) & 0 & 0 & 0 & 0 \\ 0 & 0 & 0 & 0 & \phi_{65}(t) & \phi_{66}(t) & 0 \\ 0 & 0 & 0 & 0 & 0 & \phi_{76}(t) & \phi_{77}(t) \end{array}\right). \tag{2.17}$$

The upper left and lower right blocks describe production of females by females and males by males, respectively. The entries in the lower left block describe production of males by females.

When constructing a population projection matrix, transition probability and fertility terms are often estimated from two separate data sets (Caswell, 2001), but the fertility terms can be directly estimated using the MSMR method if the stage structure includes mothers that give birth between two consecutive sampling periods (i.e. stage 4 in our example). Each time an individual enters this stage, it gives birth; therefore, transition probabilities into the fertile stage are also probabilities of giving birth. If the number of female and male births at each reproductive event are b_f and b_m, respectively, the fertility terms in the projection matrix are given by the product of the number of offspring and the transition probabilities:

$$F_2(t) = b_f \phi_{42}(t), \tag{2.18}$$

$$F_3(t) = b_f \phi_{43}(t), \tag{2.19}$$

$$F_6(t) = b_m \phi_{42}(t), \tag{2.20}$$

$$F_7(t) = b_m \phi_{43}(t). \tag{2.21}$$

An important assumption in these fertility terms is that mothers and their newborns have the same capturability during sampling. To ensure that this condition is satisfied, when mothers are captured, their offspring should also be captured and entered into the data as new individuals. Similarly, when newborns were captured, their mothers should be captured and identified as mothers. Later, we will show one example of remedial methods when the equal capturability assumption is not met.

The model (2.17) is female-dominant; males do not affect population dynamics. This assumption is often legitimate when the population size of males is large enough that searching for a partner does not limit reproduction by females. Thus for calculation of population growth rate, the two-sex matrix may be reduced to the female matrix

$$\mathbf{A}_t = \begin{pmatrix} 0 & F_2(t) & F_3(t) & 0 \\ \phi_{21}(t) & \phi_{22}(t) & 0 & 0 \\ 0 & \phi_{32}(t) & \phi_{33}(t) & \phi_{34}(t) \\ 0 & \phi_{42}(t) & \phi_{43}(t) & 0 \end{pmatrix}. \tag{2.22}$$

2.4.2 Confidence Intervals for Population Growth Rate

The long-term population growth rate implied by a projection matrix $\mathbf{A}_t$ is given by the dominant eigenvalue λ of $\mathbf{A}_t$. A confidence interval for λ can be approximated from the MSMR statistics, using eigenvalue sensitivity formula and the covariance matrix of the parameters.

The eigenvalue sensitivity formula is

$$\frac{\partial \lambda}{\partial\, a_{ji}} = \frac{v_j w_i}{< \mathbf{w}, \mathbf{v} >}, \tag{2.23}$$

where $\mathbf{v}$ and $\mathbf{w}$ are the left and right dominant eigenvectors of the population projection matrix (Caswell, 1978, 2001). If the a_{ij} are functions of some other parameters θ_r, the sensitivity of λ to θ_r is

$$\frac{\partial \widehat{\lambda}}{\partial \theta_r} = \sum_j \sum_i \frac{\partial \widehat{\lambda}}{\partial a_{ji}} \frac{\partial \widehat{a_{ji}}}{\partial \theta_r}. \tag{2.24}$$

Now let $\boldsymbol{\theta}$ be a vector of parameters estimated by the MSMR method. An approximate 95% confidence interval for λ is calculated by

$$\widehat{\lambda} \pm 1.96 \sqrt{\sum_{q,r} \widehat{c}_{qr} \left(\frac{\partial \widehat{\lambda}}{\partial \theta_q}\right) \left(\frac{\partial \widehat{\lambda}}{\partial \theta_r}\right)}, \tag{2.25}$$

where $\widehat{c}_{qr}$ is (qr)th entry of the estimated covariance matrix $\widehat{\mathbf{C}}$. The covariance matrix $\mathbf{C}$ can be estimated by inverting the Hessian matrix (the information matrix) (e.g. Burnham et al., 1987). This method of constructing the confidence interval is an application of the delta method (see Seber, 1982, Chapter 1), taking advantage of the existence of the eigenvalue sensitivity formula (2.23).

2.5 Application to the North Atlantic Right Whale

We have applied the MSMR method to data on the North Atlantic right whale (*Eubalaena glacialis*). The northern right whale is considered one of the most endangered large whale species in the world (Waring et al., 1999). The current population in the western North Atlantic contains fewer than 300 individuals. They migrate from the Bay of Fundy, which is a summer feeding ground, to the coast of Florida, which is a winter calving ground. Caswell et al. (1999) showed that the crude survival probability of individuals in this population has been declining since 1980.

Data on the North Atlantic right whale have been collected by New England Aquarium and consist of annual sighting histories of photographically identified animals from 1980 to 1997 (Crone & Kraus, 1990). For the purpose of our analysis, we consider individuals to have been marked on the occasion of their first identification, and recaptured when they

were resighted during a subsequent year. Of the 372 individuals used for the analysis, 141 are known to be females and 143 to be males. We assumed the remainder to be either female or male with 50% probabilities. A few sightings of dead individuals exist but are not included in this analysis.

2.5.1 Stage-assignment matrices

We attempted to assign each individual at each capture to one of the stages shown in Fig. 2.1. A whale was considered mature if it was known to be at least 9 years old or, for females, if it had been observed with a calf. Stages could be assigned with certainty in 78% of the captures. The remainder were known to be either immature or mature, and for these captures, we must calculate the entries u_2, u_3, u_5, and u_6 of the stage-assignment matrices (2.5) and (2.6). In the absence of information to the contrary, we assume that these probabilities are constant over time and across individuals, but differ between females and males. Because we use different criteria to assign females and males to stages, we expect that the probability distribution of stages among the unknown staged captures would differ for females and males.

When the stage of a captured individual is uncertain, the (2,2) entry of the stage-assignment matrix is the probability that the individual is immature, given that the stage is uncertain. Similarly, the (3,3) entry is the probability that the individual is mature, given that the stage is uncertain. The other entries are all zero. To express these probabilities in mathematical form, let X be a random variable giving the stage of an individual and Y be a random variable taking the value 1 if the stage is known and 0 if the stage is uncertain. Then the two probabilities are

$$u_2 = Pr(X = 2|Y = 0) \tag{2.26}$$

$$\begin{aligned} u_3 &= Pr(X = 3|Y = 0) \\ &= 1 - u_2. \end{aligned} \tag{2.27}$$

To calculate $Pr(X = 2|Y = 0)$, we use Bayes' Rule to derive:

$$Pr(X = 2|Y = 0) = \frac{Pr(X = 2) - Pr(X = 2|\ Y = 1)Pr(Y = 1)}{1 - Pr(Y = 1)}. \tag{2.28}$$

Here, $Pr(Y = 1)$ is the probability that the stage of a captured immature or mature individual is known, and can be estimated from the capture history data as

$$Pr(Y = 1) = \frac{N_2 + N_3}{N_2 + N_3 + N_u}, \tag{2.29}$$

where N_2, N_3, and N_u are numbers of captures of immature, mature, and uncertain stages, respectively. $Pr(X = 2|Y = 1)$ is the probability that the stage of a detected immature or mature individual is immature given that the stage is known. This probability can be calculated from the capture history data as

$$Pr(X = 2|Y = 1) = \frac{N_2}{N_2 + N_3}. \tag{2.30}$$

Finally, $Pr(X = 2)$ is the probability that the stage is immature given that the stage is either immature or mature, regardless of whether the stage is known or uncertain. To estimate this probability, we estimated the parameters for a time-invariant projection matrix from the subset of the data containing only certain captures. From the stable stage distribution $\mathbf{w}$ (i.e. the right eigenvector associated with the dominant eigenvalue) of this matrix, we calculated the proportion of individual in stage 2 among stages 2 and 3 and used it as our estimate of $Pr(X = 2)$:

$$Pr(X = 2) = \frac{w_2}{w_2 + w_3} \tag{2.31}$$

For males, the same method was applied to the male stages (5 and 6). It should be noted that these calculations work best when the capture probability of stages 2 and 4 (5 and 6 for males) are similar. Otherwise, each count in (2.29) and (2.30) should be divided by the corresponding capture probability (Nichols et al., 1994). The end result of these calculations is in $u_2 = 0.87$, $u_3 = 0.13$, $u_5 = 0.30$, and $u_6 = 0.70$.

2.5.2 Capture probabilities

Capture probabilities were modeled as binary logistic functions of estimated sampling effort levels in the Northern and Southern regions, which are major feeding and calving grounds, respectively. These effort levels were approximated by the number of sampling dates per year in each region. We created models by including all possible combinations of effort levels for all possible combination of stages. This resulted in 1024 models. The best capture model among the 1024 candidate models was selected using Akaike Information Criteria (AIC; Akaike (1973)). Because the sample size is large, we did not use the small sample adjustment to AIC (i.e. AIC_c in Burnham & Anderson (1998)). The differences in AIC between the best and the second-best capture models was about 2, indicating that the support for the best model relative to the second best model is high (Burnham & Anderson, 1998). Furthermore, the 4 best models differ only in how capture probability of mothers depends on effort, and in all cases the capture probability was consistently close to 1 throughout the sampling period. Therefore, we used only the best model shown in Table 2. The capture probabilities of immature males and females did not differ significantly in the best model based on a likelihood ratio test. Therefore, we set these two capture probabilities equal and used the resulting capture probability model for further analysis (Table 2.5.2).

Table 2.2: Dependence of the best capture model for the North Atlantic right whale on effort level and time.

Stage*	Northern Effort	Southern Effort
Immature Female (2)	Yes	Yes
Mature Female (3)	Yes	Yes
Mature Female with Calf (4)	No	No
Immature Male (6)	Yes	Yes
Mature Male (7)	Yes	Yes

* Sighting probability of calves cannot be estimated because the capture of a calf is always the first capture of that individual.

2.5.3 Transition Probabilities

Although we have shown the vital rates have varied over time (Chapter 5), for this example we fit a model in which the transition probabilities are constant over time (i.e. no covariates). We also assumed that the survival probabilities of female and male calves are the same. This model gives a time-averaged picture of right whale demography. Estimated capture and transition probabilities are shown in Fig. 2.2 and Table 2.3, respectively.

The population projection matrix for female right whales is

$$\mathbf{A} = \begin{pmatrix} 0 & 0.5\phi_{42}\sqrt{\phi_{34}} & 0.5\phi_{43}\sqrt{\phi_{34}} & 0 \\ \phi_{21} & \phi_{22} & 0 & 0 \\ 0 & \phi_{32} & \phi_{33} & \phi_{34} \\ 0 & \phi_{42} & \phi_{43} & 0 \end{pmatrix} \tag{2.32}$$

Table 2.3: Estimated transition probabilities for the North Atlantic right whale.

Transition Probability	Mean	95% Confidence Interval
ϕ_{21}	0.92	[0.74 0.98]
ϕ_{22}	0.86	[0.81 0.89]
ϕ_{32}	0.08	[0.06 0.12]
ϕ_{42}	0.02	[0.01 0.03]
ϕ_{33}	0.80	[0.77 0.83]
ϕ_{43}	0.19	[0.16 0.22]
ϕ_{34}	0.83	[0.77 0.88]
ϕ_{66}	0.76	[0.72 0.79]
ϕ_{76}	0.19	[0.16 0.23]
ϕ_{77}	0.95	[0.94 0.96]

Note: The confidence intervals were estimated from 1000 parametric bootstrap samples generated assuming multivariate normal distributions of parameters. For the covariance matrix of the distribution was estimated as the inverse of the Hessian matrix (Burnham et al., 1987; Lebreton, 1995).

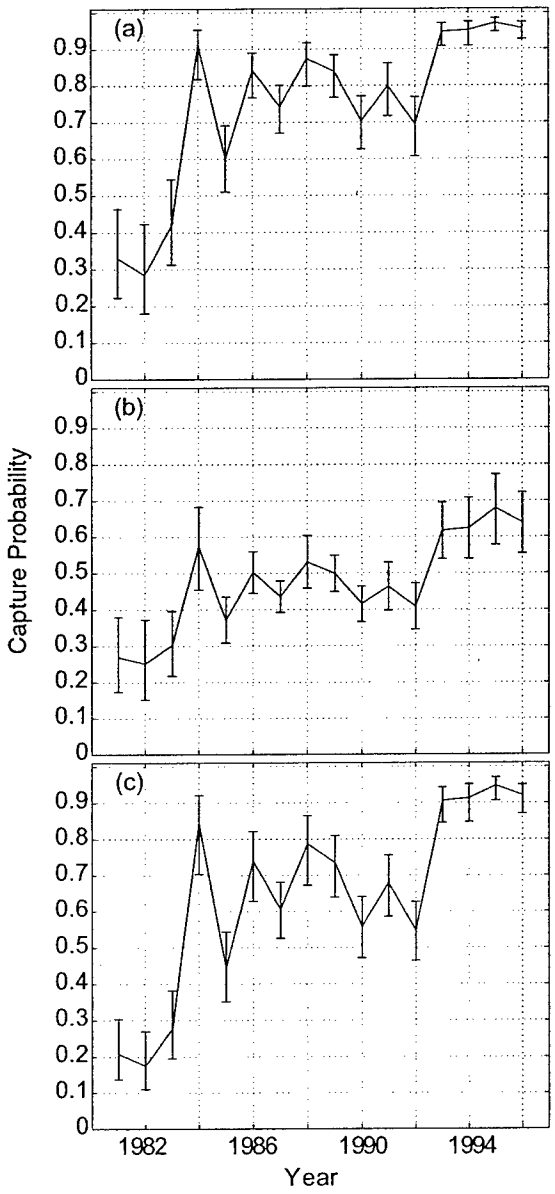

Figure 2.2: Stage-specific capture probabilities for (a) immature male and female, (b) mature female, and (c) mature male right whales. Error bars indicate point-wise 95% confidence intervals estimated from 1000 parametric bootstrap samples generated assuming a multivariate normal distribution of the logit of parameters. The covariance matrix of the distribution was estimated as the inverse of the Hessian matrix (see Burnham et al., 1987; Lebreton, 1995). Mothers had a constant capture probability 0.99 (95% CI =[0.98, 1.00]).

This matrix is the same as (2.22) but with a particular set of assumptions defining the fertility terms. Consider $F_2(t)$ in (2.22). When a female moves from stage 2 to stage 4 (with probability ϕ_{42}), she gives birth; the newborn is female with probability 0.5. To appear as a calf in stage 1 at $t+1$, the newborn calf must survive long enough to be cataloged. Although newborn calves have distinct markings, they are harder to distinguish individually than other stages. Therefore, calf survival is estimated from the time when the calf is seen sufficiently well to permit identification, which is not necessarily on its first sighting. We assumed calves are identified on average midway through their first year, and that the mother must survive this long (with probability $\phi_{34}^{0.5}$) in order for the calf to survive. $F_3(t)$ is calculated in a similar manner.

From this matrix, we estimated the long term population growth rate and its confidence interval. They are $\widehat{\lambda} = 1.01$ (95% CI =[1.00, 1.02]). This result shows that the North Atlantic right whale population has been growing by 1% annually on average from 1980 to 1997. (In fact, a time-varying model estimated by this same procedure concludes that the growth rate has declined from $\lambda = 1.03$ to $\lambda = 0.98$ over this time period Chapter 5) This matrix can now be analyzed to obtain the stable stage distribution, reproductive value, damping ratio, sensitivity and elasticity of λ, and other demographic statistics.

2.6 Discussion

The method presented here estimates a population projection matrix from mark-recapture data, which is one of the most commonly available data types for animal populations. Once the population projection matrix is estimated, it is subject to complete demographic analysis; such analyses provide powerful tools for conservation biology (e.g Caswell, 1989; Tuljapurkar & Caswell, 1997; Caswell, 2001). They can be used to assess the causes of past population declines, and to predict the effect of possible future management actions. Because population projection matrices contain many parameters, it has been difficult to estimate them accurately. This has been especially true for animals that are not captured

at every sampling period.

The likelihood calculations here are simpler than those described in Nichols et al. (1992b). This allows the use of mathematical software packages such as MATLAB, so the transition and capture probability models need not be limited to those available in mark-recapture packages such as MARK (White & Burnham, 1999) , MSSURVIV (Hines, 1994), or SURVIV (White, 1983).

Our method permits the use of capture histories with uncertain stage and sex. Individuals with such uncertainties tend to have lower survival rates than the rest of a population because individuals that survive longer have more chances for accurate assessment of stage and sex identification. For example, right whales are considered mature at 9 years of age. If animals that die within 9 years from their first capture are excluded because their stage is uncertain, then we would overestimate the survival probability. Observations with uncertain stage or sex should not be discarded in parameter estimation. Our approach is one way to deal with this problem.

The stage structure we used in this paper contains as a stage females that have given birth between consecutive sampling periods. This stage makes the conversion of the transition matrix into a population projection matrix relatively simple. Because the purpose of the MSMR statistics often is to estimate a population projection matrix, we recommend the use of this type of stage structure when possible.

The polychotomous logistic function is a flexible way to allow transition probabilities to decrease or increase with a covariate while satisfying the requirement that each column of the transition matrix sum to one. When time is used as a covariate, the polychotomous function allows inferences about temporal trends in stage-specific transition rates. This approach has been applied to the North Atlantic right whale data (Chapter 5).

Multi-stage mark-recapture data arise in many applications. For example, Nichols & Kendall (1995) use them in population genetics context to test trade-offs between survival and reproduction. Hestbeck et al. (1991) use them to estimate spatial movement of individuals. We have applied them to deal with the problem of temporary emigration (Chapter

3). We hope the extentions of the analytical method presented here will make them even more useful.

Mark-recapture data are expensive to collect, and they should be analyzed as completely as possible. If information on the stage of individuals (e.g., age, size, other developmental stages, or geographic locations) is collected in addition to the basic mark-recapture data, then MSMR statistics can be applied. The stage information need not be complete because our method incorporates uncertainties in stage identifications. The value of being able to use matrix population models for conservation makes it worthwhile to collect stage-specific data whenever possible.

Chapter 3

A general approach to temporary emigration in mark-recapture analysis

3.1 Introduction

In mark-recapture studies, survival probability is estimated from capture histories of individually identified animals. Those histories contain information on whether or not each individual was captured at each sampling occasion. The analysis assumes that all individuals have identical capture probabilities. This assumption is violated when some individuals temporarily leave the sampling area and return during subsequent sampling occasions. We refer to this as "temporary emigration." The capture probability of the individuals that have emigrated is zero, while the rest of individuals that are alive have a non-zero capture probability. Therefore, assuming that all individuals have the same capture probability, regardless their location, results in under- and over-estimation of the capture probability for individuals inside and outside the sampling area, respectively. The biased capture probability estimate often biases survival probability estimates.

The temporary emigration process we consider in this paper is deterministic; i.e., we assume that all animals in the sampling area emigrate, with probability 1, before the next sampling occasion. This type of temporary emigration process is common during immature stages and between reproductive events. We refer to these as the "immature emigra-

tion process" and "inter-birth emigration process," respectively. For example, albatrosses (*Diomedeidae* spp.) leave their breeding islands immediately after fledging (immature emigration process) and do not return for 5-15 years. Once they return, they are recaptured only when they breed (inter-birth emigration process) (Weimerskirch et al., 1997). Similarly, grey seals (*Halichoerus gryprus*) are marked when young, but cannot be recaptured before they mature (immature emigration process) (Schwarz & Stobo, 2000). Right whales (*Eubalaena* sp) are monitored at their calving ground, which they leave after reproduction and return at intervals of several years for calving (inter-birth emigration process) (Payne et al., 1990). Similarly, sea turtles are often individually identified only at their natal beach when they come back to lay their eggs (inter-birth emigration process).

Deterministic temporary emigration is different from permanent emigration and purely random temporary emigration, which are also common. Permanent emigration occurs when animals leave the sampling area and never come back. In usual mark-recapture analyses, permanent emigration is either assumed to be a part of mortality as a loss from a population (e.g. Lebreton et al., 1992) or assumed not to occur (e.g. Caswell et al., 1999). In purely random temporary emigration, individuals leave and return independently of their location at the previous sampling occasion. This type of temporary emigration occurs commonly when only a part of a habitat is sampled. When mark-recapture methods are applied to a population exhibiting purely random temporary emigration, the estimated capture probability is the product of the probability that individuals are in the sampling area and the probability that individuals within the sampling area are captured. However, survival probability is not affected by the emigration process (Brownie et al., 1993).

In this paper, we show how to estimate survival probability and other demographic transitions in the presence of deterministic temporary emigration. Our method includes location (temporarily emigrated or not) as a property of the individual and uses a multi-stage mark-recapture method. Our approach is related to the methods used by Arnason (1972), Arnason (1973), and Hestbeck et al. (1991) to estimate movement rates, but applies to populations that exhibit temporary emigration. Because individuals that have emigrated

are unobservable, the capture history data usually do not contain enough information to estimate all parameters separately. In order to add necessary information, we introduce constraints among the parameters. These constraints may be based on biologically reasonable models (e.g., that temporary emigration does not influence survival), or may be provided by independent estimates of some parameters from other data sets. The constraints reduce the number of parameters to be estimated, and allow us to estimate all the remaining parameter values separately. The possibility of modeling mark-recapture data with stage structures that contain unobservable stages was suggested by Lebreton (1995). Here, we apply the idea to populations that exhibit the two types of temporary emigration and analyze the estimability of parameters. Our results generalize those of Clobert et al. (1994), Lebreton et al. (1999), and Pradel & Lebreton (1999) in that we apply the method to inter-birth temporary emigration, analyze more general cases of immature temporary emigration, and use a formal method to determine estimable parameters.

As usual, estimating stage-specific transition and capture probabilities involves constructing an appropriate stage structure, expressing the likelihood function in terms of the parameters, and finding the best fit parameter values using maximum likelihood (e.g. Nichols et al., 1992b, also Chapter 2). The likelihood function can be written down directly using Markov chains that specify transition probabilities among stages, assuming independence of fates among individuals (i.e. assuming the number of outcomes falling into the possible capture history sequences is multinomial) (Caswell, 2001, also Chapter 2). This likelihood can be maximized numerically to find the best fit parameter values. This method allows simple programming using software such as MATLAB. Alternatively, in many but not all cases, parameters can be estimated using softwares that are specifically designed for mark-recapture analyses such as MARK (White & Burnham, 1999), MSSURVIV (Hines, 1994), and SURVIV (White, 1983).

3.2 Temporary-emigration stage structures

Figures 3.1 and 3.2 show examples of life cycle graphs including temporary emigration.

Each arrow indicates a possible stage transition from time t to $t+1$ and has a transition probability associated with it. We denote the transition probability from stage i to j by ϕ_{ji}. It should be noted that the subscripts for the transition probability are reversed from the traditional notation (e.g. Arnason, 1973; Hestbeck et al., 1991) so that they indicate the entry in a matrix population model (e.g. Caswell, 2001) and the column stochastic transition matrix used in Chapter 2. Individuals in a capturable stage have a non-zero probability of being recaptured. This probability is denoted by p_i for stage i.

The stage structure for the inter-birth emigration process (Fig. 3.1a) includes a breeding adult stage (stage 1) in which individuals can be recaptured with a probability p_1, and $k-1$ inter-breeding adult stages in which individuals cannot be recaptured. The value of k depends on the minimum inter-birth interval. For example, Wandering Albatrosses never breed successfully in two consecutive years (Weimerskirch et al., 1997). Those that give birth in one year will be missing from the breeding ground in the following year. After two years, they return to the breeding ground with some probability that is independent of age. Therefore, $k = 2$ for Wandering Albatross (Fig. 3.1b). Similarly, individual right whales do not give birth for at least two years after successful reproduction, so $k = 3$ for the right whale (Fig. 3.1c).

The stage structure for the immature emigration process (Fig. 3.2a) contains a newborn stage (stage 0) in which individuals are first captured and marked, $k-1$ immature stages (stage 1 through $k-1$) in which individuals cannot be captured due to temporary emigration, and a mature stage (stage k) in which individuals can be captured with a probability p_k. If $k > 1$, the first $k-1$ stages (i.e. newborn and the first $k-2$ immature stages) represent individuals that cannot mature before the following sampling period, and these stages also correspond to ages of individuals. Stage $k-1$ may mature (with probability $\phi_{k,k-1}$), remain immature (with probability $\phi_{k-1,k-1}$), or die (with probability $1-(\phi_{k-1,k-1}+\phi_{k,k-1})$).

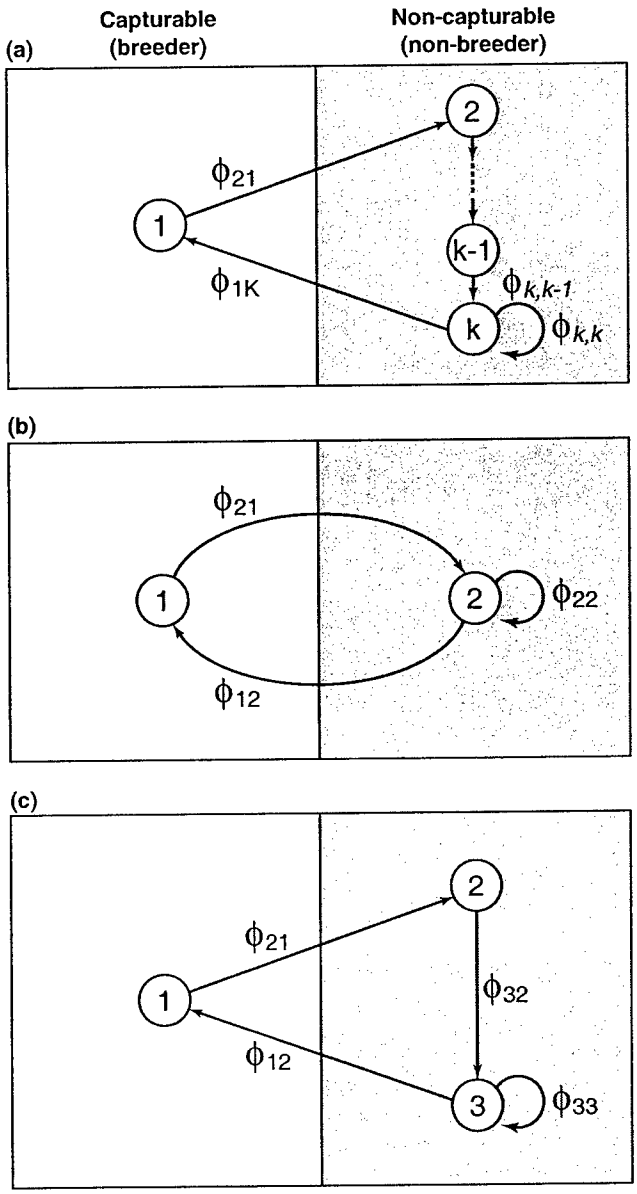

Figure 3.1: Inter-birth temporary-emigration stage structures. (a) General stage structure. (b) Stage structure with $k = 1$. This represents the temporary emigration of Wandering Albatross. (Models 1.1, 1.2, and 1.3). (b) Stage structure with $k = 2$. This represents the temporary emigration of the right whale. (Models 2.1, 2.2, and 2.3). Parameters for these stage structures are ϕ_{ij} a transition probability from stage j to i, and p_1 a capture probability of stage 1. Stages other than stage 1 have a zero recpature probability.

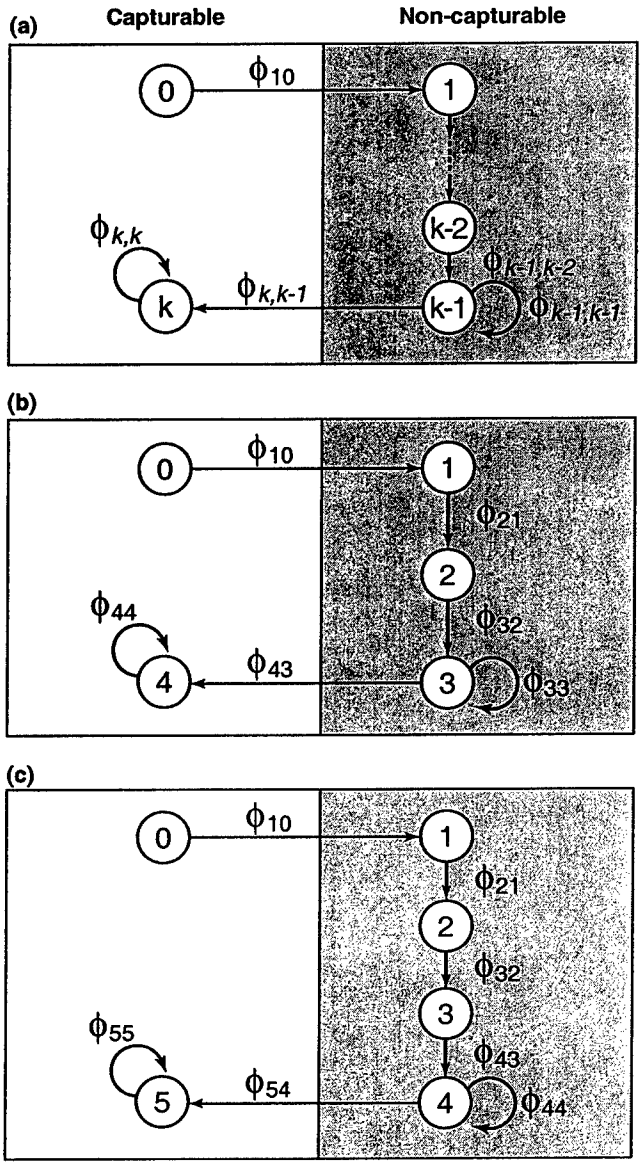

Figure 3.2: Immature temporary-emigration stage structure. (a) General stage structure. (b) Stage structure with $k = 4$. This represents the temporary emigration of the grey seal. (Models 3.1, 3.2, 3.3, 3.4, and 3.5). (c) Stage structure with $k = 5$. This represents the temporary emigration of Wandering Albatross. (Models 4.1, 4.2, 4.3, and 4.4). Parameters for these stage structures are ϕ_{ij} the transition probability from stage j to i, and p_k the recapture probability of the mature stage. Stages other than stage k have a zero recpature probability.

For example, grey seals do not give birth before reaching age 4 (Schwarz & Stobo, 2000). Therefore, an appropriate stage structure for them is one with $k = 4$ (Fig. 3.2b). Similarly, albatrosses do not mature before reaching the age of 5 (Weimerskirch et al., 1997); therefore, $k = 5$ in their stage structure (Fig. 3.2c). When $k = 1$, the stage structure does not contain a separate immature stage (i.e. newborn and immature stages are the same), and newborn individuals can mature directly or remain immature. In this stage-structure, immature individuals can be marked but cannot be recaptured; therefore, they still exhibit temporary emigration. These stage structures include as special cases the model of Clobert et al. (1994), but relax their assumption of a maximum age in immature stage.

Other population parameters (e.g., stage-specific survival probabilities, stage-specific probabilities of death, and probabilities of breeding) can be calculated from the ϕ_{ij}. For examples, the stage specific survival probability (s_i) is given by $\sum_j \phi_{ji}$ and the stage specific probability of death is given by $1 - \sum_j \phi_{ji}$. In the immature emigration model, the breeding probability, conditional on survival of individuals in stage $k-1$ (we denote this probability by ψ) is

$$\psi = \frac{\phi_{k,k-1}}{\phi_{k,k-1} + \phi_{k-1,k-1}}. \tag{3.1}$$

We will show how to calculate some other population indices in Section 6. More details can be found in (Caswell, 2001).

3.3 Estimability of parameters

Unfortunately, some of the parameters in the stage structures for temporary emigration processes may not be estimable, because of the lack of observations of the emigrated stages. In general, whether best-fit parameter values can be found uniquely or not depends on how the parameters appear in the likelihood function. If two or more parameters are confounded (i.e. they appear only in the same arithmetic form throughout the likelihood function), they cannot be estimated separately. The solution is to impose constraints on the parameters by specifying a model for the relationships among them.

Confounded parameters may result from model specification (intrinsic identifiability problem) or a lack of variation among observed data (extrinsic identifiability problem) (McCullagh & Nelder, 1989). When parameters are intrinsically confounded, the only way to eliminate the problem is to constrain parameters or modify the stage-structure so that other useful parameters can be estimated separately. When parameters are confounded because of lack of variation among observed data, the solution is to constrain parameters, modify the stage-structure, or increase the sample size. We will show how to determine whether model has the intrinsic and extrinsic identifiability problems or not in the next section and give examples in Section 4 and 5.

3.3.1 Determining estimability of parameters

Whether parameters are confounded in the likelihood function or not can be determined using the method of Catchpole & Morgan (1997). Their method uses the Jacobian matrix, which contains the derivatives of the likelihood functions with respect to parameters. If the rank of the Jacobian equals the number of parameters, then all parameters can be estimated separately. Here, we give a heuristic description of the method as it applies to temporary emigration models; for details see Catchpole & Morgan (1997).

We start with data consisting of capture histories of n individuals. The contribution of individual i to the likelihood function is proportional to the probability of its capture history. Let l_i be this contribution and assume that the model contains m parameters (x_1, x_2, ..., x_m). Then, l_i is a function of the parameters:

$$l_i = f_i(x_1, x_2, ..., x_m). \tag{3.2}$$

Taking the partial derivatives of the function l_i with respect to the parameters results in

$$\mathrm{d}l_i = \frac{\partial f_i}{\partial x_1}\mathrm{d}x_1 + \frac{\partial f_i}{\partial x_2}\mathrm{d}x_2 + ... + \frac{\partial f_i}{\partial x_m}\mathrm{d}x_m. \tag{3.3}$$

Because the data consist of n captured individuals, n such functions exist. In a vector

notation, they are:

$$\mathrm{d}\mathbf{l} = \mathbf{J}\mathrm{d}\mathbf{x} \tag{3.4}$$

where,

$$\mathrm{d}\mathbf{l} = \begin{pmatrix} \mathrm{d}l_1 & \mathrm{d}l_2 & \mathrm{d}l_3 & \cdots & \mathrm{d}l_n \end{pmatrix}^{\mathsf{T}},$$

$$\mathrm{d}\mathbf{x} = \begin{pmatrix} \mathrm{d}x_1 & \mathrm{d}x_2 & \cdots & \mathrm{d}x_m \end{pmatrix}^{\mathsf{T}},$$

$$\mathbf{J} = \begin{pmatrix} \frac{\partial f_1}{\partial x_1} & \frac{\partial f_1}{\partial x_2} & \cdots & \frac{\partial f_1}{\partial x_m} \\ \frac{\partial f_2}{\partial x_1} & \frac{\partial f_2}{\partial x_2} & \cdots & \frac{\partial f_2}{\partial x_m} \\ \frac{\partial f_3}{\partial x_1} & \frac{\partial f_3}{\partial x_2} & \cdots & \frac{\partial f_3}{\partial x_m} \\ \vdots & \vdots & \ddots & \vdots \\ \frac{\partial f_n}{\partial x_1} & \frac{\partial f_n}{\partial x_2} & \cdots & \frac{\partial f_n}{\partial x_m} \end{pmatrix}.$$

Here, $\mathbf{J}$ is the Jacobian matrix of the likelihood function with respect to the parameters. Equation (3.4) is a system of linear equations with $\mathbf{J}$ as a coefficient matrix. For $\mathbf{x}$ to be estimated uniquely, the Jacobian matrix must map $\mathrm{d}\mathbf{x}$ to $\mathrm{d}\mathbf{l}$ uniquely. This requires that the rank of the Jacobian matrix be m (i.e. columns of the Jacobian matrix must be independent). Therefore, if the rank of $\mathbf{J}$ is equal to the number of parameters, values for the parameters can be estimated separately using the maximum likelihood method. Otherwise, some parameters cannot be estimated separately, and the number of parameters that can be estimated separately is given by the rank of $\mathbf{J}$.

If multiple individuals have the same capture history sequence, the likelihoods associated with their capture histories are the same. Therefore, only one such copy needs to be included in the likelihood vector, and the duplicated likelihoods can be eliminated. If we do the analysis assuming that every possible capture history is observed at least once for each stage structure, then the above analysis can be used to detect intrinsic identifiability problems. On the other hand, if we use likelihood associated with the available capture history sequences, the analysis can be used to detect extrinsic identifiability problems.

3.3.2 An example of the Jacobian method

As an example, we apply the above method to the inter-birth emigration model with $k = 2$ (Fig. 3.1b). We assume all individuals are marked at the first sampling occasion, and there are 4 subsequent sampling occasions for recaptures (i.e. 5 capture occasions). Under these assumptions, there are five possible capture histories:

$$h_1 = 10101,$$

$$h_2 = 10100,$$

$$h_3 = 10001,$$

$$h_4 = 10010,$$

$$h_5 = 10000,$$

where 1 indicates an individual was captured and 0 indicates it was not captured.

The likelihood functions corresponding to these capture histories are:

$$l_1 = \quad p_1^2\phi_{21}^2\phi_{12}^2, \tag{3.5}$$

$$l_2 = \quad p_1\phi_{21}\phi_{12} - p_1^2\phi_{21}^2\phi_{12}^2 \tag{3.6}$$

$$l_3 = \quad [\phi_{21}^2\phi_{12}(1-p_1) + \phi_{21}\phi_{22}^2]\phi_{12}p_1 \tag{3.7}$$

$$l_4 = \quad p_1\phi_{21}\phi_{22}\phi_{12}[\phi_{21} + (1-\phi_{21})] \tag{3.8}$$

$$l_5 = \quad 1 - l_1 - l_2 - l_3 - l_4. \tag{3.9}$$

A likelihood function can be determined by creating a list of event sequences that could lead to the capture history, calculating the probability of the sequences, and then summing the probabilities. For example, h_1 can only arise for an animal that makes the transition back to stage 1 immediately after each observation occasion in stage 2, and is observed on each occasion it is in stage 1. The corresponding likelihood function (equation 3.5) is simply the product of this unique sequence of transition and recapture probabilities,

with some collection of terms. Likelihood functions l_2 through l_4 are more complicated because more than one sequence of events can lead to the observation sequence h_2 through h_4. For example, h_3 could arise from an animal that remained in stage 2 during sampling occasions 2-4 and then made the transition to stage 2 for sampling occasion 5 and was recaptured. However, this sequence could also arise if the animal went through the same stage transitions that produced h_1, but was not recaptured during sampling occasion 3. l_5 is calculated simply as the probability that capture histories h_1 through h_4 do not occur.

There are 4 parameters (p_1, ϕ_{21}, ϕ_{22}, and ϕ_{12}) and 5 likelihoods; therefore, the Jacobian is a 5x4 matrix. Its rank is the number of independent columns in $\mathbf{J}$. The Jacobian and its rank can be found easily using software for symbolic calculations; we used the SYMBOLIC MATH TOOLBOX in MATLAB. The rank of the Jacobian is 3, so only 3 of the 4 parameters can be estimated separately; therefore, this model has an intrinsic identifiability problem. This does not necessarily imply that any 3 parameters can be estimated; we include a discussion on which 3 parameters can be estimated in the next section.

3.4 Estimable parameters in temporary emigration models

To evaluate estimability of parameters in selected temporary emigration models, we applied the Jacobian method to 15 models based on the four stage structures in Fig. 3.1b, 3.1c, 3.2b, and 3.2c. Table 3.1 lists the models and also shows (1) constraints on transition probabilities, (2) parameters whose values are assumed to be known, (3) the number of parameter to be estimated, and (4) the rank of the Jacobian matrix. After imposing constraints and eliminating known parameters, all the remaining parameters become estimable in some models, which are indicated by (*).

Consider the inter-birth emigration model of Wandering Albatross (Fig. 3.1b, $k = 2$). Adults can be captured on the breeding grounds, but then disappear until they breed next. If no constraints are placed on the parameters (Model 1.1), the rank of the Jacobian is 3, so we can estimate only at most 3 of the 4 parameters. However, this does not imply that

any 3 parameters can be estimated. For example, if p_1 is known independently (Model 1.2), the number of parameters is reduced to 3, but the rank of the Jacobian is reduced to 2. On the other hand, we can fit a model that assumes that survival probability of breeding and non-breeding adults is the same, which implies the constraint $\phi_{21} = \phi_{12} + \phi_{22}$ (Model 1.3). In this model, both the number of parameters and the rank of the Jacobian are 3, indicating that all three parameters can be estimated.

For the inter-birth emigration model of the right whale without constraints (Model 2.1), the rank of the Jacobian is 3, while the number of parameters is 5. If we assume that

Table 3.1: Parameter constraints, number of parameters, and the rank of the Jacobian matrix for the 15 temporary emigration models. * indicates that values of all the free parameters are estimable.

Species	Model	Constraints on survival probabilities	Parameters set to known values	Number of parameters	Rank of Jacobian
Albatross	1.1	none	none	4	3
(Fig. 3.1b)	1.2	none	p_1	3	2
	1.3*	$\phi_{21} = \phi_{12} + \phi_{22}$	none	3	3
Right Whale	2.1	none	none	5	3
(Fig. 3.1c)	2.2	none	p_1	4	2
	2.3*	$\phi_{21} = \phi_{32} = \phi_{13} + \phi_{33}$	none	3	3
Grey Seal	3.1	none	none	6	3
(Fig. 3.2b)	3.2*	$\phi_{10} = \phi_{21} = \phi_{32}$ $= (\phi_{33} + \phi_{43}) = \phi_{44}$	none	3	3
	3.3*	$\phi_{10} = \phi_{21} = \phi_{32}$ $= (\phi_{33} + \phi_{43})$	p_4	3	3
	3.4*	$\phi_{21} = \phi_{32}$ $= (\phi_{33} + \phi_{43}) = \phi_{44}$	p_4	3	3
Albatross	4.1	none	none	7	3
(Fig. 3.2c)	4.2*	$\phi_{10} = \phi_{21} = \phi_{32} = \phi_{43}$ $= (\phi_{44} + \phi_{54}) = \phi_{55}$	none	3	3
	4.3*	$\phi_{10} = \phi_{21} = \phi_{32} = \phi_{43}$ $= (\phi_{44} + \phi_{54})$	p_5	3	3
	4.4*	$\phi_{21} = \phi_{32} = \phi_{43}$ $= (\phi_{44} + \phi_{54}) = \phi_{55}$	p_5	3	3
	4.5*	Logistic Model[1]	p_5	3	3

1: See Equations (3.10)–(3.17)

survival probability is unaffected by reproduction ($\phi_{21} = \phi_{32} = \phi_{13} + \phi_{33}$; Model 2.3), both the rank of the Jacobian and the number of parameters become 3, indicating that all the three remaining parameters (ϕ_{13}, ϕ_{33}, and p_1) can be estimated.

For the immature emigration model of the grey seal without constraints (Model 3.1), the rank of the Jacobian is 3, while the number of parameters is 6. While keeping the rank of the Jacobian at 3, we can reduce the number of parameters to 3 in several ways depending on assumptions on how mortality varies among the emigrated stages. Here we show some specific examples. Model 3.2 assumes that survival probabilities of all stages are the same. Under this assumption the three parameters ϕ_{33}, ϕ_{43}, and p_4 can be estimated separately, which also provides estimates of the survival of other stages (ϕ_{21}, ϕ_{32}, and ϕ_{44}). The next two models use an independent estimate of the capture probability of stage 4 (p_4). This permits estimation of an extra survival probability. For example, Model 3.3 assumes that all immature stages (0, 1, 2, and 3) have the same survival probability, which may differ from that of adults (stage 4). Model 3.4 assumes that the survival of newborn individuals (stage 0) may differ from that of all other stages.

The capture probability p_4 required for Models 3.3 and 3.4 could be obtained using Pollock's robust design (Pollock, 1982) if multiple samples of the mature individuals are collected within each primary sampling occasion, or by using a Cormack-Jolly-Seber type mark-recapture method (e.g. Burnham et al., 1987; Lebreton et al., 1992) if capture histories of the mature individuals over multiple sampling occasions are available. The latter method is used by Clobert et al. (1994) to estimate survival probability and age-specific breeding probability. This method also provides a separate survival probability estimate for mature stage (ϕ_{44}). This survival probability could also be provided in these models, reducing both the number of parameters and the rank of the Jacobian by one.

The situation for the immature temporary emigration models for Wandering Albatross is the same as the grey seal models. After reducing the number of parameters by assuming that survival probability of all stages are the same ($\phi_{21} = \phi_{32} = \phi_{43} = \phi_{44} + \phi_{54} = \phi_{55}$; Model 4.2), we can estimate all remaining parameters (ϕ_{44}, ϕ_{54}, p_5). Alternatively, different

distributions of survival probability during temporary emigration can be used. Model 4.3 assumes that survival probability is the same for the first 4 stages ($\phi_{21} = \phi_{32} = \phi_{43} = \phi_{44} + \phi_{54}$) and a separately estimated capture probability (p_5) is provided. Then we can estimate the remaining three parameters (ϕ_{44}, ϕ_{54}, and ϕ_{55}). Similarly, model 4.4 assumes that survival probability is the same for the last 4 stages ($\phi_{32} = \phi_{43} = \phi_{44} + \phi_{54} = \phi_{55}$) and p_5 is provided. Then we can estimate ϕ_{21}, ϕ_{44}, and ϕ_{54}, separately. This result suggests that the length of temporary emigration in our immature emigration model does not change the number and types of parameters that can be estimated.

Another approach to constraining parameters in the immature temporary emigration models is to write the survival probability as a parametric function of the stage and estimate the parameters in that function. For example, with the stage structure of Wandering Albatross, we might model the survival probability as a logistic function of age with the last immature stage and mature stage having the same survival probability. In many organisms, survival probability increases with age; therefore, this model may be realistic in many cases. Let s_i be survival probability of individuals in stage i, then

$$s_i = \frac{\exp(\gamma + \delta i)}{1 + \exp(\gamma + \delta i)} \qquad \text{for } i = 0, ..., 4, \tag{3.10}$$

where γ and δ are intercept and slope parameters. From the survival probability, transition probabilities can be calculated as

$$\phi_{01} = s_0 \tag{3.11}$$

$$\phi_{21} = s_1 \tag{3.12}$$

$$\vdots \tag{3.13}$$

$$\phi_{43} = s_3 \tag{3.14}$$

$$\phi_{44} = (1 - \psi)s_4 \tag{3.15}$$

$$\phi_{54} = \psi s_4 \tag{3.16}$$

$$\phi_{55} = s_5, \tag{3.17}$$

where ψ is the probability of transition from stage 4 to stage 5 conditional on survival. If p_5 is known, the rank of the Jacobian is 3, permitting estimation of γ, δ, and ψ separately.

3.5 Bias caused by temporary emigration

To examine the bias of the estimates, we applied Models 1.3, 2.3, 3.4, 4.2, and 4.5, shown in Table 1, to simulated data. Each simulated data set contained 75 individuals marked at the first sampling occasion. For each individual, the stage at the next sampling occasion was selected at random from the possible states (including death) with probabilities given by the column of the transition matrix corresponding to the current stage. An individual in a capturable stage was captured randomly with a probability equal to the capture probability of that stage. For Models 1.3 and 2.3, the data sets consisted of 9 resampling occasions; for Models 3.4, 4.2, and 4.5, sequences of 19 resampling occasions were generated.

From the data we estimated the parameters in the corresponding model. This process was repeated to obtain 1000 sets of parameter estimates. From the same data, we also estimated survival probability under the erroneous assumption that there was no temporary emigration, using the Cormack-Jolly-Seber method (Cormack, 1964; Jolly, 1965; Seber, 1965) with constant survival and capture probabilities.

Table 3.2 compares the values of parameters that were used to generate data and the means of 1000 estimates for the five models. Biases in both capture probability and transition probability are very small. Model 1.3 performs most poorly, but even here, the survival probability ($\phi_{22} + \phi_{12}$) appears to be without bias. On the other hand, Table 3.3 compares actual values and the means of 1000 estimates under the false assumption that there was no temporary emigration. Assuming there was no temporary emigration while there was in fact temporary emigration caused overestimations of survival probability for Models 1.3 and 2.3 and underestimations for most stages in Models 3.4 and 4.2, showing that these biases are a serious problem.

In the parameter estimation processes above, we were not always able to estimate pa-

rameters. Under Models 1.3 and 2.3 with 75 marked individuals, about 14% and 9%, respectively, of the numerical optimization failed to converge. These appear to be primar-

Table 3.2: Actual and mean of estimated parameters for Models 1.3, 2.3, 3.4, 4.2, and 4.5. Values in parentheses are standard deviations. Results based on simulating 1000 replicate datasets.

Model	Parameter	Actual Value	Mean Estimate (SD)
Model 1.3	p_1	0.80	0.79 (0.09)
	ϕ_{22}	0.40	0.38 (0.08)
	ϕ_{12}	0.50	0.52 (0.08)
Model 2.3	p_1	0.90	0.90(0.06)
	ϕ_{33}	0.30	0.30 (0.06)
	ϕ_{13}	0.60	0.60 (0.05)
Model 3.4	p_4	0.90	known
	ϕ_{10}	0.50	0.50 (0.10)
	ϕ_{33}	0.40	0.40 (0.08)
	ϕ_{43}	0.50	0.51 (0.08)
Model 4.2	p_5	0.80	0.80 (0.02)
	ϕ_{44}	0.45	0.45 (0.06)
	ϕ_{54}	0.50	0.50 (0.06)
Model 4.5	p_5	0.80	known
	γ	1.3863	1.40 (0.36)
	δ	0.3895	0.39 (0.13)
	ψ	0.4737	0.46 (0.07)

Table 3.3: Estimated capture and survival probabilities wrongly assuming no temporary emigration (simple Cormack-Jolly-Seber model with constant capture and survival probability). Data were generated assuming Models 1.3, 2.3, 3.4, and 4.2. Values in parentheses are standard deviations. Results based on simulating 1000 replicate datasets.

Model	Parameter	Actual Value	Mean Estimate (SD)
Model 1.3	Capture Probability (p)	0.80 for stage 1	0.20 (0.02)
	Survival Probability (s)	0.90	0.94 (0.02)
Model 2.3	Capture Probability (p)	0.90 for stage 1	0.14 (0.01)
	Survival Probability (s)	0.90	0.98 (0.01)
Model 3.4	Capture Probability (p)	0.90 for stage 4	0.52 (0.05)
	Survival Probability (s)	0.5 for stage 0	
		0.9 for stage > 0	0.83 (0.03)
Model 4.2	Capture Probability (p)	0.80 for stage 5	0.63 (<0.01)
	Survival Probability (s)	0.95	0.72 (<0.01)

ily caused by extrinsic identifiability problems as repeating the analysis with 150 marked individuals reduced the incidence of non-convergence to 5% and 1%, respectively.

3.6 An example: the right whale

As an example, we apply our method to data on the North Atlantic right whale (*Eubalaena glacialis*). This is one of the most endangered mammal populations in the world, currently consisting of fewer than 300 individuals. There is evidence to suggest that this number is slowly declining because of declined survival probability (Caswell et al., 1999). The right whale is found along the east coast of the United States. In summer, they feed in the northwest Atlantic, including Massachusetts Bay, Great South Channel, Bay of Fundy, and Brown's Bank. In winter, some females migrate to the coast of Florida and Georgia for calving. Their inter-birth interval is 3-5 years.

The capture history data we use here are based on photographs taken by members of the North Atlantic right whale consortium during annual surveys along the east coast of the United States. Because right whales have unique markings called callosity patterns on their heads, individuals can be identified from photographs. Based on these photographs, the New England Aquarium has been accumulating capture history data of individuals since 1980. Here, we use only sightings of mothers (i.e. females with their calf). We consider individuals to have been marked on the occasion of their first identification as mothers, and recaptured when they were resighted with a calf during a subsequent year. If the data had actually been collected this way, females would exhibit an inter-birth temporary emigration with an interval of at least 3 years. This corresponds to the data structure in the ongoing study of southern right whales (*Eubalaena australis*) in their breeding ground off Peninsula Valdes, Argentina (Payne et al., 1990).

We use the stage structure shown in Figure 3.1c. This stage structure is consistent with the fact that right whales do not give birth for at least two years after successful reproduction. Because previous analyses have detected time-variation in survival and transition

probabilities (Caswell et al., 1999), we divided the data into two periods, 1980-1988 ($t = 1$) and 1989-1997 ($t = 2$). Transition and survival probabilities are assumed constant within each period. We further assumed that the survival probabilities are the same for all stages (Model 2.3). The Jacobian indicates that this model, given the available data, is identifiable. Because individuals in stage 3 have three possible fates (remaining in stage 3, moving to stage 1, and death) the probability of which must sum to 1, the transition probabilities (ϕ_{13} and ϕ_{33}) in each period ($t = 1, 2$) were modeled with polychotomous logistic equations:

$$\phi_{13}^{(t)} = \frac{\exp(\alpha_t)}{1 + \exp(\alpha_t) + \exp(\beta_t)} \tag{3.18}$$

$$\phi_{33}^{(t)} = \frac{\exp(\beta_t)}{1 + \exp(\alpha_t) + \exp(\beta_t)}, \tag{3.19}$$

where α_t and β_t are the parameters to be estimated. Because the model assumes that the survival probability of all stages are the same, $\phi_{21}^{(t)} = \phi_{32}^{(t)} = \phi_{13}^{(t)} + \phi_{33}^{(t)}$. We expressed the likelihood associated with the data using the method in Chapter 2, and the negative log of the likelihood was numerically minimized using MATLAB function `fminu` to estimate the six parameters (p_1, p_2, α_1, α_2, β_1, and β_2).

To compare the estimated parameters between the two periods in terms of demographic context, we calculated survival probability as

$$s^{(t)} = \phi_{13}^{(t)} + \phi_{33}^{(t)}. \tag{3.20}$$

We also calculated the number of reproductive events based on Markov chain theory:

$$\widehat{\mathbf{R}}^{(t)} = \mathbf{F}\left(\mathbf{I} - \widehat{\mathbf{A}}^{(t)}\right)^{-1}, \tag{3.21}$$

where

$$\widehat{\mathbf{A}}^{(t)} = \begin{pmatrix} \widehat{\phi}_{13}^{(t)} & 0 & 0 \\ \widehat{\phi}_{21}^{(t)} & 0 & 0 \\ 0 & \widehat{\phi}_{32}^{(t)} & \widehat{\phi}_{33}^{(t)} \end{pmatrix}, \tag{3.22}$$

$$\mathbf{F} = \begin{pmatrix} 1 & 0 & 0 \\ 0 & 0 & 0 \\ 0 & 0 & 0 \end{pmatrix}, \tag{3.23}$$

and $\mathbf{I}$ is the identity matrix. The value r_{11} gives the expected number of future reproductive events from a female that has just given a birth. More details of this calculation can be found in Chapter 2.

Figure 3.3 compares survival probability and expected number of reproductive events between the two periods. Error bars in the figures are point-wise 95% confidence intervals based on a parametric bootstrap sampling procedure. We drew bootstrap samples of the four parameters $\widehat{\alpha}^{(1)}$, $\widehat{\alpha}^{(2)}$, $\widehat{\beta}^{(1)}$, and $\widehat{\beta}^{(2)}$ from a multivariate normal distribution, with mean vector equal to the maximum likelihood estimates and covariance matrix calculated from the inverse of the last Hessian matrix obtained during model fitting. A thousand bootstrap samples were generated and, for each bootstrap sample of the parameters, the survival probabilities and expected number of reproductive events were calculated. The 95 % confidence intervals for these parameters were defined by the 2.5 and 97.5 percentiles of the simulated distributions.

As expected, Figure 3.3 shows confidence intervals for survival and reproductive events are wide because of the small sample size. However, the results suggest that both survival and the expected number of reproductive events have declined. This result is consistent with the previous finding in Fujiwara & Caswell (2001) although the declines revealed by the analysis of the full data set are greater than those found here.

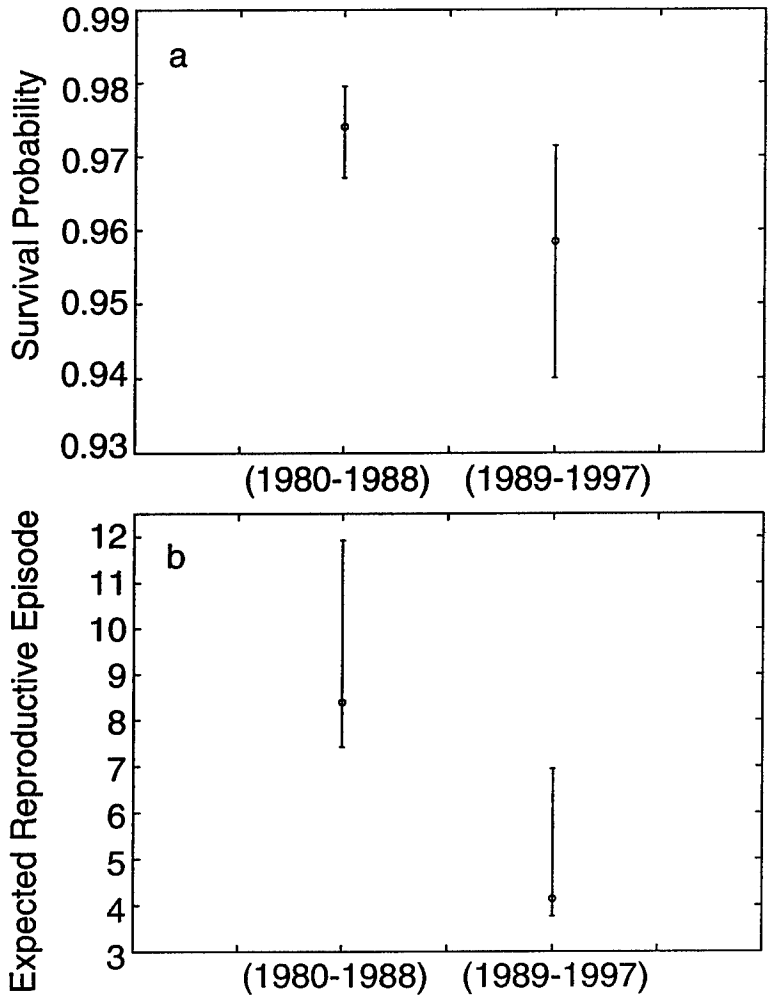

Figure 3.3: Analyses of North Atlantic right whale data. (a) Survival probability of females that have previously given birth at least once during periods between 1980 and 1988 and between 1989 and 1997. (b) Expected number of future reproductions during the lifetime of females that have given birth at least once.

3.7 Discussion

Temporary emigration causes an extreme case of heterogeneity in capture probability. Temporarily emigrated individuals have zero capture probability, while the rest of individuals have a non-zero capture probability. Ignoring temporary emigration when it exists leads to biased estimates of survival probability. By explicitly modeling the emigration process, the

method presented in this paper eliminates this bias.

The temporary emigration problem is often encountered in sampling large animals such as seabirds, sea turtles, and marine mammals. When the same problem is encountered with smaller organisms such as fish or insects, researchers may be able to eliminate the temporary emigration problem by experimental manipulation. For example, it has been suggested that when organisms can be marked and released into unobservable stages in the inter-birth temporary emigration stage structures (e.g., Models 3.1 and 4.1), all the parameters may be estimated separately (G. White, *personal communication*). In such cases, the methods outlined here to determine the estimability of parameters are still useful.

Our results are complementary to the approach of Kendall et al. (1997) and Kendall (1999), who use the Pollock's robust design method (Pollock, 1982) to deal with temporary emigration. In their method, a closed population model is used to estimate capture probabilities, which are incorporated into an open population model to estimate survival probabilities. This method has an advantage over our method in that it permits estimation of survival probabilities that vary freely from one sampling occasion to the next. The robust design method, however, requires multiple secondary samplings within each primary sampling period in order to obtain information on the capture probability. The method presented here does not require secondary sampling, although it can be combined with the robust design method when such samples are available.

In this paper, we focused on two stage structures, representing two different emigration processes, and considered only selected constraints on the parameters. We emphasize that the method can be applied to any biologically interesting age- or stage-classified life cycle, with any pattern of observed and unobserved stages. Each such structure may admit several choices for constraining parameters to make estimation possible. Choosing biologically relevant constraints is part of the data analysis process. We are certain that many useful stage structures and parameter constraints exist and are yet to be discovered.

Chapter 4

Estimating dispersal kernels from individual mark-recapture data

4.1 Introduction

A dispersal kernel is a probability density function for the location of an individual at time $t+1$ ($t = 0, 1, 2, \ldots$) conditional on the location of the individual at time t. This kernel is often incorporated in an integrodifference equation to model movements of individual organisms (e.g. Kot et al., 1996; Van Kirk & Levis, 1996; Van Kirk & Lewis, 1999; Lewis & Pacala, 2000; Neubert & Caswell, 2000; Neubert et al., 2000; Clark et al., 2001b). When the kernel is the probability density function of the Normal distribution (Gaussian distribution), the corresponding integrodifference equation model is a discrete-time equivalent of a simple diffusion process. The dispersal kernel can take other shapes to represent different hypotheses about movements of individuals (Neubert et al., 1995). For example, organisms may tend to either stay where they are or to travel long distances when they decide to travel. Such a movement pattern can be modeled with leptokurtic probability density functions such as the Laplace and Cauchy density functions. In fact, leptokurtosis is a ubiquitous feature of dispersal data in ecology (Okubo, 1980; Kot et al., 1996).

Recent studies in theoretical ecology have shown that different movement patterns (i.e. different shapes of the kernels) can produce qualitatively different population dynamics. For example, Kot et al. (1996) showed that invading organisms with frequent long-distance

dispersals (i.e. "fat-tailed" dispersal kernels) can have an accelerating speed of invasion. Clark (1998) showed that a dispersal pattern modeled by the fat-tailed kernel can explain the extremely fast spread of trees during the Pleistocene. In other studies, Kot (1989) and Neubert et al. (1995) showed that dispersal-driven instability may produce stable spatial patterns of population density in predator-prey systems under some patterns of predator and prey dispersal. Van Kirk & Levis (1996) also showed that the scale of a dispersal kernel relative to the size of a fragmented habitat can determine persistence of a population. These theoretical developments are prompting ecologists to measure dispersal kernels in the field.

Here, we present a method for estimating dispersal kernels from individual mark-recapture data. The mark-recapture data consist of information on whether or not each uniquely marked individual was captured at each sampling occasion along with its captured location. From the data, we derive a likelihood function, and a maximum likelihood method is used to estimate parameters associated with the dispersal kernels.

When an individual is not recaptured, we do not know its location. One possibility is that it was outside of the sampling area; in this case, there was zero probability of it being captured. The other possibility is that the individual was actually within the sampling area but was not captured by chance. To account for these two possibilities, we explicitly model the sampling process using a function for the capture probability at a given location; we call this function the capture probability function. The capture probability function is 0 where sampling was not conducted, and bounded between 0 and 1 where sampling was conducted. The capture probability function and dispersal kernel are used in integrodifference equations to express the likelihood.

In Section 4.2 and 4.3, we describe examples of dispersal kernels and capture probability functions, respectively. In Section 4.4, an algorithm for formulating the likelihood function is provided. In Section 4.5, we show examples of joint probability densities of locations of individuals at time t and their capture history sequences up to time $t-1$. These probability densities are used to demonstrate how a sampling process changes the probability densities of locations of individuals. In Section 4.6, we evaluate the performance of the estimators

using simulated data sets. In Section 4.7, we compare some results in Section 4.6 and equivalent results from the same data but falsely assuming that a sampling domain was large enough to include all individuals at all sampling occasions and falsely assuming a wrong dispersal kernel shape. In Section 4.8, we examine the performance of the method in selecting the true dispersal kernel shape based on Akaike Information Criteria (AIC). Up through Section 4.8, we assume individuals do not die, or that deaths occur on a much longer time-scale than spatial movements. In Section 4.9, we discuss how we can incorporate the deaths in a likelihood formulation when data for a longer time-scale are also available. Other extensions of the spatial mark-recapture method are also discussed in the last section.

4.2 Dispersal Kernels

Gaussian, Laplace, and Cauchy functions are used in our analysis as dispersal kernels; these functions are denoted by g, l, and c, respectively. These three kernels differ in kurtosis and fatness of their tails, which are important characteristics that can determine qualitatively different ecological dynamics (*e.g.* Kot et al., 1996; Neubert et al., 1995; Van Kirk & Levis, 1996). The Gaussian distribution is (by definition) nonleptokurtic and has exponentially bounded tails. The Laplace distribution is leptokurtic and has exponentially decaying tails. The Cauchy distribution is leptokurtic and its tails are not exponentially bounded. Although we focus on these three distributions, the approach we outline in this paper can be extended to many other shapes of dispersal kernels.

Let $X_t \in \Re$ be a random variable for the location of an individual at time $t = 0, 1, 2, \ldots, T$ where T is the time of the last sampling. Then a kernel $k_d(x_{t+1}|x_t)$ of shape d ($d = g, l, c$) is the probability density function for X_{t+1} conditional on $X_t = x_t$. With the further assumption that the kernel depends only on the relative locations of an individual at times t and $t+1$, the Gaussian kernel is

$$k_g(x_{t+1} - x_t) = \frac{1}{\alpha\sqrt{2\pi}} \exp\left[\frac{-(x_{t+1} - x_t - \mu)^2}{2\alpha^2}\right], \tag{4.1}$$

where $\alpha > 0$. Similarly, the Laplace kernel is

$$k_l\left(x_{t+1} - x_t\right) = \frac{1}{2\beta} \exp\left(-\frac{|x_{t+1} - x_t - \mu|}{\beta}\right), \tag{4.2}$$

where $\beta > 0$. Finally, the Cauchy kernel is

$$k_c(x_{t+1} - x_t) = \left\{\pi\gamma\left[1 + \left(\frac{x_{t+1} - x_t - \mu}{\gamma}\right)^2\right]\right\}^{-1}, \tag{4.3}$$

where $\gamma > 0$. In the above density functions, α, β and γ are parameters that define the scale of dispersal distances (displacements), and μ is a parameter that defines a directional movement of the individual between consecutive sampling occasions (i.e. a shift in the location of the center of a kernel).

4.3 Capture Probability Functions

The capture probability function $p_t(x_t)$ gives the probability of capturing an individual conditional on its location at time t is x_t. This function depends on how sampling is conducted. For example, the sampling may be done uniformly within a sampling area $[-d, d]$. Under this sampling protocol (M_1), the capture probability function is

$$p_t(x_t) = \begin{cases} u_t & \text{for} \quad |x_t| \leq d, \\ 0 & \text{for} \quad |x_t| > d. \end{cases} \tag{4.4}$$

In addition to the first protocol, an intense sampling area [-r,r] within the sampling domain may be added. Under this second protocol (M_2), the capture probability function is

$$p_t(x_t) = \begin{cases} 1 & \text{for} \quad |x_t| \leq r, \\ u_t & \text{for} \quad r < |x_t| \leq d, \\ 0 & \text{for} \quad |x_t| > d, \end{cases} \tag{4.5}$$

with $r < d$.

In the third protocol (M_3), sampling is only done outside of the center region:

$$p_t(x_t) = \begin{cases} 0 & \text{for} \quad |x_t| < d, \\ u_t & \text{for} \quad |x_t| \geq d. \end{cases} \tag{4.6}$$

This type of sampling protocol is sometimes used to obtain information on the shape of tail regions.

In the all three sampling models, u_t is the parameter to be estimated. The other parameters (d and r) are sizes of a sampling domain and an intense sampling region, respectively. Because they are determined before sampling, they are known constants.

Although we focus on capture probability functions (4.4)-(4.6) for simplicity, other functions can be incorporated in the method outlined in this paper. In Section 4.9, we discuss other functions that may be useful.

4.4 An Algorithm for the Likelihood

Let $\boldsymbol{\theta}$ be a parameter set that defines the dispersal kernel (the scale and shift parameters) and the capture probability function (u_t). A likelihood $l_i(\boldsymbol{\theta})$ associated with the ith individual in the data is a function of $\boldsymbol{\theta}$ and depends on the capture history of individual i.

Let $s^{(i)}_{x_{t_1+j}}(x_{t_1}, x_{t_1+1}, \ldots, x_{t_1+j})$ be the joint probability density function for the locations $\mathbf{X}_t$ $(t = t_1, \ldots, t_1 + j)$ of individual i $(i = 1, \ldots, n)$ and for its capture history sequence up to time $t_1 + j$. We assume that individual i was first captured (i.e. marked) at time t_1 and at location x_{t_1}. The likelihood can then be calculated by the following algorithm:

1. Obtain the probability density function for the locations X_{t_1} and X_{t_1+1} of individual i:

$$s^{(i)}_{t_1+1}(x_{t_1}, x_{t_1+1}) = k_d(x_{t_1+1} - x_{t_1}). \tag{4.7}$$

2. Obtain the joint probability density function of the locations X_{t_1}, X_{t_1+1}, and X_{t_1+2}

of individual i. If individual i was captured at location x_{t_1+1} at time t_1+1:

$$s^{(i)}_{t_1+2}(x_{t_1}, x_{t_1+1}, x_{t_1+2}) = s^{(i)}_{t_1+1}(x_{t_1}, x_{t_1+1}) p_{t_1+1}(x_{t_1}+1) k_d(x_{t_1+2} - x_{t_1+1}). \quad (4.8)$$

If individual i was not captured at t_1+1:

$$s^{(i)}_{t_1+2}(x_{t_1}, x_{t_1+1}, x_{t_1+2}) = \int_{-\infty}^{\infty} s^{(i)}_{t_1+1}(z)\{1 - p_{t_1+1}(z)\} k_d(x_{t_1+2} - z) dz. \quad (4.9)$$

3. Obtain the joint probability density function of the locations X_{t_1}, X_{t_1+1}, ..., X_{t_1+t+1} of individual i. If individual i was captured at location x_{t_1+t} at time t_1+t:

$$s^{(i)}_{t_1+t+1}(x_{t_1}, x_{t_1+1}, \ldots, x_{t_1+t+1}) = s^{(i)}_{t_1+t}(x_{t_1}, \ldots, x_{t_1+t}) p_{t_1+t}(x_{t_1+t}) k_d(x_{t_1+t+1} - x_{t_1+t}). \quad (4.10)$$

If individual i was not captured at t_1+t:

$$s^{(i)}_{t_1+t+1}(x_{t_1}, x_{t_1+1}, \ldots, x_{t_1+t+1}) = \int_{-\infty}^{\infty} s^{(i)}_{t_1+t}(z)\{1 - p_{t_1+t}(z)\} k_d(x_{t_1+t+1} - z) dz. \quad (4.11)$$

4. Repeat step 3 until the time of the final sampling occasion T.

5. Calculate the probability density of the final observation and reinterpret it as a likelihood. If individual i was captured at location x_T at time T,

$$\ell_i(\boldsymbol{\theta}) = s^{(i)}_T(x_T). \quad (4.12)$$

If individual i was not captured at time T,

$$\ell_i(\boldsymbol{\theta}) = \int_{-\infty}^{\infty} s^{(i)}_T(z)(1 - p_T(z)) dz. \quad (4.13)$$

□

It should be noted that equation (4.11) is a convolution of two functions and can there-

fore be calculated quickly using a fast Fourier transform convolution method.

The above algorithm is repeated for all marked individuals. Assuming that individual movements are independent of one another, the likelihoods associated with individual capture history sequences can be multiplied to get the likelihood of the data including all marked individuals. This likelihood can be numerically maximized to estimate the parameters.

4.5 Joint Probability Density of Location and Past Capture History Sequence

To calculate the likelihood in the previous section, we used the joint probability density function $s_t^{(i)}(x_0, \ldots, x_t)$ of the locations of individuals from time 0 to t. Here, we assume the individual was marked at time 0. In this section, we show how $s_t^{(i)}(x_0, \ldots, x_t)$ may change with time.

As examples, we use two marked individuals released at different locations at $t = 0$. We simulated movements of the two individuals using the Gaussian kernel ($\alpha = 1, \mu = 0$), and their capture was simulated using the M_1 sampling protocol with probability $u = 0.85$ within $d = [-1, 1]$ and $u = 0$ outside. The marginal probability density, which does not depend on past capture histories, can also be calculated by convolving the kernels at each time step. We have plotted the joint probability density function $s_t^{(i)}(x_0, \ldots, x_t)$ sliced at actual capture history sequence up to time t-1 (solid lines) and a marginal probability density function of location (dotted lines) at time $t = 1, 2, 3$ in Figure 4.1.

Figures 4.1a and 4.1d show the joint probability densities of the individuals at $t = 1$. They are just Gaussian probability densities and the same as the marginal probability densities because they do not have any previous sampling occasions.

Figures 4.1b and 4.1e show the joint probability densities (solid lines) of the two individuals at $t = 2$ when the individuals were not captured at $t = 1$. Because they were not captured at $t = 1$, the probability that individuals were within the sampling domain at

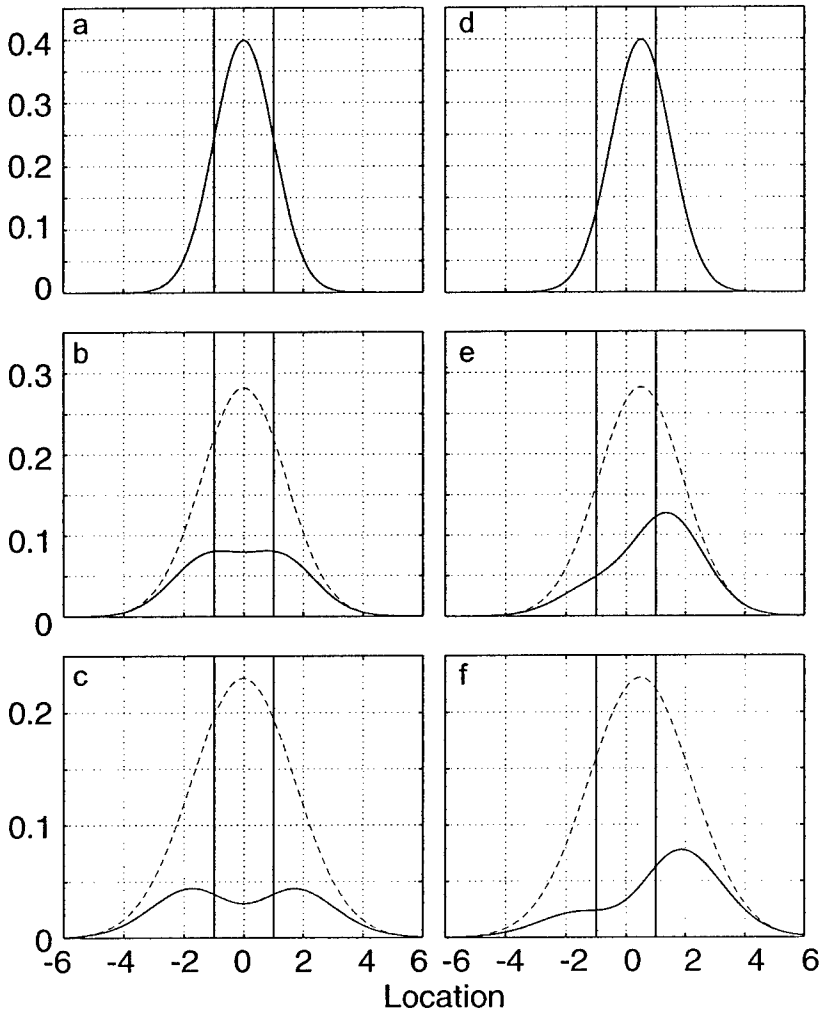

Figure 4.1: Joint probability density of location of an individual and its past capture history sequence (solid line) and the marginal probability density of location of the individual (dashed line). We simulated movements of the two individuals using the Gaussian kernel ($\alpha = 1, \mu = 0$), and their capture was simulated using the M_1 sampling protocol with probability $u = 0.85$ within $d = [-1, 1]$ and $u = 0$ outside. (a) The probability densities at $t = 1$ when an individual was released at $x = 0$ at $t = 0$. (b) The probability densities at $t = 2$ when an individual was released at $x = 0$ at $t = 0$ but not recaptured at $t = 1$. (c) The probability densities at $t = 3$ when an individual was released at $x = 0$ at $t = 0$ but not recaptured at $t = 1$ and $t = 2$. (d)-(f) The same as (a)-(c) except the individual is released at $x = 0.5$ at $t = 0$. Vertical lines indicate the edges of the sampling domain.

$t = 1$ was reduced. Compared with the marginal probability densities (dotted lines), the shape as well as the height of the joint probability densities are changed noticeably.

Figures 4.1c and 4.1f show the joint probability densities of the two individuals at $t = 3$ when the individuals were captured at neither $t = 1$ nor $t = 2$. Because the individuals were not captured in two previous sampling occasions, the degree of concavity in the middle of the joint probability densities are magnified. Comparison between the joint and marginal probability densities show how the shapes of the two probability densities depart from each other because of the sampling process.

For the infinite integrals in equations (4.11) and (4.13), we truncated the kernels at $x_{min} = -333$ and $x_{max} = 333$, renormalized them so that the kernels integrate to 1, and the equations were integrated over a domain $[-1000, 1000]$. This assumes that individuals can only travel the maximum distance of 333 in one time step. This truncation has almost no effect on the calculation because the probability of individual traveling beyond the distance 333 according to the Gaussian kernel ($\alpha = 1, \mu = 0$) is infinitesimally small.

Comparisons of the two individuals (compare Fig 4.1b and 4.1c with Fig 4.1e and 4.1f, respectively) demonstrate that the shape of the joint probability density function depends on where an individual was released. For example, if an individual was released near the edge of the sampling domain, it is more likely to leave the sampling domain than if it was released in the middle of the sampling domain before the next sampling occasion. These differences in probability influence the probability distribution of location of an individual at the subsequent sampling occasions. These results show that although the movements of the individuals are modeled with a memoryless process, the calculation of $s_t^{(i)}(\mathbf{x})$ depends on the past capture history sequences. This makes further simplification of the likelihood calculation difficult.

4.6 Bias of Parameter Estimates

We demonstrate performance of estimators using simulated data sets. We considered 7 scenarios that differed in kernel shapes, time-dependence of capture probability, and size of sampling domain; these scenarios are listed in Table 4.1. Under each scenario, we generated data and estimated parameters from the data. Each data set consisted of 100 individuals marked and released at the origin at $t = 0$ and resampled 4 subsequent sampling occasions using the sampling protocol M_1. This was repeated 50 times to obtain means and standard errors of the estimates.

Scenarios 1, 2, and 3 differ in their kernel shapes; they are Gaussian, Laplace, and Cauchy, respectively (Table 4.1). Here, we assume that movement of individuals is symmetric so that they are always centered at the location of the previous capture. We also assume that capture probability is constant over time. Under these scenarios, there are two parameters to be estimated: the scaling parameter for the kernel (α, β, or γ) and the capture probability within the sampling domain (u).

Table 4.1: Sampling and movement scenarios used to examine parameter estimation performance.

Scenario	Kernel	Capture Probability	Sampling Domain
Scenario 1	Gaussian ($\mu = 0$, $\alpha = 1.0$)	Constant (0.85)	[-1.5,1.5]
Scenario 2	Cauchy ($\mu = 0$, $\gamma = 1.0$)	Constant (0.85)	[-1.5,1.5]
Scenario 3	Laplace ($\mu = 0$, $\beta = 1.0$)	Constant (0.85)	[-1.5,1.5]
Scenario 4	Gaussian ($\mu = 0.2$, $\alpha = 1.0$)	Constant (0.85)	[-1.5,1.5]
Scenario 5	Gaussian ($\mu = 0$, $\alpha = 1.0$)	Time Varying (0.8, 0.5, 0.7, & 0.9)	[-1.5,1.5]
Scenario 6	Gaussian ($\mu = 0$, $\alpha = 1.0$)	Constant (0.75)	[-1.5,1.5]
Scenario 7	Gaussian ($\mu = 0$, $\alpha = 1.0$)	Constant (0.85)	[-1.0,1.0]

Under Scenario 4, the Gaussian kernel is nonsymmetric and shifted by μ. This shift is equivalent to an advection term in a simple diffusion-advection model. Under this scenario, there are three parameters (α, u, and μ) to be estimated.

Under Scenario 5, the simulated capture probability is varied at each sampling occasion. In actual mark-recapture studies, it is very difficult to maintain a constant level of sampling effort, and it is often even more difficult to keep the same sampling conditions over multiple sampling occasions. Therefore, the changes in capture probability among sampling occasions are often expected. Under this scenario, we have five parameters (α, u_1, u_2, u_3, and u_4) to be estimated.

Scenario 6 and 7 are the same as Scenario 1, but use lower capture probability and reduced sampling domain size, respectively.

For all kernel shapes, we truncated the kernels at $x_{min} = -300$ and $x_{max} = 333$, renormalized them so that the kernels integrate to 1, and the equations were integrated over a domain $[-1000, 1000]$ to calculate the infinite integrals in equations (4.11) and (4.13). This process slightly changed the heights of the kernels and makes the shape tighter in the middle for a kernel with fatter tails (e.g. the Cauchy kernel). We expect that this truncation of kernels causes small overestimations of the scale parameter and the capture probability.

Table 4.2 shows the result comparing true and estimated parameter values. Most of the estimates agree reasonably well with the true values. However, with such a small sample size (50 estimates for each model), some estimates deviate from the true values. In Scenario 2, β is underestimated, and in Scenarios 3 and 4, γ and α, respectively, are overestimated. In part, these small deviations can be attributed to errors associated with the truncation and the numerical integration of kernels. Furthermore, likelihood methods do not necessarily give unbiased estimates. In the next section, we will show how these deviations change when we make the incorrect assumptions that the sampling was done in a larger sampling domain than the actual size and that the shape of dispersal displacements were approximated by a Gaussian kernel when in fact come from a leptokurtic distribution.

4.7 Bias Caused by Assuming Large Sampling Domain

When analyzing mark-recapture data, one might be tempted to assume that (1) the kernel is approximately Normal and that (2) the sampling domain was large enough to include all individuals at all sampling occasions. If the first assumption were true, the integrodifference model would be a discrete-time equivalent of a simple diffusion model. If the second assumption were true (which is rarely the case) and sampling was done uniformly over the sampling domain, then the algorithm for calculating likelihood could be simplified because the shape of the joint probability function in Section 4.5 would remain the same regardless of where individuals were released and recaptured previously. When both assumptions are true, we can obtain the value of α that maximizes the likelihood, which is expressed using

Table 4.2: Comparison between true and estimated parameter values (sample size 50).

Scenario	Parameter	True Value	Estimated Value (SE)
Scenario 1	α	1.00	1.005 (0.010)
	u	0.85	0.850 (0.005)
Scenario 2	β	1.00	0.976 (0.015)
	u	0.85	0.833 (0.007)
Scenario 3	γ	1.00	1.075 (0.020)
	u	0.85	0.862 (0.008)
Scenario 4	α	1.00	1.037 (0.012)
	μ	0.2	0.193 (0.010)
	u	0.85	0.866 (0.006)
Scenario 5	α	1.00	0.993 (0.012)
	u_1	0.80	0.794 (0.008)
	u_2	0.50	0.505 (0.009)
	u_3	0.70	0.704 (0.010)
	u_4	0.90	0.886 (0.011)
Scenario 6	α	1.00	0.995 (0.012)
	u	0.75	0.743 (0.007)
Scenario 7	α	1.000	1.001 (0.022)
	u	0.85	0.843 (0.014)

the algorithm in Section 4.4, by

$$\widehat{\alpha} = \sqrt{\frac{1}{n}\sum_{i=1}^{n}\left(\frac{h_i^2}{v_i}\right)}, \tag{4.14}$$

where n is the number of observed dispersal distances, h_i is the length of the ith observed interval, and v_i is the time taken to travel that distance (see Appendix). The right side of equation (4.14) is a standard deviation of the length of the observed dispersal intervals in a unit time.

To demonstrate how falsely assuming a large sampling domain causes bias in the parameter estimation, we applied the equation 4.14 to the data generated under Scenarios 1, 5, 6 and 7 in the previous section.

Furthermore, when the true kernel was the Laplace or the Cauchy (Scenario 2 and 3, respectively), we applied the algorithm presented in Section 4.4 but inappropriately assumed a large sampling domain ($d = m$) to the data generated in the previous section.

In the results of these calculations, any deviations from the true vales in addition to the deviations found in the previous section are caused by the wrong assumption on the sampling domain size. The estimates from these calculations and the estimates in the previous section, which set the sampling domain sizes appropriately, are compared in Table 4.3.

Table 4.3: Comparisons of scale parameters (α, β, or γ) when appropriately setting the size of the sampling domain and when wrongly assuming that the sampling domain was large enough to include all individuals at all sampling occasions (sample size 50).

Scenario	True Value	Estimated Value (SE) using the kernel method	Estimated Value (SE) using equation (4.14)
Scenario 1	1.00	1.005 (0.010)	0.747 (0.004)
Scenario 2	1.00	0.976 (0.015)	0.566 (0.004)
Scenario 3	1.00	1.075 (0.020)	0.428 (0.004)
Scenario 5	1.00	0.993 (0.012)	0.728 (0.005)
Scenario 6	1.00	0.995 (0.012)	0.734 (0.005)
Scenario 7	1.00	1.001 (0.022)	0.561 (0.004)

Comparing the results under the false and correct assumptions, it is clear that if the sampling domain was falsely assumed to be large, the scaling parameters (α, β, and γ) are underestimated (Table 4.3). This results from the fact that any long-distance movements were not observed at all because they were actually outside of the sampling domain; however, they were assumed to be always observable under the false assumption. As expected, the bias increases as the size of the actual sampling domain is reduced from $d = 1.5$ in Scenario 1 to $d = 1.0$ in Scenario 7 because more individuals are located outside of the sampling domain when it is smaller.

Figures 4.2a, 4.3a, and 4.4a show the kernels based on the $5th$ largest and the $5th$ smallest of the 50 parameter values estimated in the previous section under Scenario 1, 2, and 3, respectively, along with the true kernel that was used to generate the data. In all three cases, the true kernel is within the upper and lower estimates. For the same scenarios, Figures 4.2b, 4.3b, and 4.4b show the kernels based on the $5th$ largest and the $5th$ smallest of the 50 estimated parameter values under the false assumption (large sampling domain size). These are compared with the true kernel. For all three scenarios, the estimated kernels are tighter than the true kernel.

These deviations from the true kernels are expected to be even more severe if the true kernel were the Laplace or the Cauchy but was assumed to be Gaussian. This is because more individuals are lost to unsampled tail regions when true kernels are leptokurtic, so analyses that assume they are observable produce bigger errors. To demonstrate this, we applied estimator (4.14) to the data generated under Scenario 2 (Laplace kernel) and under Scenario 3 (Cauchy kernel). In doing so, we are falsely assuming that the kernel was Gaussian as well as assuming that the sampling domain was large enough to include all individuals at all sampling occasions. Again, we plot the kernels based on the $5th$ largest and the $5th$ smallest parameter values along with the true kernel (Fig. 4.3c and 4.4c). In both cases, under the wrong assumptions, more individuals were falsely expected to be nearer to the center than the true distributions (Fig. 4.3c, and 4.4c).

These results suggests that it is important to record where sampling was conducted as

(a)

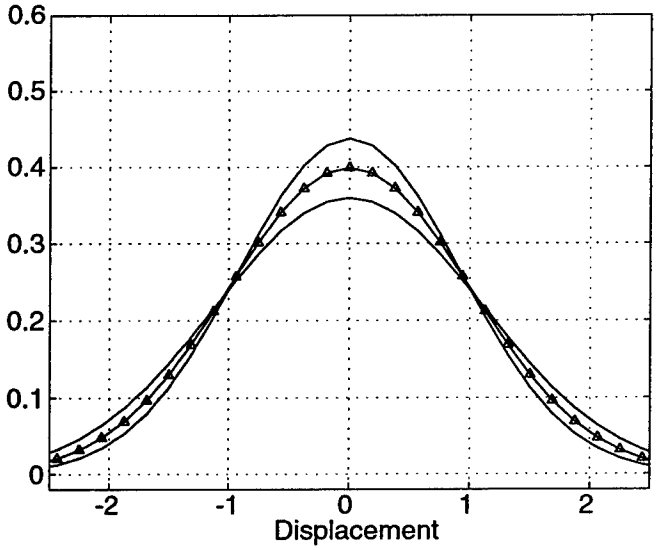

(b)

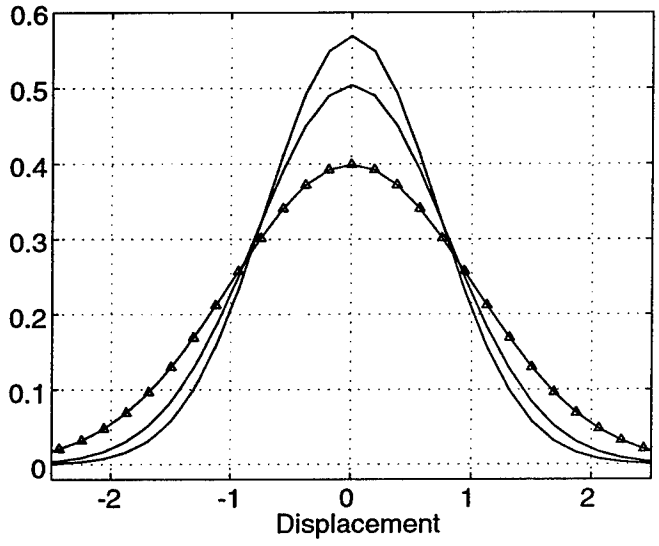

Figure 4.2: Kernels based on the $5th$ largest and the $5th$ smallest of the 50 estimated parameter values (solid lines) and the true kernel (Gaussian) used to generate the data (solid line with triangles). (a) Parameters estimated applying Gaussian kernel and the true sampling domain size (algorithm in Section 4.4). (b) Parameters estimated applying Gaussian kernel but assuming the sampling domain size was large enough to include all individuals at all sampling occasions (Equation 4.14). See the text in Section 4.6 for how data were generated.

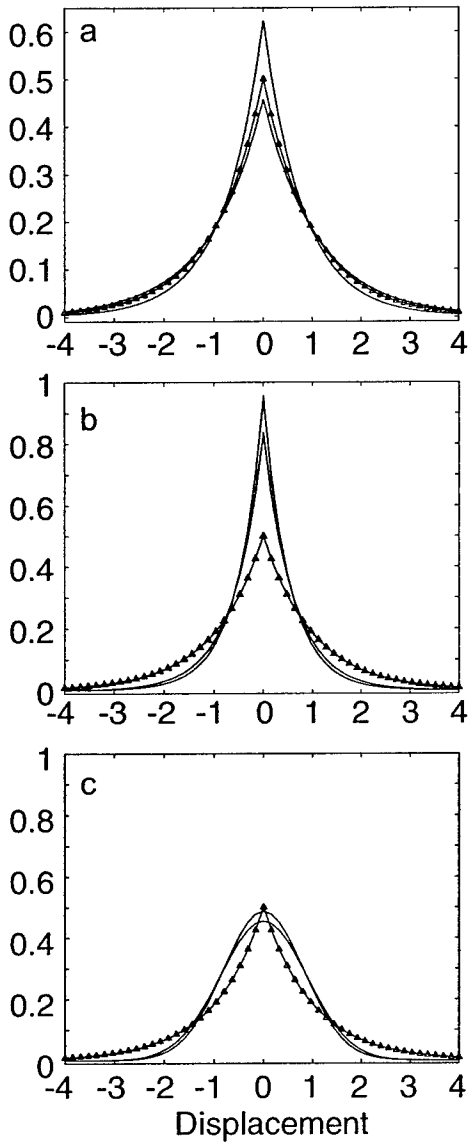

Figure 4.3: Kernels based on the $5th$ largest and the $5th$ smallest of the 50 estimated parameter values (solid lines) and the true kernel (Laplace) used to generate the data (solid line with triangles). (a) Parameters estimated applying Laplace kernel and using an appropriate sampling domain size (algorithm in Section 4.4). (b) Parameters estimated applying Laplace kernel but using a larger than actual sampling domain size ($d = m$ in the algorithm in Section 4.4). (c) Parameters estimated applying Gaussian kernel and assuming the sampling domain size was large enough to include all individuals at all sampling occasions (4.14). See the text in Section 4.6 for how data were generated.

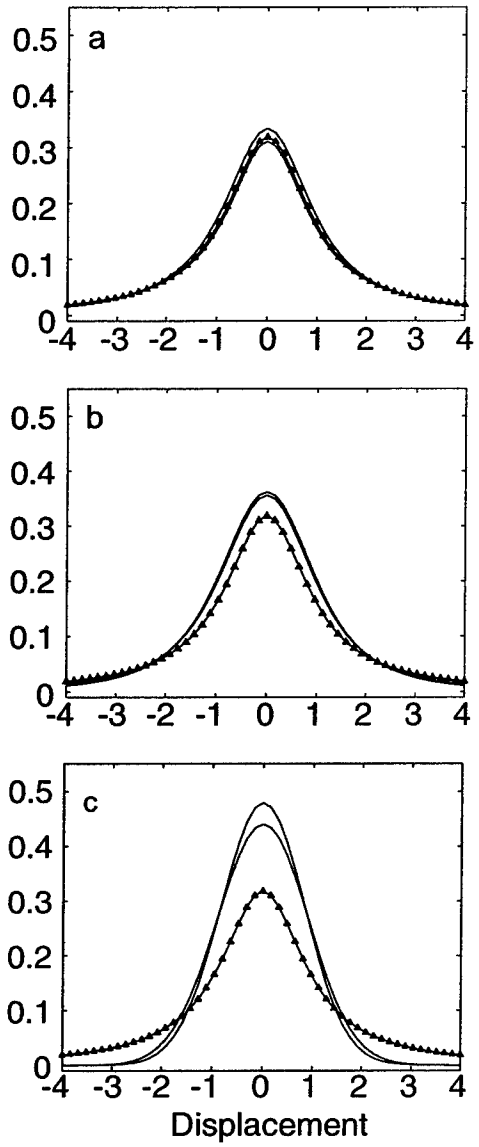

Figure 4.4: Kernels based on the $5th$ largest and the $5th$ smallest of the 50 estimated parameter values (solid lines) and the true kernel (Cauchy) used to generate the data (solid line with triangles). (a) Parameters estimated applying Cauchy kernel and using an appropriate sampling domain size (algorithm in Section 4.4). (b) Parameters estimated applying Cauchy kernel but using a larger than actual sampling domain size ($d = m$ in the algorithm in Section 4.4). (c) Parameters estimated applying Gaussian kernel and assuming the sampling domain size was large enough to include all individuals at all sampling occasions (4.14). See the text in Section 4.6 for how data were generated.

a part of the mark-recapture data and use the kernel that best approximates the true one.

4.8 Dispersal Kernel Selection Performance

When analyzing data, we often do not know the true shape of the kernel in advance. Thus we must fit several different kernels and try to select the one closest to the true kernel, a challenging task. Especially when different shapes of kernels result in different population dynamics, it is very important that we can select the best-fit kernel. Here, we evaluate the performance of Akaike's Information Criteria (AIC) (Akaike, 1973) as a tool for kernel selection.

We generated a data set using each of the three dispersal kernels, fitted the three dispersal kernels to the data set, and selected the best-fit kernel according to AIC. Each data set consisted of 100 individuals released at the origin at $t = 0$ and resampled at 3 subsequent occasions. This was repeated 20 times to obtain the probability of selecting the true model. The same process was repeated with different sampling domains (d) under the sampling protocol M_1. For each true kernel, we set the scaling parameter (α, β, or γ) equal to $\sqrt{2}$ and set the capture probability (u) to 0.85 within the sampling domain.

Figures 4.5, 4.6, and 4.7 show changes in the probability of selecting the true kernel shape with the size of sampling domain when the true kernel was Gaussian, Laplace, and Cauchy, respectively.

Associated error bars show the point-wise estimates of 95% confidence intervals. In each figure, we also show the size of the sampling domain that contains 50% of individuals at time $t = 1$ (left line) and at time $t = 3$ (right line). We call the two points reference points and compare the probabilities for the three kernels at these points.

As expected, the probability of selecting the true kernel shape increases as the sampling domain increases in all three cases. Comparisons among the three kernels reveal that when the true kernel was Cauchy, there is a high probability of selecting the true kernel even when the sampling domain is small (Figure 4.7). When the true kernel was Gaussian, the

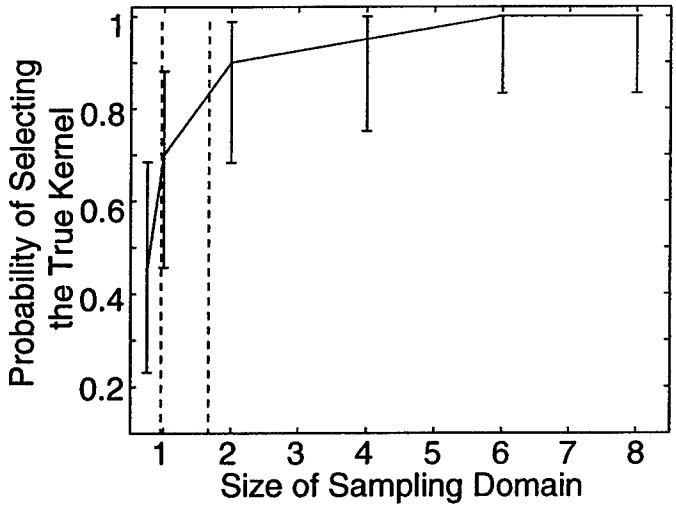

Figure 4.5: The probability of selecting the true kernel shape when the true kernel shape was Gaussian as the sampling domain is changed. Error bars indicate estimated point-wise 95% confidence intervals. Vertical lines on the left and right indicate the size of sampling domain where 50% of individuals are expected to be within the sampling domain at $t = 1$ and $t = 3$, respectively.

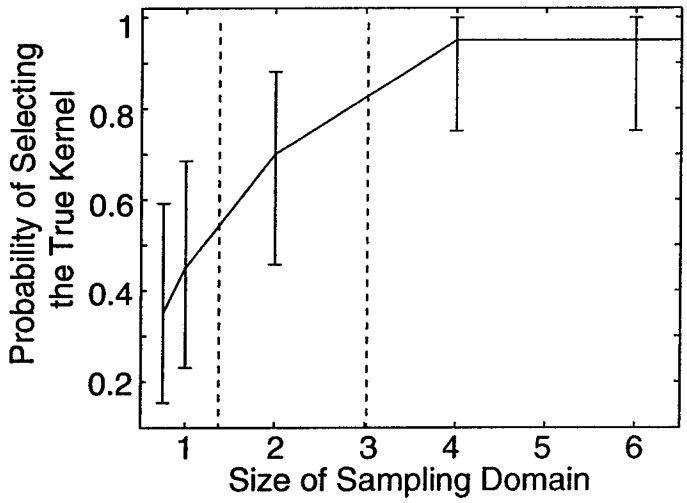

Figure 4.6: The probability of selecting the true kernel shape when the true kernel shape was Laplace as the sampling domain is changed. Error bars indicate estimated point-wise 95% confidence intervals. Vertical lines on the left and right indicate the size of sampling domain where 50% of individuals are expected to be within the sampling domain at $t = 1$ and $t = 3$, respectively.

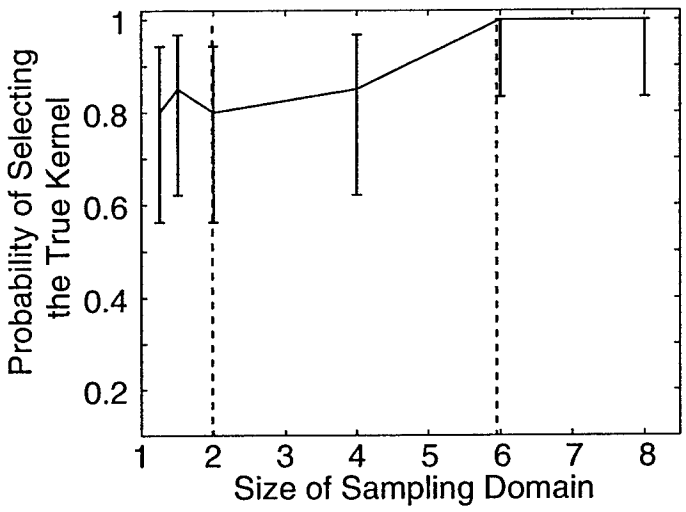

Figure 4.7: The probability of selecting the true kernel shape when the true kernel shape was Cauchy as the sampling domain is changed. Error bars indicate estimated point-wise 95% confidence intervals. Vertical lines on the left and right indicate the size of sampling domain where 50% of individuals are expected to be within the sampling domain at $t = 1$ and $t = 3$, respectively.

probability of selecting the true kernel is also relatively high at the two reference points. The probability of selecting the true kernel when it was actually Gaussian, declines rapidly to the left of the smaller reference point. We speculate that this rapid decline is due to the nonleptokurtic nature of the distribution. The middle part of the kernel tends to be flat and it may not contain much information about the shape of the kernel. When the true kernel was Laplace function, the probability of selecting the true kernel is the lowest (Figure 4.7). This result is consistent with the fact that the shape of the Laplace distribution is intermediate between Gaussian and Cauchy distributions in terms of their kurtosis.

When the true kernel was Cauchy and the true kernel was not selected, wrongly selected kernels tended to be Laplace kernel. Similarly, when the true kernel was Gaussian, wrongly selected kernel tended to be Laplace. However, when the true kernel was Laplace, both Cauchy and Gaussian kernels were selected wrongly. This result also suggests that selecting between Laplace and Cauchy or between Laplace and Gaussian is more difficult than selecting between Cauchy and Gaussian. If such model selection is important, one should

consider ways to improve the model selection performance. Two obvious ways to improve the performance are to increase sampling domain size and number of marked individuals.

Alternatively, we can fix the size of sampling domain and add small area of the intensive sampling within the domain to try to improve chances of selecting right kernel. We examined how the probability of selecting the true kernel changes as the size of intense sampling region is changed in M_2 sampling protocol (Fig. 4.8). We used the same Gaussian kernel as before ($\alpha = \sqrt{2}$ and $\mu = 0$) and the sampling domain $d = 0.75$. Without the intense sampling domain, there is only 0.45 probability of selecting the true kernel. However, adding a small intense sampling region $r = 0.1$ in Equation (eq:intense) increases this probability to 0.8. This suggests that intense sampling over a small part of the domain provides an alternative way of improving the model selection performance instead of simply increasing the sampling domain size or increasing the number of marked individuals.

Finally, we examined the performance of selecting the true kernel under the sampling protocol M_3, in which only outer region is sampled. This protocol may be used when trying to collect information on the shape of the tail regions of kernels. Under this protocol, there

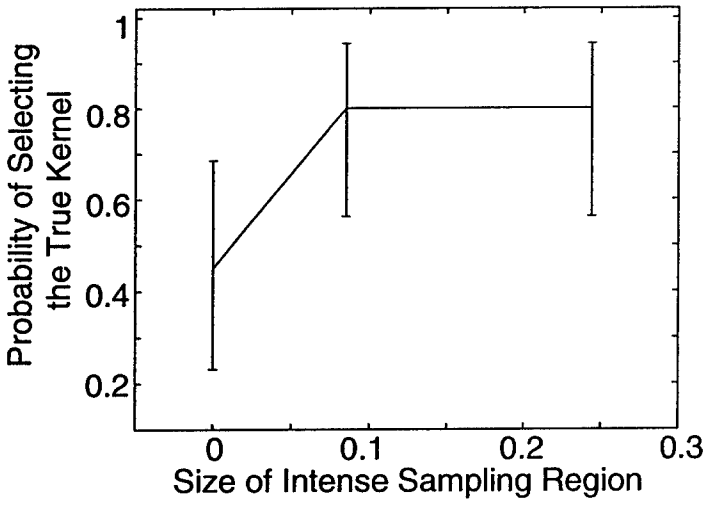

Figure 4.8: The probability of selecting the true kernel shape when the true kernel shape was Gaussian as the region of intense sampling was increased under sampling protocol M_2. Error bars indicate estimated point-wise 95% confidence intervals.

was high probability of selecting the true kernel. However, when the sampling region was reduced by increasing d in equation 4.6, very small number of individuals were recaptured. This was especially true when the kernel was Gaussian. As a result, it was very difficult for likelihood to converge in the numerical optimization even when applying the true kernel shape. This suggests that although the important part of the kernel in terms of ecological dynamics may be the distribution in the tail regions, it is also necessary to sample the center region to estimate kernels.

4.9 Extension of the Method

We have considered estimation and performance of selecting kernel shapes under different sampling protocols; however, the method is flexible enough to be used in other circumstances. Here, we discuss possible extensions of the method.

4.9.1 Kernel Shape

We used three kernel shapes (Gaussian, Laplace, and Cauchy) in this paper because of differences in their kurtosis. Other kernel shapes can be incorporated in the method, but there are exceptions. For example, a rectangular kernel cannot be incorporated in the method. The parameters in the rectangular kernel define the height of the kernel and the parameters of the capture probability function also define the height of the function. As a result, the parameters in the rectangular kernel and capture probability function become confounded. It should also be noted that the individual mark-recapture method permits estimation of scale parameters (α, β, and γ) and a shift parameter (μ), however, a shape parameter such as the one in the standard Student's t distribution appears to be unestimable. The estimated parameters, therefore, are conditional on the shape of kernel, and the model selection approach to select the best-fit kernel as presented in Section 4.8 becomes important.

In this paper, data in a one-dimensional space were considered. However, it is simple to

extend the method to data in a two-dimensional space. One way of doing so is to collapse a two-dimensional into a one-dimensional problem using a polar coordinate if the kernels are symmetric about their centers (see Shigesada & Kawasaki, 1997, for this approach in a simple diffusion model). Alternatively, we can fit two-dimensional kernels such as bivariate Gaussian and bivariate Cauchy distributions directly to the data.

4.9.2 Mortality

The method presented here assumes that there were very few deaths of marked individuals within the entire sampling period ($t = 0, \ldots, T$). This assumption is needed because deaths would add another reason for not capturing individuals. When there is mortality, survival probability will be multiplied to the dispersal kernel. The product is the kernel with a reduced height. A kernel with a similar height can also be produced by letting more individuals to travel outside of sampled region. As a result, kernel parameters become confounded with survival probability. The same problem is encountered in the discrete multi-stage mark-recapture method, in which individuals temporarily emigrate out of sampled region (Kendall et al., 1997; Kendall, 1999, Chapter 3). In the discrete case, some transition probability parameters are also confounded (see Chapter 3).

Under certain circumstances, however, parameters associated with survival probability can be estimated along with the dispersal kernel and capture probability. One such example is when the dispersal kernel has finite support and the sampling is conducted over the entire region within which individuals move. Then there is no temporary emigration, and survival probability can be estimated in addition to the parameters associated with the kernel. In this case, survival probability is given by the area under the kernel.

Alternatively one can collect data on two different time-scales (one on the scale of movement, and the other on the scale of the mortality process) to estimate parameters associated with both kernel and survival probability. Movement on the faster-time scale can be modeled assuming no mortality. The data on the slower time-scale can be modeled with dispersal kernel, survival probability, and capture probability. A single likelihood

associated with both sets of data can be used to estimate all the parameters. This method is similar to Pollock's robust design method (Pollock, 1982) in which no mortality was assumed in a short-time scale to estimate capture probability.

4.9.3 Sampling Design

In this paper, we considered only three different types of sampling protocols. However, there are many other possibilities. In Section 4.8, we demonstrated that even with a small sampling domain relative to the shape of the kernel, adding a small intense sampling region within the sampling domain (sampling protocol M_2) can improve model selection performance. For the protocol we considered , we added the intense sampling region in the middle of the sampling domain. However, the intense sampling region can be moved to other locations within the sampling domain. It is also possible to sample at many isolated small regions intensively or also possible to sample only toward the left (or right) half of the space. How the sampling effort should be allocated is an important question to ask before actual sampling and will likely vary from study to study. To answer such a question, different movement and sampling scenarios can be explored using simulated data sets as we demonstrated in this paper.

In actual sampling, it may not be possible to maintain a constant capture probability over the whole sampling domain. For example, vegetation coverage or topography of the ground may influence capturability of individuals. However, when such data as degree of vegetation coverage or index of topographic feature are available, they can be incorporated into the capture probability function as covariates using a function such as the logistic function

$$p_t(x_t) = \frac{\exp(\psi + \omega c(x_t))}{1 + \exp(\psi + \omega c(x_t))} \tag{4.15}$$

where ψ and ω are the intercept and slope parameters and $c(x_t)$ is the value of covariate at location x at time t. This ability to model the capture probability function is one strength of the individual mark-recapture method presented in this paper.

4.10 Discussion

The individual mark-recapture method presented here permits estimation of parameters associated with non-Gaussian as well as Gaussian kernels from individual mark-recapture data that are sampled in a finite sampling domain. We analyzed the performance of estimators and the model selection method using simulated data sets. Each data set consisted of only 100 marked individuals, but both the parameter estimators and the model selection worked reasonably well.

The method presented in this paper can be considered as a continuous-stage equivalent to a multi-stage (or multi-type) mark-recapture method (e.g. Nichols et al., 1992b, also Chapter 2). In the method presented in this paper, "stage" corresponds to the spatial location of the individual. There are several studies that attempt to quantify movements of individuals using a discrete-stage multi-stage mark-recapture method (e.g. Arnason, 1973; Hilborn, 1990; Hestbeck et al., 1991; Brownie et al., 1993). However, the discrete-space approach loses the detailed information on where individuals were located within the discrete patches. As shown in Section 4.5, it is very important information when estimating dispersal kernels accurately.

Other types of data are also collected to quantify movements of organisms. For example "seed shadow" data contain locations of seeds released from a single plant. From these data, non-Normal dispersal kernels (e.g. Werner, 1975; Carey & Watkinson, 1993) or invasion speed of the population (Clark et al., 2001a) can be estimated. The data are excellent when organisms have both dispersal and sessile stages and the source of seeds can be identified. Another type of data is mass mark-recapture data in which markings are not unique to each individual (e.g. Dobzhnsky & Wright, 1943; Taylor, 1978; Kareiva, 1983; Turchin & Thoeny, 1993). These data contain locations of captured individuals, but do not contain information on which individuals were captured. This type of data is excellent when large number of individuals can be marked and sampling process can be controlled to be constant over space and time. The individual mark-recapture method presented in this paper is an

addition to these existing ways for estimating dispersal kernel. We expect this method to be particularly useful to estimate kernels associated with animals that can potentially travel a long distance when only small numbers of them can be marked.

4.11 Appendix

We derive equation (4.14) from the likelihood function in Section 4.4. Here, we are assuming that movement is modeled with the Gaussian kernel without any shift ($\mu = 0$), capture probability is constant in time and space, and sampling is done over the entire universe.

First, we divide the capture history into segments when the individual was recaptured, and note that the probability density for the capture history sequence is a product of the probability densities for the segments. For example, suppose that an individual was marked and released at x_1 at time 1, recaptured the first time at x_3 at time 3, but never recaptured again when the sampling ended at time 5. This capture history is separated into two segments: one from time 1 to 3 and the other from time 3 to 5. The probability density for the second segment is conditional on the release at x_3 at time 3. Consequently, the product of the probability density for the first and second segments gives the probability density of the entire capture history sequence.

After separating the capture history sequences of individuals into segments, we classify the segments into two forms. In one form, individuals are released at x_t at time t and recaptured at x_{t+v} at time $t+v$ ($v = 1, 2, \ldots$) the first time since t, and in the other form, individuals are released at x_t at time t but never recaptured again. With these two forms, we can construct any capture history sequences. We derive general expressions for the probability density of these two types of the segments.

For the jth segment of the first form, we write down the probability density function for the location $X_{t+v} = y$ of an individual in which it was released at x_t at time t. If the individual was recaptured immediately after the release ($v = 1$),

$$s_{t+1}^{(j)}(y) = k_g(y - x_t)p \tag{4.16}$$

where

$$k_g(y - x_t) = \frac{1}{\alpha\sqrt{2\pi}} \exp\left[\frac{-(y - x_t)^2}{2\alpha^2}\right]. \tag{4.17}$$

Similarly, if the individual was recaptured the first time at $t + 2$ ($v = 2$),

$$\begin{aligned} s_{t+2}^{(j)}(y) &= \int_{-\infty}^{\infty} k_g(z - x_t)(1 - p)k_g(y - z)p dz \\ &= (1 - p)p \int_{-\infty}^{\infty} k_g(z - x_t)k_g(y - z)dz. \end{aligned} \tag{4.18}$$

$$\tag{4.19}$$

If the individual was recaptured the first time at $t + 3$ ($v = 3$),

$$\begin{aligned} s_{t+3}^{(j)}(y) &= \int_{-\infty}^{\infty}\int_{-\infty}^{\infty} k_g(z - x_t)(1 - p)k_g(w - z)dz(1 - p)k_g(y - w)p dw \\ &= (1 - p)^2 p \int_{-\infty}^{\infty}\int_{-\infty}^{\infty} k_g(z - x_t)k_g(w - z)dz k_g(y - w)dw. \end{aligned} \tag{4.20}$$

By inspection of the above equations, we obtain the general probability density function associated with the first form of the capture history segments as

$$s_{t+v}^{(j)}(y) = (1 - p)^{v-1} p f_v(y, x_t), \tag{4.21}$$

where $f_v(y, x_t)$ is the probability density function obtained by convolving the Gaussian kernel, which is centered at x_t, with $v - 1$ Gaussian kernels, which are centered at the origin, sequentially. By convolving two Gaussian kernels, we get the Gaussian kernel with its variance being the sum of the variances of the two convolved Gaussian kernels. Therefore, equation (4.21) becomes

$$s_{t+v}^{(j)}(y) = (1 - p)^{v-1} p \frac{1}{\sqrt{2\alpha^2 v\pi}} \exp\left[\frac{-(y - x_t)^2}{2\alpha^2 v}\right]. \tag{4.22}$$

Similarly for the second form of the capture history sequence, which ends without observing the individual, we write down the probability of not recapturing the individual i

that was released at x_t at time t:

$$s_T^{(i)} = (1-p)\int_{-\infty}^{\infty} f_1(z-x_t)dz \quad \text{for} \quad T-t=1, \tag{4.23}$$

$$s_T^{(i)} = (1-p)^2\int_{-\infty}^{\infty} f_2(z,x_t)dz \quad \text{for} \quad T-t=2, \tag{4.24}$$

$$s_T^{(i)} = (1-p)^3\int_{-\infty}^{\infty} f_3(z,x_t)dz \quad \text{for} \quad T-t=3, \tag{4.25}$$

$$\vdots$$

where T is the time of the last sampling occasion. The integrals in equations (4.23)-(4.25) are 1 because integrands are probability density functions. Thus, we obtain the general equation for the probability as

$$s_T^{(j)} = (1-p)^{T-t}. \tag{4.26}$$

The likelihood in Section 4.4 (Equations 4.12 and 4.13) can be expressed as a product of equations (4.22) and (4.26). In both equations(4.22) and (4.26), the capture probability (p) can be factored from the dispersal kernels because the capture probability is independent of location. Therefore, the likelihood can be expressed by a product of two terms each consisting of only dispersal kernel or only capture probability. Consequently, we can maximize the terms for capture probability and dispersal kernel the likelihood separately to find the maximum likelihood estimates of the parameters. In other words, capture probability does not affect the parameters associated with kernels in the estimation. Since we are only interested in estimating the parameter associated with the dispersal kernel, we can ignore the capture probability part. Furthermore, equation (4.26) contains only the capture probabilities. Thus the part of the likelihood that we are interested is just a product of equations (4.22) each expressed for observed dispersal intervals. We denote this special likelihood as ℓ_{sp}. After collecting terms in ℓ_{sp}, we obtain

$$\ell_{sp} = \frac{1}{\sqrt{2\alpha^2\pi\prod_{j=1}^{n}(v_j)}}\exp\left[\frac{-1}{s\alpha^2}\sum_{j=1}^{n}\frac{h_j^2}{v_j}\right], \tag{4.27}$$

where n is the number of observed dispersal intervals, h_j is the length of the jth observed interval, and v_j is the time taken to travel that distance.

Taking the derivative of equation (4.27) with respect to the parameter α, setting the derivative equal to zero, and solving for α results in equation (4.14).

Chapter 5

Demography of the endangered North Atlantic right whale

Fujiwara, M. and Caswell, H. (2001)[1] Demography of the endangered North Atlantic right whale. *Nature* **414**(29): 537-541.

[1]Reprinted with permission of Nature Publishing Group. Any right to copy and/or distribute this chapter when not incorporated in this thesis shall require further permission of Nature Publishing Group.

Demography of the endangered North Atlantic right whale

Masami Fujiwara & Hal Caswell

Biology Department, MS34, Woods Hole Oceanographic Institution, Woods Hole, Massachusetts, USA

Northern right whales (*Eubalaena glacialis*) were formerly abundant in the northwestern Atlantic, but by 1900 they had been hunted to near extinction. After the end of commercial whaling the population was thought to be recovering slowly; however, evidence indicates that it has been declining since about 1990 (ref. 1). There are now fewer than 300 individuals, and the species may already be functionally extinct[2,3] owing to demographic stochasticity or the difficulty of females locating mates in the vast Atlantic Ocean (Allee effect[4]). Using a data set containing over 10,000 sightings of photographically identified individuals we estimated trends in right whale demographic parameters since 1980. Here we construct, using these estimates, matrix population models allowing us to analyse the causes of right whale imperilment. Mortality has increased, especially among mother whales, causing declines in population growth rate, life expectancy and the mean lifetime number of reproductive events between the period 1980–1995. Increased mortality of mother whales can explain the declining population size, suggesting that the population is not doomed to extinction as a result of the Allee effect. An analysis of extinction time shows that demographic stochasticity has only a small effect, but preventing the deaths of only two female right whales per year would increase the population growth rate to replacement level.

Conservation biology uses population models to assess population performance, to diagnose the causes of poor performance, to prescribe management interventions, and to make prognoses of population viability (see chapter 18 of ref. 5). We have developed a stage-structured matrix population model[5–7] that addresses all four of these tasks. This matrix model uses the life cycle shown in Fig. 1 (a similar model has been successfully applied to a killer whale population[8]). The parameters in the matrix model were defined by a series of statistical models, the parameters of which were estimated by applying stage-structured mark–recapture analysis[5,9,10] to photographic identification data collected by the New England Aquarium (NEA)[11]. The best model was selected using Akaike Information Criteria (AIC)[12–14] (see Methods).

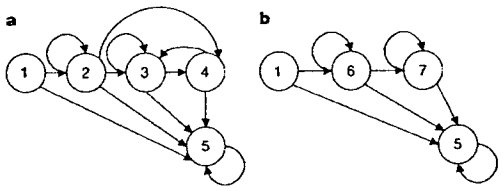

Figure 1 Life cycle graphs of female (**a**) and male (**b**) right whales. Numbers represent different stages: 1, calf; 2, immature female; 3, mature female; 4, mature females with newborn calves (mothers); 5, dead; 6, immature male; 7, mature male. Each arrow represents a possible transition in stage from one year to the next; the arrows going to stage 5 represent stage-specific mortalities. A calf is an individual that was sighted along with its mother. An immature is an individual known to be less than 9 years old. Mature individuals are known to be at least 9 years old, or in the case of females, have been sighted previously with a calf. Mothers are females that are sighted with a newborn offspring. If the sex of an individual is unknown, we assume it has an equal chance of being either female or male, as our data contain almost equal numbers of individuals (141 and 143) known to be female and male, respectively. Maturity status (whether an individual is immature or mature) is unknown in 22% of sightings. When maturity status was unknown, we estimated the probability that the individual was immature (0.30 for males, 0.87 for females) using the method described in ref. 10. These probabilities were used in stage-assignment matrices[10] for likelihood calculations.

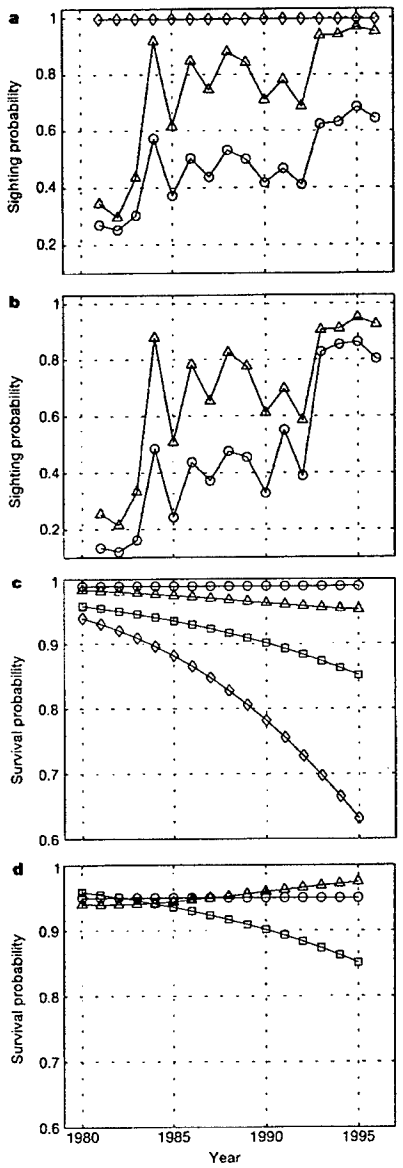

Figure 2 Stage-specific sighting and survival probabilities for males and females. **a**, **b**, Stage-specific sighting probabilities of the best model (M_2) for females (**a**) and males (**b**). **c**, **d**, Stage-specific survival probabilities (M_2) for females (**c**) and males (**d**). Squares, calf; triangles, immature; circles, mature; diamonds, mothers.

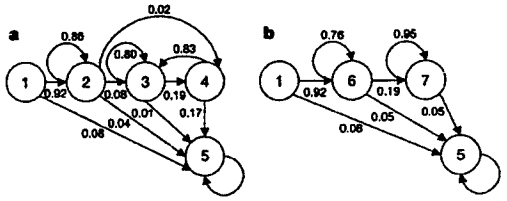

Figure 3 Constant transition probabilities estimated using the best sighting model (M_t). Life cycle graphs of female (a) and male (b) right whales. The numbers in the circles are the same as in Fig. 1.

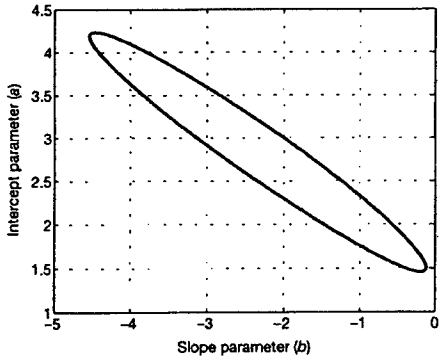

Figure 4 Joint 95% profile likelihood confidence region for the logistic parameters of survival probability of mothers.

In the resulting model, the sighting probability of most stages depends on both northern and southern effort levels (Fig. 2a, b; see Methods for definition). This is consistent with a previous study[1], which found a significant correlation between total effort and sighting probability in a simpler model that did not distinguish sex or stages. In contrast to other stages, mothers have a consistently high sighting probability (Fig. 2a). This suggests that they are easier to sight than other stages, and that the survey effort in the two regions has been sufficient to detect almost all births with high probability.

Using the best sighting probability model, we estimated two transition models. One model assumed time-invariant transition probabilities (M_1) and the other was the best time-varying model according to the AIC criterion (M_2). The time-invariant model (M_1, $b_{ji} = 0$ for all j and i in equation (2)) gives a weighted, time-averaged picture of transition probabilities. In this model, survival probability is low for calves, higher for immature and mature females and much lower for mothers (Fig. 3). According to the best time-varying model (M_2), the transition probabilities of mature females and males have been constant, whereas the other stages have transition probabilities that change with time. The survival probability of mothers shows the most pronounced decline over time (Fig. 2c, d). This trend is statistically significant, as the slope parameter (b_{34}) in the polychotomous logistic function (equation (2)) is significantly below 0 (Fig. 4).

A series of population projection matrices, A_t, was constructed by augmenting the female transition probability matrix with elements describing reproduction[10] (see Methods). These matrices were used to calculate population growth rate, life expectancy and expected lifetime number of reproductive events experienced by a female.

The asymptotic population growth rate (λ) is given by the dominant eigenvalue of the population projection matrix. When $\lambda > 1$, the population is asymptotically growing; when $\lambda < 1$, the population is asymptotically declining. Therefore, λ is an important indicator of the status of a population. If we assume all demographic parameters have been constant from 1980 to 1995 (M_1), we find that $\lambda = 1.01$ (95% confidence interval = [1.00, 1.02]; the confidence interval was estimated using the estimated covariance of parameters by taking the inverse of the Hessian matrix[10]), suggesting a population increase of 1% per year, on average, between 1980 and 1995. However, time-specific asymptotic growth rates (λ_t)—calculated from the time-varying matrices A_t using model M_2—declined from $\lambda_{1980} = 1.03$ to $\lambda_{1995} = 0.98$ (Fig. 5c). Population growth rate declined below 1 at around 1992. If the 1995 population growth rate were maintained, the population would go extinct.

The decline in λ_t is the net result of all the changes in the vital rates (a collective term for transition, survival, fertility and mortality rates). We determined how much the decline in each vital rate contributed to the decline in λ_t using a life table response experiment (LTRE) analysis[5,9]. This analysis decomposes the changes in λ_t into contributions from each entry in A_t. Figure 5d shows the sum of the contributions of all matrix entries involving each stage. The results of this analysis show that the decline in λ_t is caused mainly by the decline in the survival probability of mothers (Fig. 5d).

The life expectancy at birth is the mean age at which individuals born in a given year would die if conditions of that year were maintained. It can be calculated by treating the transition matrix as an absorbing Markov chain and calculating the mean time to absorption (that is, death)[5]. During the early 1980s, the life expectancy of females was twice that of males (Fig. 5a). This may be typical of large cetaceans. (Killer whales (*Orcinus orca*), for example, exhibit a similar difference in life expectancy between females and males[15].) Female life expectancy has declined from about 51.8 years in 1980 to about 14.5 years in 1995. Until recently, life expectancy of females has exceeded that of males, but that is no longer true owing to the reduced survival probability of females.

The expected number of reproductive events during a female's lifetime[5] has declined from about 5.27 in 1980 to about 1.26 in 1995 (Fig. 5b). A mature female could once expect to reproduce 6.48 times; that number is now about 1.80.

The growth rate projections in Fig. 5c are deterministic. The right whale population is small, however, and the population of any single stage is even smaller. Because of this, it has been suggested that population projections should include demographic stochasticity (chance fluctuations due to the random fates of a small number of individuals; see ref. 5). To evaluate the effect of demographic stochasticity, we transformed the matrix A_{1995} into a multitype branching process[5], and calculated the probability distribution of times to extinction (Fig. 6). We compared this distribution with the deterministic prediction obtained by using A_{1995} and defining extinction as the time when total population size reached 1 individual. For both calculations, we used an initial condition of 150 females distributed according to the stable stage distribution. This simulates the hypothetical situation in which the vital rates of 1995 remain constant and neither environmental trends nor environmental fluctuations affect them.

The mean time to extinction under demographic stochasticity is 208 years (similar to the estimate of 191 years in ref. 1). The deterministic time to extinction is 245 years. Thus demographic stochasticity reduces expected extinction time by 15%. Figure 6 gives the complete distribution of extinction times; there is a 5% chance of extinction within 130 years and a 25% chance of extinction within 165 years. These calculations exclude other factors such as continued declining survival trends, environmental stochasticity and Allee effects, all of which would hasten extinction. Thus the expected time of 208 years should be considered an upper bound.

Right whale conservation efforts are directed towards reducing mortality due to entanglement and ship collisions. Because the

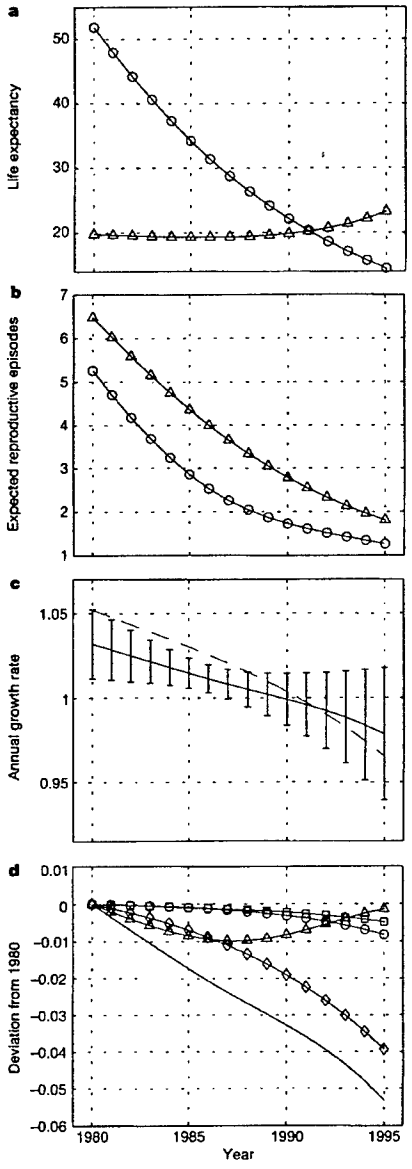

Figure 5 Demographic parameters calculated from the time-varying matrices A_t. **a**, The mean life expectancy at birth for males (triangles) and females (circles). **b**, The mean number of lifetime reproductive episodes, estimated from birth (circles) and from maturity (triangles). **c**, Asymptotic population growth rates λ_t (solid line) calculated from the population projection matrices A_t produced by the best model (M_2) and from the unstructured model of ref. 1 (dotted line). The error bars were standard errors, which were calculated using the series approximation to the variance of λ and the covariance matrix obtained from the information matrix. **d**, The result of a LTRE decomposition analysis for the trend in λ. The demographic rates in 1980 are used as the reference matrix, and the contributions of all matrix entries involving each stage were summed. The solid line shows the actual trend in λ, measured as a deviation from the value in 1980. It is closely approximated by the sum of all the other lines. Squares, calf; triangles, immature; circles, mature; diamonds, mothers.

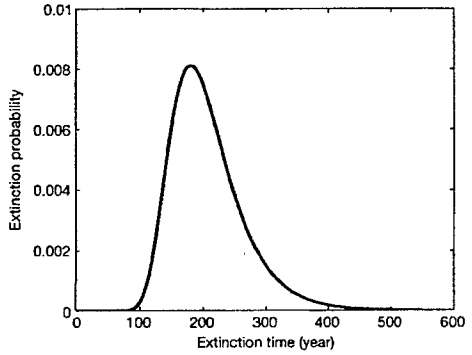

Figure 6 The probability distribution of time to extinction assuming demographic stochasticity. The distribution was calculated from a multi-type branching process, treating transitions and reproduction as independent events (multinomial and Bernoulli, respectively; see ref. 5).

population is so small, a single death represents a significant mortality rate. Conversely, significant reduction in mortality rate can be obtained by preventing just a few deaths. Figure 7 shows the effect on λ of preventing female deaths, using the vital rates of 1995 and assuming a starting population of 150 females distributed according to the stable stage distribution. The results indicate that prevention of just two female deaths every year would suffice to increase λ to 1. This gives a sense of the magnitude of the initial management action needed for the protection of the population. However, as population size increases owing to successful management, more deaths will have to be prevented to maintain a positive population growth rate because the number of deaths that translates into a given mortality rate also increases with the population size.

The causes behind the decline in survival probability of mothers are still unknown; however, collisions with ships, entanglement with fishing gear and changes in food availability due to climate fluctuations are suspected to contribute towards mortality[16,17]. Although right whales are distributed from the coast of northern Florida to the Bay of Fundy, it is primarily females and calves that are sighted in the calving ground off the coast of Florida and Georgia[18]. The calving ground is close to shipping lanes where large vessel traffic has increased since 1980 (ref. 19). More than 60% of North Atlantic right whales have scars from entanglement in fishing gear such as lobster pots and sink gillnets[17]. We have found a significant rank correlation between crude survival probability[1] (the survival probability of individuals without distinguishing stage differences) and North Atlantic Oscillation index (NAO), which is often used as an index for climate fluctuations[20]. Studies that focus on the effects of these three factors are urgently needed.

This study combines multi-stage mark–recapture methods and matrix population model analyses. Both methods incorporate differences in vital rates that are experienced by different stages within a population. Multi-stage mark–recapture analysis also incorporates stage-specific heterogeneity in sighting probability within the population. We succeeded in identifying a life cycle stage that is experiencing reduced survival probability, and were able to use the model to document the implications of that reduced survival probability for population growth.

Like any mark–recapture analysis, ours can be influenced by heterogeneity in sighting probability among individuals within a stage. If the sighting probability of mature females (stage 3) was heterogeneous, the survival probability of mothers towards the end of the study period would be underestimated. However, heterogeneity in sampling alone cannot explain the observed decline in the

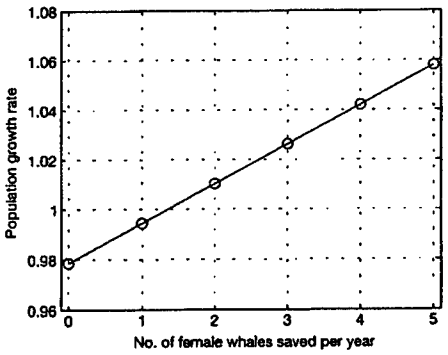

Figure 7 The predicted population growth rate that would result from preventing deaths of females regardless of their stage.

survival probability. Furthermore, during the winter of 1996, an unusually large number of confirmed mortalities were reported in the southeast United States, which is the only known calving ground[17]. This evidence suggests that the declining trend in the survival of mothers is both real and a great concern.

The North Atlantic right whale is currently seriously endangered owing to declining survival probability, especially among mothers. This finding, together with the unprecedented calf production in the spring of 2001 (ref. 21), suggests that Allee effects are not yet limiting this population. Our analysis also shows that the population was experiencing a positive growth rate in the early 1980s (Fig. 5c). This implies that it is not necessary to return the vital rates to those of the pre-whaling period to obtain a positive growth rate. There is every reason to hope that prompt management intervention can improve survival enough to permit the recovery of the North Atlantic right whale. □

Methods

Photographic identification data

Since 1980, the NEA has accumulated photographs of approximately 350 right whales taken on more than 10,000 sighting occasions. Individual right whales can be recognized by natural markings such as scars and callosity patterns. On the basis of these identifications the NEA has constructed a database of individual sighting histories, which consist of information on whether or not each individual was sighted at least once in each year. These data can be treated as if individuals were marked on the occasion of their first identifications, and recaptured at subsequent sightings. We used the data from 1980 to 1996, which were complete at the beginning of this analysis.

Statistical models

Sighting probabilities of each stage and transition probabilities among stages were estimated by fitting a series of statistical models to the sighting history data by maximum likelihood. The statistical models describe sighting probability as a function of sampling effort in two regions. The northern effort level is measured by the total annual survey days in Massachusetts Bay, Great South Channel, Bay of Fundy, and in Brown's Bank; the southern effort level is measured by the total annual survey days off the coast of Florida and Georgia. The dependence of sighting probability on the northern effort, the southern effort, both efforts, or neither effort was modelled with binary logistic functions. Let $s_i(t)$ be the sighting probability of stage i at time t. Then

$$s_i(t) = \frac{\exp(x_i + y_i e_{1,t} + z_i e_{2,t})}{1 + \exp(x_i + y_i e_{1,t} + z_i e_{2,t})} \quad (1)$$

where x_i is an intercept parameter, and y_i and z_i are slope parameters associated with northern ($e_{1,t}$) and southern ($e_{2,t}$) effort levels, respectively.

We modelled the transition probabilities of each stage as polychotomous logistic functions of time[10,22]. Let $p_{ij}(t)$ be the transition probability from stage i at time t to j at time $t+1$. Then

$$p_{ij}(t) = \frac{\exp(a_{ij} + b_{ij}t)}{1 + \sum_{-1} \exp(a_{ij} + b_{ij}t)} \quad (2)$$

where a_{ij} and b_{ij} are intercept and slope parameters, respectively. When all the slope parameters are set to zero, the transition probabilities are time-invariant.

Model selection

Model selection was done in the following sequence. First, 1,024 sighting models were created by including all possible combinations of effort levels for all possible combinations of stages (equation (1)). These models were combined with the transition model in equation (2) in which all probabilities are functions of time. We selected the best of these models using AIC[12]. The AIC difference between the best and the second-best sighting models was about 2, indicating that the support for the best model relative to the second best model is high[14]. Therefore, we used only the best model. Because sighting probabilities of immature males and females did not differ significantly, by a likelihood ratio test, they were set equal. Using the resulting model for sighting, we selected the best time-varying transition matrix from all 64 models created by allowing the transition probabilities of all possible combination of stages to depend on time according to equation (2). The four best transition models had AIC differences from the best model of less than 2, indicating that the data provide some support for all these models. All of these models, however, had time-dependent survival probability of mothers.

Projection matrix

The projection matrix is

$$A_t = \begin{pmatrix} 0 & F_2 & F_3 & 0 \\ p_{21}(t) & p_{22}(t) & 0 & 0 \\ 0 & p_{32}(t) & p_{33}(t) & p_{34}(t) \\ 0 & p_{42}(t) & p_{43}(t) & 0 \end{pmatrix} \quad (3)$$

where

$$F_2 = 0.5p_{21}(t)p_{44}^{0.5}(t+1) \quad (4)$$

and

$$F_3 = 0.5p_{43}(t)p_{44}^{0.5}(t+1) \quad (5)$$

The first row of A_t describes reproduction; the other entries are transition probabilities. Consider F_2. When a female moves from stage 2 to stage 4 (with probability $p_{42}(t)$), she gives birth; the newborn calf is female with probability 0.5. Although newborn calves have distinct markings, they are harder to distinguish individually than other stages. Therefore, calf survival is estimated from the point where the calf is seen sufficiently well to permit identification, which is not necessarily on its first sighting. To appear as a calf in stage 1 at $t+1$, the newborn calf must survive long enough to be catalogued. We assume calves are catalogued on average midway through their first year, and that the mother must survive this long (with probability $p_{44}^{0.5}(t+1)$) in order for the calf to survive. F_3 is similar.

Received 18 May; accepted 21 September 2001.

1. Caswell, H., Fujiwara, M. & Brault, S. Declining survival probability threatens the North Atlantic right whale. *Proc. Natl Acad. Sci. USA* 96, 3308–3313 (1999).
2. Knowlton, A. R., Kraus, S. D. & Kenney, R. D. Reproduction in North Atlantic right whales (*Eubalaena glacialis*). *Can. J. Zool.* 72, 1297–1305 (1994).
3. Gerber, L. R., DeMaster, D. P. & Roberts, S. P. Measuring success in conservation. *Am. Sci.* 88, 316–324 (2000).
4. Allee, W. C. *Animal Aggregations* (Univ. Chicago Press, Chicago, 1931).
5. Caswell, H. *Matrix Population Models: Construction, Analysis and Interpretation* 2nd edn (Sinauer Associates, Sunderland, Massachusetts, 2001).
6. Caswell, H. *Matrix Population Models* (Sinauer Associates, Sunderland, Massachusetts, 1989).
7. Tuljapurkar, S. & Caswell, H. *Structured-population Models in Marine, Terrestrial, and Freshwater Systems* (Chapman & Hall, New York, 1997).
8. Brault, S. & Caswell, H. Pod-specific demography of killer whales (*Orcinus orca*). *Ecology* 74, 1444–1454 (1993).
9. Nichols, J. D., Sauer, J. R., Pollock, K. H. & Hestbeck, J. B. Estimating transition probabilities for stage-based population projection matrices using capture-recapture data. *Ecology* 73, 306–312 (1992).
10. Fujiwara, M. & Caswell, H. Estimating population projection matrices from multi-stage mark-recapture data. *Ecology* (in the press).
11. Crone, M. J. & Kraus, S. D. *Right Whale (Eubalaena glacialis) in the Western North Atlantic: a Catalog of Identified Individuals* (New England Aquarium, Boston, Massachusetts, 1990).
12. Akaike, H. in *International Symposium on Information Theory* 2nd edn (eds Petran, B. N. & Csaki, F.) 267–281 (Akademiai Kiado, Budapest, 1973).
13. Lebreton, J.-D., Burnham, K. P., Clobert, J. & Anderson, D. R. Modeling survival and testing biological hypotheses using marked animals: a unified approach with case studies. *Ecol. Monogr.* 62, 67–118 (1992).
14. Burnham, K. P. & Anderson, D. R. *Model Selection and Inference: a Practical Information-theoretic Approach* (Springer, New York, 1998).
15. Olesiuk, P. F., Bigg, M. A. & Ellis, G. M. in *Individual Recognition of Cetaceans: Use of Photo-identification and Other Techniques to Estimate Population Parameters* (eds Hammond, P. S., Mizroch, S. A. & Donovan, G. P.) 209–243 (Rep. Int. Whaling Comm. Special Issue 12, Cambridge, 1990).
16. Kraus, S. D. Rates and potential causes of mortality in North Atlantic right whales (*Eubalaena glacialis*). *Mar. Mamm. Sci.* 6, 278–291 (1990).
17. Waring, G. T. *et al. U.S. Atlantic and Gulf of Mexico Marine Mammal Stock Assessments—1999*. NOAA Technical Memorandum NMFS-NE-153 (Northeast Fisheries Science Center, Woods Hole, Massachusetts, 1999).

18. Kraus, S. D., Prescott, J. H., Knowlton, A. R. & Stone, G. S. in *Right Whale: Past and Present Status* (eds Brownell, R. L. Jr, Best, P. B. & Prescott, J. H.) 145–151 (Rep. Int. Whaling Comm. Special Issue 10, Cambridge, 1986).
19. Knowlton, A. R. in *Shipping/Right Whale Workshop* (eds Knowlton, A. R., Kraus, S. D., Meck, D. F. & Mooney-Seus, M. L.) 31–36 (New England Aquarium Aquatic Forum Series Report 97-3, Massachusetts, 1997).
20. Planque, B. & Reid, P. C. Predicting *Calanus finmarchicus* abundance from a climatic signal. *J. Mar. Biol. Ass. UK* **78**, 1015–1018 (1998).
21. Holden, C. Whale baby boomlet. *Science* **291**, 429 (2001).
22. Hosmer, D. W. & Lemeshow, D. *Applied Logistic Regression* (Wiley, New York, 1989).

Acknowledgements

We thank S. Kraus, A. Knowlton, P. Hamilton and the NEA for data. We also thank S. Brault, M. Hill, P. Kareiva, J.-D. Lebreton, M. Neubert, J. Nichols and the participants of the first Woods Hole Workshop on the Demography of Marine Mammals for discussions and suggestions. This project was funded by the Woods Hole Oceanographic Institution Sea Grant Program, the Rinehart Coastal Research Center, the David and Lucile Packard Foundation and The Robert W. Morse Chair.

Correspondence and requests for materials should be addressed to M.F. (e-mail: mfujiwara@whoi.edu).

Chapter 6

Stage-structured demographic analysis of North Atlantic right whale: Effects of environmental and demographic stochasticity on population viability

6.1 Introduction

North Atlantic right whales (*Eubalaena glacialis*) are one of the most endangered mammal populations in the world. By the beginning of the $20th$ century, the population in the western Atlantic had been hunted to near extinction. Despite more than a half century of international protection, no clear sign of their recovery has been detected. This population currently consists of fewer than 300 individuals, and there is evidence to suggest that this number is slowly shrinking because of declining survival probability (Caswell et al., 1999, also Chapter 5). A previous study (Chapter 5) has shown that this reduction in survival is primarily a result of an increase in the mortality of females during the year after giving birth. The same study has also concluded that if the environmental conditions experienced by this population in 1995 were maintained in future years, the population would be expected to go extinct in about 200 years. The survival of this population depends on prompt and effective conservation efforts based on our understanding of the population.

Results of any demographic analysis has inherent uncertainties because a population is affected by many factors; the North Atlantic right whales are not an exception. For example, demographic stochasticity can reduce the time to extinction (Caswell, 2001). The results in Chapter 5 and Pershing & Greene (2002) showed that the estimated survival probability and reproductive rate, respectively, are significantly correlated with an index for climate pattern in the North Atlantic (the North Atlantic Oscillation index), suggesting that the environmental forcing is also affecting the population. In this paper, we present the results of a demographic analysis of the North Atlantic right whale that analyzes effects of demographic stochasticity and environmental stochasticity on population viability.

Another uncertainty inherent in demographic analyses are the uncertainties in parameter estimation and model selection. In this paper, we will assess the parameter estimation uncertainty using a parametric bootstrap method. We also apply the Akaike Information Criteria (AIC) to select the best-fit models from multiple candidate models. This method takes into account model selection uncertainty.

6.2 Method

6.2.1 Matrix Population Model for the North Atlantic right whales

Our analysis uses a stage-structured matrix population model (e.g. Caswell, 2001). This model takes into account the differences in vital rates among life stages. The model in a general form is expressed as

$$n(t+1) = \mathbf{A}^{(t)} n(t) \tag{6.1}$$

where $n(t)$ is a vector containing the number of individuals at year t, and $\mathbf{A}^{(t)}$ is a matrix that projects the number of individuals in each stage from year t to $t+1$. The entries in $\mathbf{A}^{(t)}$ are determined by a life cycle structure of a population of interest.

For the North Atlantic right whales, we developed a life cycle structure based on available information on their life history Figure 6.1. In the figure, the numbers indicate stages, solid arrows indicate possible transitions that an individual can make from one year to the next

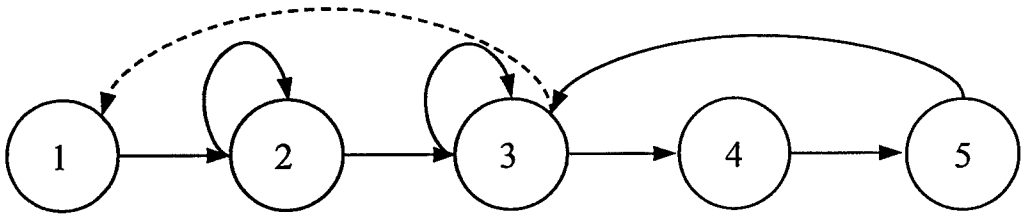

Figure 6.1: Life cycle graph of the North Atlantic right whales: 1: calves, 2: immature females, 3: mature females, 4: mothers, 5: mature females during a year after the mother stage

if it survives, and the dashed arrow represents reproduction of offspring by mature females (i.e. fertility). Each of the solid arrows has an associated transition probability $\phi_{ij}^{(t)}$, which gives the probability that an individual in stage j in year t is in stage i in the following year. This stage structure is slightly different from the one in Chapter 5. In the new stage structure, females have an extra stage after giving birth (stage 5) during which they cannot reproduce again. This reflects the fact that individual right whales rarely give birth within two years after a successful reproduction.

Based on the stage structure in Figure 6.1, we wrote down a projection matrix for the North Atlantic right whales:

$$\mathbf{A}^{(t)} = \begin{pmatrix} 0 & 0 & F_3^{(t)} & 0 & 0 \\ \phi_{21}(y) & \phi_{22}^{(t)} & 0 & 0 & 0 \\ 0 & \phi_{32}^{(t)} & \phi_{33}^{(t)} & 0 & \phi_{35}^{(t)} \\ 0 & 0 & \phi_{43}^{(t)} & 0 & 0 \\ 0 & 0 & 0 & \phi_{54}^{(t)} & 0 \end{pmatrix}. \tag{6.2}$$

The first row of $\mathbf{A}^{(t)}$ describes reproduction; the other entries are the transition probabilities. Here, we assume that population dynamics are determined only by female vital rates and there are always enough males to fertilize them. Therefore, we only keep track of number of females.

Because of the way the stage structure is defined, the fertility $F_3^{(t)}$ can be expressed in terms of transition probabilities as

$$F_3^{(t)} = 0.5\phi_{43}^{(t)} \left(\phi_{54}^{(t+1)}\right)^{0.5}. \tag{6.3}$$

This relationship is based on the following arguments. When a female moves from stage 3 to stage 4 (with probability $\phi_{43}^{(t)}$), she gives birth; the calf is female with probability 0.5. Although calves have distinct markings, they are more difficult to distinguish individually than other stages. Therefore, calf survival is estimated from the point where the calf is seen sufficiently well to permit identification, which is not necessarily on its first sighting. To appear as a calf in stage 1 in year $t+1$, the newborn calf must survive long enough to be cataloged. We assume calves are cataloged on average midway through their first year, and that the survival probability is equal to that of mother during the same period (with probability $(\phi_{54}^{(t+1)})^{0.5}$). Ordinarily, when estimating a population projection matrix, transition probabilities and fertility terms must be estimated separately, often requiring different sets of data. Because we can express the fertility term with the transition probabilities, we only need data to estimate the transition probabilities.

6.2.2 Data

The data we used to estimate transition probabilities are individual sighting histories of the right whales. They are based on photographs taken by members of the North Atlantic right whale consortium along the east coast of the United States from 1980 to 1998. Major survey areas include Massachusetts Bay, Great South Channel, Bay of Fundy, Brown's Bank, and off the coast of Florida and Georgia. Because right whales have unique markings called callosity patterns on their head and scars from entanglement in fishing gear, individuals can be identified from the photographs. Based on these photographs, New England Aquarium has been accumulating annual sighting histories of individual right whales. For the purpose of our analysis, individuals were considered captured and marked at the occasion of their

first sighting and recaptured when they were resighted at least once in a later year.

Of the 406 individuals captured between 1980 and 1998, 158 were identified as female and 163 were identified as male. The rest were assumed to be female or male with an equal probability. At each sighting occasion, we also categorized the sighted individual into one of the five life stages (calf, immature, mature, mother, and mature female during a year after the mother stage) based on the following criteria. Calves were sighted along with their mothers. Immature individuals were known to be less than 9 years old. Mature individuals were known to be at least 9 years old, or in the case of females, had been sighted previously with a calf. A "mother" is a female during the year after a successful birth. A stage for mature female during a year after the mother is for a female that is known to have given a birth in a previous year. After assigning the stages based on these criteria, we were left with about 30% of the total sightings that belong to either immature or mature stages but did not have enough information to assign either stage with certainty. We assumed that they have an equal chance of being immature or mature.

6.2.3 Multi-stage mark-recapture statistics

We estimate the transition probabilities $\phi_{ij}^{(t)}$ from the sighting (capture) history sequences. A difficulty in estimating transition probabilities from the capture history sequences such as the ones available for the North Atlantic right whales comes from the fact that not all individuals, even if they are still alive, are captured every year. If a capture history sequence ends without capturing an individual for one or more sampling occasions, we do not know whether the individual was dead or alive. It could have died immediately after the last capture, it could have died later, or it may still be alive. Furthermore, if an individual was not captured, we often do not have enough information to determine the stage of that individual for sure.

Instead of assuming any particular whale is dead or alive, we modeled the capture history sequence using both capture probabilities $p_i^{(t)}$, which give the probability of capturing an individual that is in stage i in year t, and transition probabilities $\phi_{ij}^{(t)}$. With the capture and

transition probabilities, we calculated the sum of the probabilities of every possible sequence of events that was compatible with a given capture history to obtain the probability of that capture history. The product of all the capture history probabilities was reinterpreted as a likelihood. Finally a maximum likelihood method was applied to estimate the transition probabilities as well as the capture probabilities (see Nichols et al., 1992b, also Chapter 2).

Major assumptions of the multi-stage mark-recapture method in general include (1) individuals within the same stage make transitions into another stage independently but based on the same probability and (2) marked individuals within the same stage are captured independently but based on the same probability. However, we do not assume that any particular whale is dead or alive, nor do we assume that unmarked individuals have the same capture probability as marked individuals. For the right whale study in particular, we also assume that (1) when the stage of an individual is unknown, it is immature or mature with equal probability, (2) when the sex of an individual is unknown, it is female or male with equal probability, and (3) the capture probability of a dead individual is 0. These assumptions are incorporated into the likelihood using the method described in Chapter 2.

6.2.4 Parameters to be estimated

Figure 6.2 shows a complete transition graph of the North Atlantic right whale. This transition graph includes male stages and another stage for death. Stages in this transition graph correspond to the stages we assigned to the sighted individuals. Each arrow indicates all possible stage transitions (including death) of individuals from one year to the next and has associated transition probability $\phi_{ij}^{(t)}$. Once we estimate the transition and capture probabilities associated with this transition graph, we can use the transition probabilities associated with female stages to construct the population projection matrix (Equation 6.2). We let the survival probability of calves between females and males to be the same, and we need male data to estimate this probability. Because of this assumption, we still need to estimate parameters associated with males.

From the 19 year capture history sequences, we estimated parameters that define transi-

tion and capture probabilities. The transition graph in Figure 6.2 contain 8 live stages and 19 possible stage transitions. If all probabilities were free to vary from one year to the next, there would be about 300 parameters to estimate. The number of parameters, however, can be reduced by making reasonable assumptions about how the probabilities are related among stages and on how they change with time.

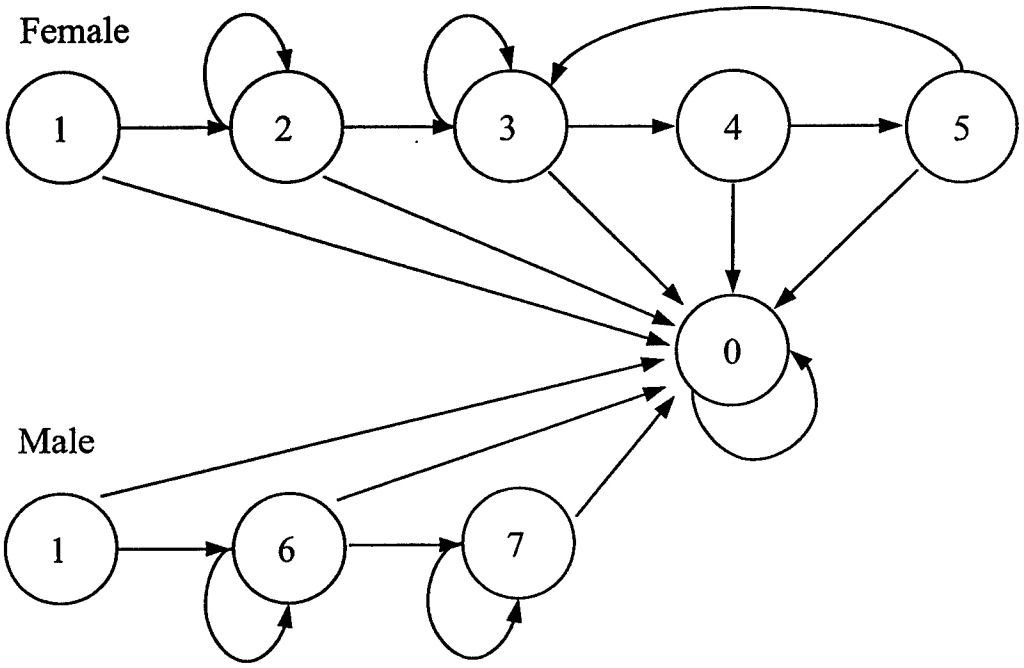

Figure 6.2: Stage transition graph of the North Atlantic right whales: 0: deaths, 1: calves, 2: immature females, 3: mature females, 4: mothers, 5: mature females during a year after the mother stage, 6: immature males, 7: mature males

Capture probability model

To reduce the number of parameters associated with capture probabilities, we assumed that they change freely from one year to the next but are correlated between stages. Let $\varphi^{(t)}$ be the logistic transform of the capture probability of mature females (stage 3) (i.e. $\varphi^{(t)} = \log \frac{p_3(t)}{1-p_3(t)}$). We let logistic transforms of capture probabilities of other stages to be linear functions of $\varphi^{(t)}$ (i.e. $\psi_i + \omega_i \varphi^{(t)} = \log \frac{p_i(t)}{1-p_i(t)}$). After we transform $\varphi^{(t)}$ and the functions back to probabilities, we obtain the following statistical model:

$$p_3(t) = \frac{\exp(\varphi^{(t)})}{1+\exp(\varphi^{(t)})}, \tag{6.4}$$

$$p_i(t) = \frac{\exp(\psi_i + \omega_i \varphi^{(t)})}{1+\exp(\psi_i + \omega_i \varphi^{(t)})} \quad \text{for} \quad i \neq 1 \text{ or } 3, \tag{6.5}$$

where t is year (for capture probability $t = 1981, \ldots, 1998$), and φ^t, ψ_i, and ω_i are parameters to be estimated. Equation (6.4) is a logit function with a different parameter for each year. Equation (6.5) is a logistic function with φ^t as a covariate. In this equation, ψ_i is an intercept and ω_i is a slope parameter. Because the capture probabilities other than mature females are expressed only with two parameters ψ_i and ω_i, this model reduces the number of parameters.

We used stage 3 (mature female) as a reference stage, for which one parameter is estimated for each year (see equation (6.4)), because the data contain this stage the most. The rest of stages use the parameters in equation (6.4) as a covariate. This model does not include the capture probability of calves. It is not needed for estimating transition probabilities because mark-recapture statistics are conditional on marking of animals. Capturing of calves always occurs at the very first capture (i.e. marking) of the individuals.

The resulting capture probability model contains 28 parameters to be estimated. We used this model for all of the analyses presented in this paper.

Transition probability models

In the current study, we focus on modeling the reproductive rate and the stage specific survival probability of calves and mothers. A previous study in Chapter 5 has shown that the survival probability of mothers and calves has declined significantly over time; on the other hand, the survival probability of other stages remained constant. The same study has also concluded that the survival probability of individuals averaged over all stages in Caswell et al. (1999) is significantly correlated with the NAO index that is lagged by 2 years. Furthermore, Pershing & Greene (2002) have shown that reproductive rate of the population has been significantly correlated with the same NAO index. Therefore, we model transition probabilities incorporating the trend associated with time and the NAO index.

In order to model the reproductive rate and the survival probability of mature females separately, we decomposed the transition probability $\phi_{43}^{(t)}$ into a stage-specific survival probability and a transition probability conditional on the survival of individuals (i.e. $\phi_{43}^{(t)} = s_3^{(t)} t_{43}^{(t)}$). We call the latter a conditional transition probability, and these two probabilities are denoted by $s_3^{(t)}$ and $t_{43}^{(t)}$, respectively. The stage-specific survival probability gives the probability of individuals in stage 3 at year t surviving to the following year, and the conditional transition probability gives the probability that individuals in stage 3 in year t will be in stage 4 in the following year conditional on the individuals survival through the year. The relationship between $\phi_{i3}^{(t)}$ and these two probabilities are

$$\phi_{03}^{(t)} = 1 - s_3^{(t)}, \tag{6.6}$$

$$\phi_{33}^{(t)} = s_3^{(t)}(1 - t_{43}^{(t)}), \tag{6.7}$$

$$\phi_{43}^{(t)} = s_3^{(t)} t_{43}^{(t)}. \tag{6.8}$$

In the above formulation, $t_{43}^{(t)}$ is a probability of mature females giving birth conditional on their survival. Thus it gives the reproductive rate of mature females.

The reproductive rate ($t_{43}^{(t)}$) and the survival probabilities of calves ($s_1^{(t)} = \phi_{21}^{(t)}$) and

mothers ($s_4^{(t)} = \phi_{54}^{(t)}$) are modeled with logistic functions of two covariates:

$$s_1(t) = \frac{\exp\left(\alpha_1 + \beta_1 c_1^{(t)} + \gamma_1 c_2^{(t)}\right)}{1 + \exp\left(\alpha_1 + \beta_1 c_1^{(t)} + \gamma_1 c_2^{(t)}\right)}, \tag{6.9}$$

$$s_4(t) = \frac{\exp\left(\alpha_2 + \beta_2 c_1^{(t)} + \gamma_2 c_2^{(t)}\right)}{1 + \exp\left(\alpha_2 + \beta_2 c_1^{(t)} + \gamma_2 c_2^{(t)}\right)}, \tag{6.10}$$

$$t_{43}(t) = \frac{\exp\left(\alpha_3 + \beta_3 c_1^{(t)} + \gamma_3 c_2^{(t)}\right)}{1 + \exp\left(\alpha_3 + \beta_3 c_1^{(t)} + \gamma_3 c_2^{(t)}\right)}, \tag{6.11}$$

where t is year (for transition probabilities $t = 1980, \ldots, 1997$), $c_1^{(t)}$ and $c_2^{(t)}$ are values of the winter NAO index (December of year $t-3$ to March of year $t-2$) and a time index $(0, \frac{1}{17}, \frac{2}{17}, \ldots, \frac{t-1980}{17}, \ldots, 1)$ for year t, α_k $(k = 1, 2, 3)$ is an intercept parameter, and β_k and γ_k are slope parameters associated with the covariates. By setting some or all of β_k and γ_k to zeros, we constructed 64 models that differ in the dependency of the probabilities on the two covariates.

To be consistent with the transition probability of mature females, we also decompose the transition probabilities of immature stages (stage 2 and 6) into stage-specific survival probabilities (s_2 and s_6) and conditional transition probabilities (t_{32} and t_{76}). However, these probabilities along with the survival probabilities of mature females and males are assumed to be constant over time. For each constant probability, its logistic transform was estimated as a parameter.

We fitted the 64 models to the capture history sequences, calculated AIC for each model, and compared the AIC values to select the best fit model.

Saturated model

In addition to the 64 models, we also used another model in which all transition probabilities vary freely from one year to the next. We call this model a saturated model. This model contains a total of 184 parameters (156 are associated with transition probabilities, 27 are associated with capture probabilities, and 1 is a confounded parameter that is a product of stage-specific survival probability from 1997 to 1998 and capture probability of mature

females in 1998).

We assume that any deviations from the best models among the 64 models are resulting from effects of environmental variability. And we used the saturated model to calculate deviations in parameter values due to the environmental stochasticity.

6.3 Results

6.3.1 Model selection

From the 64 models, we select the best model that optimize the errors of over-fitting by including too many parameters and under-fitting by over-simplifying models. This model selection was done using Akaike information criteria (AIC) (Burnham & Anderson, 1998). AIC is an index for weight of evidence in the data that a corresponding model is the best model among the ones compared. AIC values associated with 64 models were transformed into Akaike weights, which are the normalized AIC indices aso that they sum to 1. Using the index, we chose the 10 best models (Table 6.3.1). In the same table, I also show the difference between AIC for each model and one associated with the best model (i.e. Δ AIC). The best and the second best models are supported almost equally at 0.27 and 0.25,

Table 6.1: Akaike weight for the 10 best models. $\surd$ indicates that the model include the corresponding covariate (time or NAO index).

Model	Akaike Weight	Δ AIC	Calf Survival		Mother Survival		Reproduction	
			NAO	Time	NAO	Time	NAO	Time
M_1	0.27	0	$\surd$			$\surd$	$\surd$	$\surd$
M_2	0.25	0.18		$\surd$		$\surd$	$\surd$	$\surd$
M_3	0.15	1.24	$\surd$		$\surd$	$\surd$	$\surd$	$\surd$
M_4	0.10	2.06	$\surd$	$\surd$		$\surd$	$\surd$	$\surd$
M_5	0.07	2.78		$\surd$	$\surd$	$\surd$	$\surd$	$\surd$
M_6	0.05	3.47	$\surd$	$\surd$	$\surd$	$\surd$	$\surd$	$\surd$
M_7	0.03	4.50			$\surd$	$\surd$		$\surd$
M_8	0.02	5.29					$\surd$	$\surd$
M_9	0.02	5.30			$\surd$		$\surd$	$\surd$
M_{10}	0.01	6.40	$\surd$		$\surd$	$\surd$		$\surd$

respectively. In both models, the survival probability of mothers is correlated with NAO and the reproductive rate is correlated with both the time and NAO indices. However, these models differ in how survival probability of calves changes over time. The best model suggests that the survival probability depends on the time index and is monotonically declining, but the second model predicts that the survival probability is correlated with the NAO index.

The ΔAIC values for the first six models in Table 6.3.1 are less than 4 suggesting these models deserve our attention (Burnham & Anderson, 1998). In all six models, the reproductive rate is correlated with the NAO index indicating that there is a strong evidence in the data that the environmental forcing is influencing right whale reproduction. In the six models, the reproductive rate depends on the time index in addition to the NAO index, and the slope parameter associated with the time index in these models is negative. Therefore, the data also suggest that the reproductive rate has been declining over time independent of the effect of NAO. Finally, these models have survival probability of mothers that depend on NAO; there is evidence that environmental forcing is acting on the survival probability of mothers.

The ΔAIC values for the first three models in Table 6.3.1 are less than 2; so there is not strong evidence to exclude these models from potentially the best model in the data (Burnham & Anderson, 1998). Therefore, the rest of our analyses focuses on these models separately and compares the results to find the influence of model selection uncertainty. We denote these three statistical models by M_1, M_2, and M_3 as indicated in Table 6.3.1.

6.3.2 Estimated probabilities

Capture probability model

Figure 6.3 shows the estimated stage-specific capture probabilities of the three best models; they are almost identical. This suggests that the capture probability estimates are not affected by the differences in transition probability models. The capture probability of all stages appears to have increased over the course of the study. This reflects the fact that

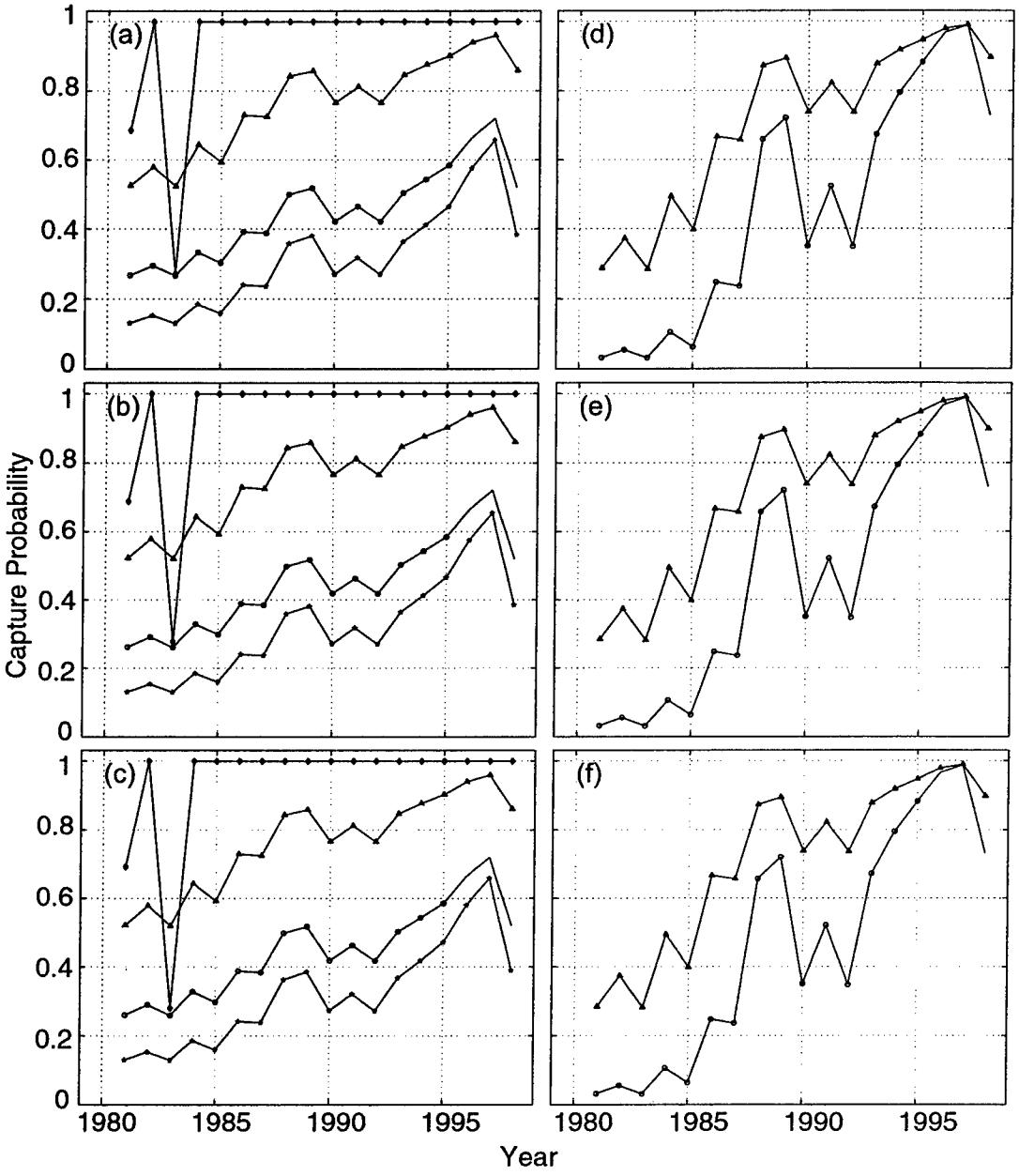

Figure 6.3: Stage-specific capture probabilities: (a) female under M_1, (b) female under M_2, (c) female under M_3, (d) male under M_1, (e) male under M_2, and (f) male under M_3 (triangles, juvenile; circles, mature; diamonds, mother; stars, year after the mother stage).

the sampling effort has increased (see Chapter 5). Compared with other stages, the capture probability of mothers is very high and close to 1 (except in some early years). This indicates that mothers are easier to observe than other stages, or the sampling program is particularly effective for detecting them. The capture probabilities of mature females during the year immediately after the mother stage and other years (stage 5 and 3, respectively) appear to be different. A likelihood ratio test indicates that this difference is significant. Individuals in stage 3 are available for reproduction in the following year, but those in stage 5 are not because of reproduction in the previous year. This difference could influence the behavior of females and affect the capturability of the individuals. All mature females (stage 3 and 5) are assumed to have the same capture probability in the previous study in Chapter 5; this difference in the capture probability could have caused slight underestimation of the previous estimate of survival probability of mothers (stage 4).

Transition probability models

Figure 6.4 shows estimated stage-specific survival probabilities. The survival probabilities of calves are different among the three models. In the first model (M_1), the survival probability is negatively correlated with the NAO index. Because the index has a slightly increasing trend over time, the survival probability also has a slightly declining trend. In the second model (M_2), the survival probability has a monotonically declining trend. In the third model (M_3), the calf survival is a function of NAO only. We do not have enough data to test whether the survival probability of calves is significantly correlated with the NAO index or not; however, the three models suggest that there is at least a slightly declining trend.

The survival probabilities of mothers in the best (M_1) and the second best (M_2) models decline monotonically with time. The same trend was also found in Chapter 5. On the other hand, the survival probability of mothers in the third model (M_3) is negatively correlated with both the time and NAO indices. This model shows that the survival probability in 1996 was dramatically low. The fact that there were unusually high observed mortalities in

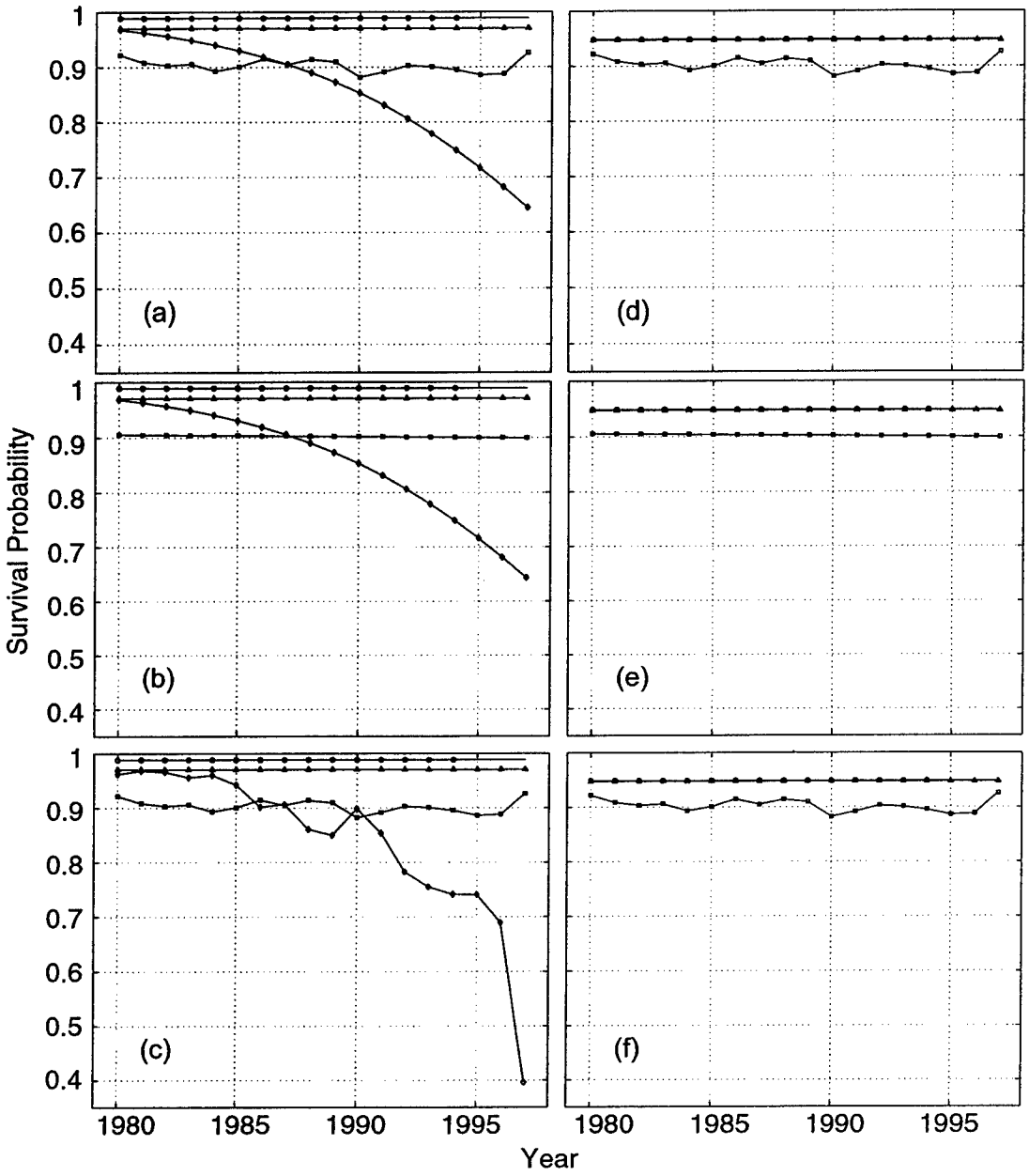

Figure 6.4: Stage-specific survival probabilities: (a) female under M_1, (b) female under M_2, (c) female under M_3, (d) male under M_1, (e) male under M_2, and (f) male under M_3. The curves are for calves (squares), juvenile (triangles), mature (circles), mother (diamonds), and year after the mother stage (stars).

the winter of 1996 (Waring et al., 1999) indicates that model M_3 may be more accurately reflecting the true state of the population. In all three models, the survival probability of mothers is declining. This decline is significant because the slope parameters associated with time (γ_2 in equation (6.10)) in all three models are significantly less than 0 based on the likelihood ratio tests.

Figure 6.5 shows estimated conditional transition probabilities from stage 3 to stage 4 of the three best models. The conditional transition probability gives the probability of mature females becoming mother provided they survive until the following year. In all three models, the probability is correlated with both the NAO and time indices. This result is consistent with the previous studies by Knowlton et al. (1994); Pershing & Greene (2002). This suggests there is declining trend in the reproductive rate upon which the effect of climate fluctuations are superimposed.

6.3.3 Uncertainty in parameter estimates

The estimated probabilities in the previous section have associated uncertainties that we would like evaluate in terms of some indicator of population health. With a lack of an universal indicator, we use the asymptotic annual population growth rate (λ) as a proxy for population health.

We drew the parameters associated with the stage-specific survival probabilities and conditional transition probabilities from a multivariate normal distribution. The covariance matrix for the distribution was approximated by the inverse of the Hessian matrix calculated at the last iteration in the numerical maximum likelihood method (see Burnham et al., 1987). The simulated parameters were transformed into the stage-specific survival probabilities and the conditional transition probabilities setting the NAO index to the mean value between 1980 to 1997 and the time to be 1 (i.e. the level in 1997) in equations (6.9)-(6.11). By setting the NAO index to the mean value, we removed the variability associated with the index. By setting the time to the 1997 level, we assume that mean environmental conditions remain at 1997 levels in future years. With these probabilities, we constructed

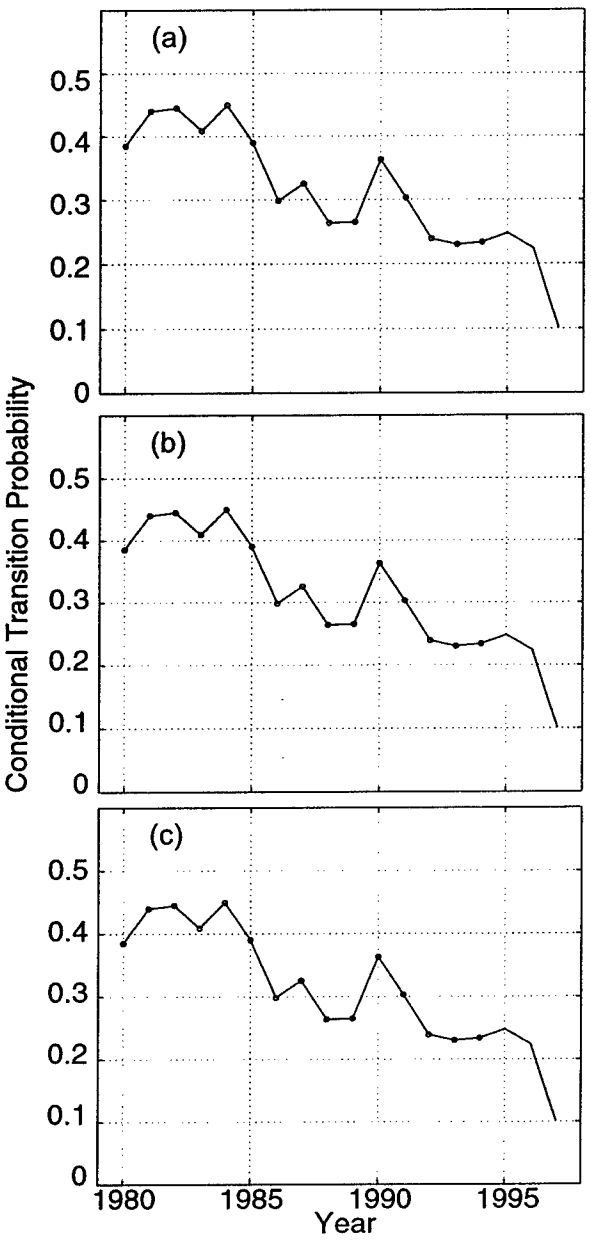

Figure 6.5: Conditional transition probabilities t_{43} under M_1 (a), M_2 (b), and M_3 (c).

a population projection matrix. From the matrix, we calculated an asymptotic population growth rate (λ), which is given by the dominant eigenvalue of the projection matrix (see Caswell, 2001). This was repeated 1000 times for each of the three models selected in the previous section.

The result shows that there are 79% (M_1), 86% (M_2), and 81% (M_3) chances that the asymptotic population growth rate (λ) is less than 1. When λ was less than 1, we calculated the quasi-extinction time (τ_d). Here, we define the quasi-extinction time to be the time that it takes a population to be reduced from 150 females distributed according to stable stage distribution to a single female. The quasi-extinction time (τ_d) was calculated as

$$\widehat{\tau}_d = \frac{\log(1/150)}{\log \widehat{\lambda}}. \tag{6.12}$$

Figure 6.6 shows the distribution of the quasi-extinction time ($\widehat{\tau}_d$) conditional on $\widehat{\lambda} < 1$. This figure shows that there is a wide range in $\widehat{\tau}_d$. It also shows that when the population goes extinct, it disappears relatively quickly. In fact, of the 1000 simulations (including the cases in which $\widehat{\lambda} > 1$ and $\widehat{\lambda} < 1$), there is 50% chance of the population going extinct within 236 (M_1), 209 (M_2), and 176 (M_3) years.

6.3.4 Environmental Stochasticity

The quasi-extinction time calculation in the previous section assumes a deterministic change in the population size and does not include any environmental stochasticity. However, populations live in stochastic environments, and we would like to assess the effect of this stochasticity on population health. Here, we analyze the effect of adding variability to the mean stage-specific survival and conditional transition probabilities in the previous section.

The variability in the probabilities (both stage-specific survival probabilities and the conditional transition probabilities) due to environmental stochasticity was approximated by the deviations in saturated models, in which probabilities change freely from one year to the next, from one of the three best models (M_1, M_2, and M_3). First, we calculated the

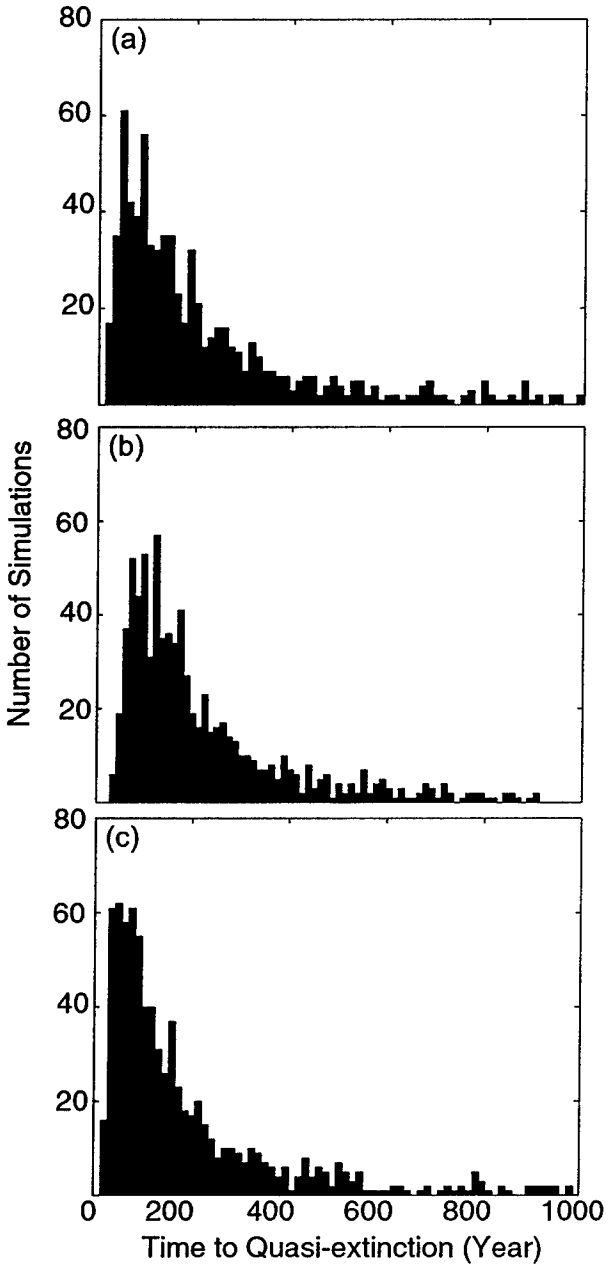

Figure 6.6: Distributions of quasi-extinction time showing parameter uncertainty under M_1 (a), M_2 (b), and M_3 (c). Parameters generated with estimated means and associated covariance matrix assuming their multivariate Normal distribution.

probabilities using the parameters estimated with the saturated model. We also calculated the probabilities using the parameters estimated with one of the three models using the mean NAO index but the time index changing with time in equations (6.9)-(6.11). Then we subtracted these probabilities from the corresponding probabilities of the saturated model to calculate the deviations. Finally, these deviations were added to the probabilities calculated using parameters of the same model (i.e. one of the three best models) but setting the NAO and time indices to the mean and the 1997 level, respectively. This resulted in 17 values for each probability. Two of the values associated with t_{34} in each model were negative; they were set to 0. Using these probabilities, we constructed 17 population projection matrices.

The 17 matrices approximate the variability in a population projection matrix around the matrix that would have been expected in the environmental condition of 1997 but under the average climate level. It should be noted that we did not subtract the sampling variations from the estimates. Therefore, the 17 matrices are over-estimating the variability due to environmental stochasticity.

Using the 17 population projection matrices, we calculated the cumulative probability density for time to quasi-extinction assuming the changes in log of the total population size are approximated by a diffusion process (e.g. Caswell, 2001; Dennis et al., 1991). For this calculation, the stochastic growth rate was calculated from a population growth rate of the average matrix using the approximation developed by Tuljapurkar (1990) and the diffusion coefficient (σ^2) was approximated by

$$\widehat{\sigma^2} = 2(\widehat{\log \mu} - \widehat{\log \lambda_s}), \tag{6.13}$$

where $\log \mu$ is the population growth rate of the average matrix and $\log \lambda_s$ is the stochastic population growth rate.

The mean deviations added to all stage-specific survival probabilities in all three models except the one for survival probability of mothers in M_3 were negative. Therefore, by adding the deviations, we reduced the survival probabilities on average. Paradoxically,

the deterministic growth rate of the projection matrix averaged over the 17 matrices was higher than the deterministic growth rate of the matrix before adding the environmental variability. As a result, the quasi-extinction time calculated using equation (6.12) increased from 361 based on the mean estimates for 1997 to 447 based on the average of the 17 matrices constructed using M_1 as the trend model, from 354 based on the mean estimates for 1997 to 437 based on the average of the 17 matrices constructed using M_2 as the trend model, and from 196 based on the mean estimates for 1997 to 248 based on the average of the 17 matrices constructed using M_3 as the trend model. This effect comes from the skewed distributions of the survival probabilities and the negative mean deviations added to t_{43}. When t_{43} is reduced, fewer individuals make the transition into the mother stage in which individuals face higher risk of mortality.

Figure 6.7 shows the cumulative probability density for quasi-extinction. In each figure, the vertical line on the left indicates the median time to the quasi-extinction and the line on the right indicates the quasi-extinction time calculated using the deterministic model (equation (6.12)). These two values are close to each other in all models.

6.3.5 Demographic stochasticity

The extinction calculations so far do not include the effect of the small population size (i.e. demographic stochasticity). In this section, we analyze this effect on the population viability. Changes in population size are determined by the fates of individuals; those fates are determined stochastically. For example, with some probability each individual survives or die, and with some probability an individual makes a transition into a different stage or remains in the same stage; these stochasticities occur even if the environment is constant. When population size is large, the effect of these events are averaged over many individuals, and as a result, the population size changes smoothly. However, when the population size is small, the fate of each individual has a magnified effect on the total population size. This is called demographic stochasticity.

The effect of demographic stochasticity on the viability of the North Atlantic right

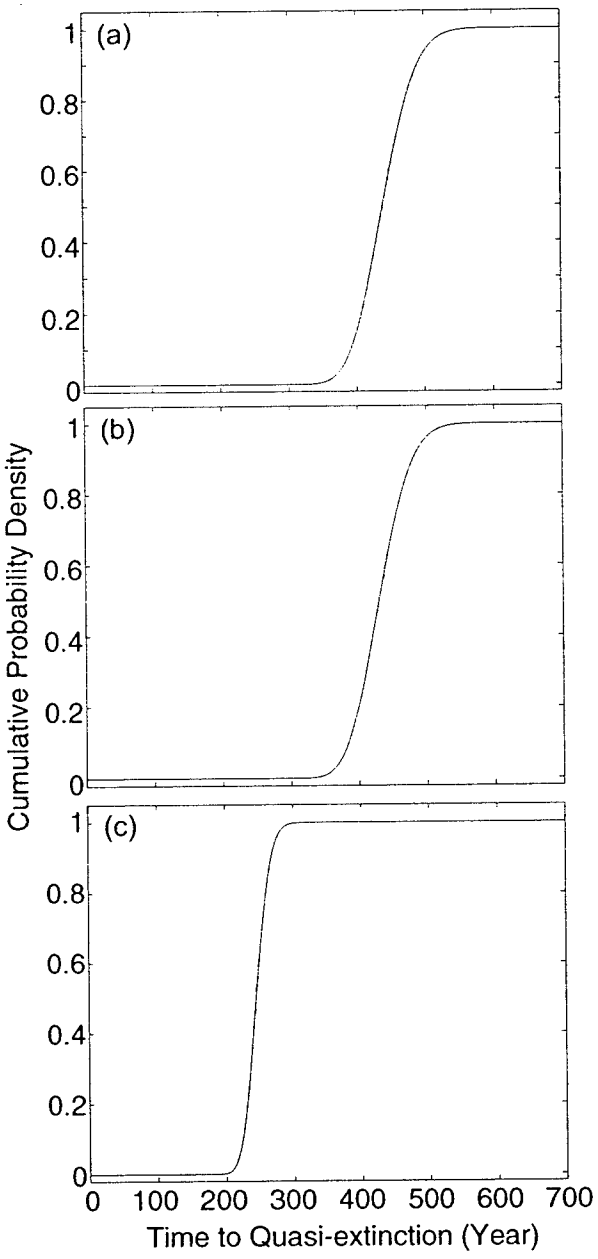

Figure 6.7: Cumulative probability density for quasi-extinction time showing the effect of environmental stochasticity under M_1 (a), M_2 (b), and M_3 (c). The left vertical line shows median, and the right vertical line shows quasi-extinction time calculated under the deterministic model. (see text for the method)

whales has been analyzed in Chapter 5. Here, we repeat the same analyses based on the new estimates. For this analysis, we used the average matrix used in the previous section. These estimates were analyzed using the multi-type branching process (see Caswell, 2001).

Figure 6.8 shows the cumulative probability density for the extinction time. As in the previous section, the vertical line on the left is the median time to extinction, and the vertical line on the right is the quasi-extinction time based on the deterministic calculation (equation 6.12). It should be noted that we are calculating the time to extinction (not quasi-extinction) using the branching process calculation. The extinction time is defined here as the time it takes a population consisting of 150 females distributed according to stable stage distribution to completely disappear. Even the comparison of the quasi-extinction and the extinction times, it is clear that there is a larger effect of the demographic stochasticity on the population viability than the environmental stochasticity.

6.3.6 Environmental and demographic stochasticity

After the separate analyses of environmental and demographic stochasticities, the next obvious step is to analyze the combined effects on the population viability. When both environmental stochasticities and demographic stochasticities are combined, there is no practical analytical method to calculate the extinction time. So we rely on simulations.

We started the population with 150 females distributed according to the stable stage distribution of the average matrix in the previous section. Then for each year, we randomly selected one of the 17 matrices with equal probabilities. Using the selected matrix, we projected the number of individuals in the ith stage in time $t+1$ coming from stage j in year t assuming multinomial distributions with the number of individuals in stage j in year t and probabilities ϕ_{ij} as parameters. This was repeated for all stages for each year of projection. The number of calves in year $t+1$ was calculated using the binomial distribution with the number of individual in mature stage (stage 3) in year y and F_3 as parameters. The population projection was repeated until the population goes to quasi- and actual extinction, and the years of these extinction events were noted. This process

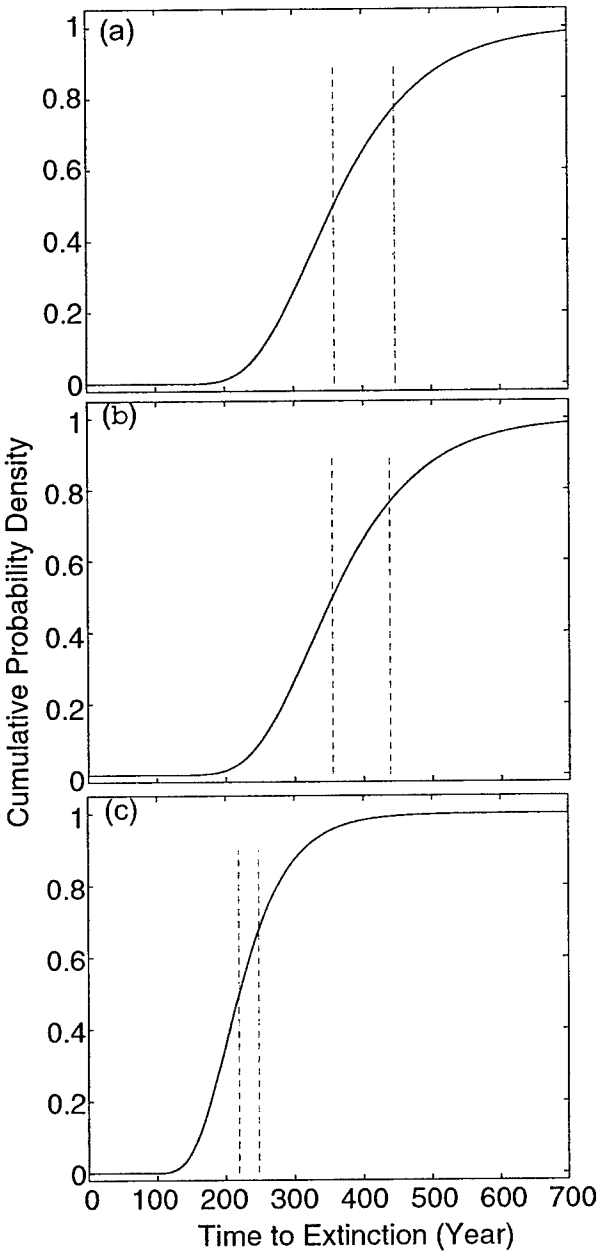

Figure 6.8: Cumulative probability density for quasi-extinction time showing the effect of demographic stochasticity under M_1 (a), M_2 (b), and M_3 (c). The left vertical line shows median, and the right vertical line shows quasi-extinction time calculated under the deterministic model. (see text for the method)

was repeated for 500 times using the parameter estimates of each model.

Figure 6.9 shows 50 randomly selected simulation paths of the total population size. The solid lines in the figures indicate the deterministic path of the population size. Figure 6.10 shows the distributions of actual extinction time. As expected, the combination of demographic and environmental stochasticities creates a range of projected extinction times.

The above simulation assumes that mature females giving birth and making transition into the mother stage are independent. This assumption was also made in all of the calculations so far. However, in reality, every individual that makes the transition from mature to mother stage also gives birth. Thus the reproduction and transition are correlated. Although incorporating this correlation in the diffusion approximation model and the branching process calculation is difficult, it can be incorporated easily in a simulation. Therefore, we repeat the same simulation as before but calculating the number of calves in year $y+1$ differently to account for the correlation. In this calculation, when individuals made the transition from mature (stage 3) to mother (stage 4) stages, we used the binomial distribution with number of individuals that made the transition and ${0.5\phi_{54}}^{0.5}$ as parameters to decide how many individuals appear as calves in the following year.

Assuming the independence between the reproduction and the transition, the median times to quasi-extinction were 317 (M_1), 315 (M_2), and 194 (M_3) years, and the median times to actual extinction were 355 (M_1), 352 (M_2), and 217 (M_3) years. However, when we assume the correlation, the median times to quasi-extinction increase to 338 (M_1), 333 (M_2), and 201 (M_3) years, and the median time to the extinction increase to 380 (M_1), 377 (M_2), and 229 (M_3) years. These increases result from the fact that individuals in the mother stage have very low survival probability compared with other stages. If the probability of individuals risking into the mother stage and reproduction are correlated, there is a less chance that mothers die without giving birth and a higher chance that the population size does not decline. We have not included the correlation between survival of mothers and calves in our model. The right whale mothers nurse their calves for almost a year. It is very likely that calves die if mothers die. This correlation would have an opposite

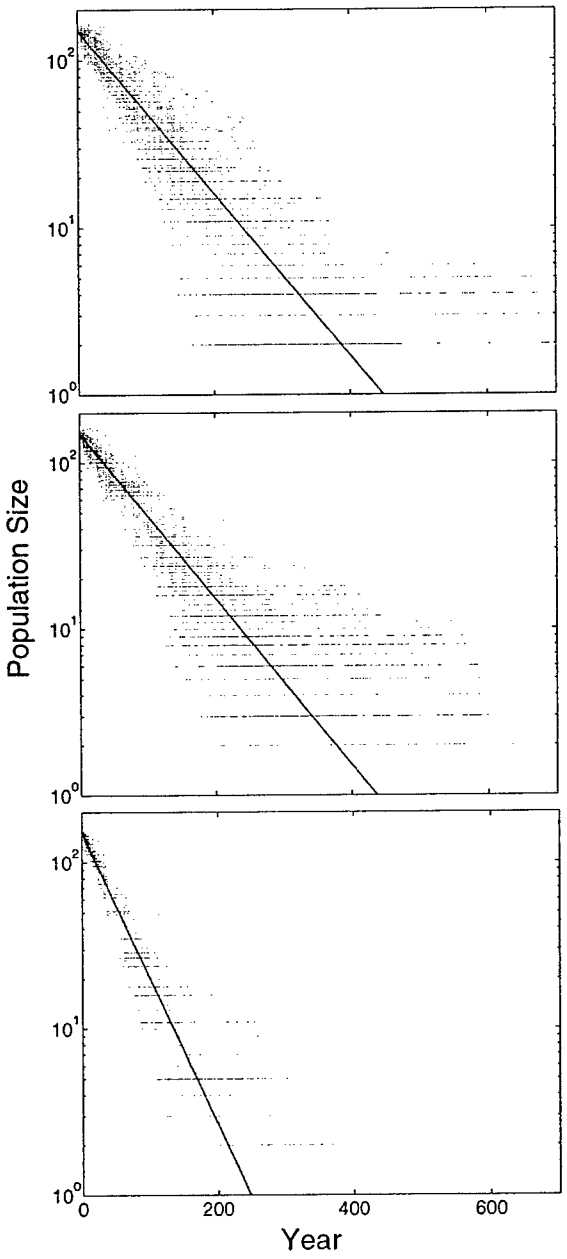

Figure 6.9: Stochastic simulations of the total population size with both environmental and demographic stochasticity under M_1 (a), M_2 (b), and M_3 (c). 50 randomly selected paths are shown. The simulation does not assume the correlation between transition into the mother stage and fertility. The solid line is a path of the deterministic model.

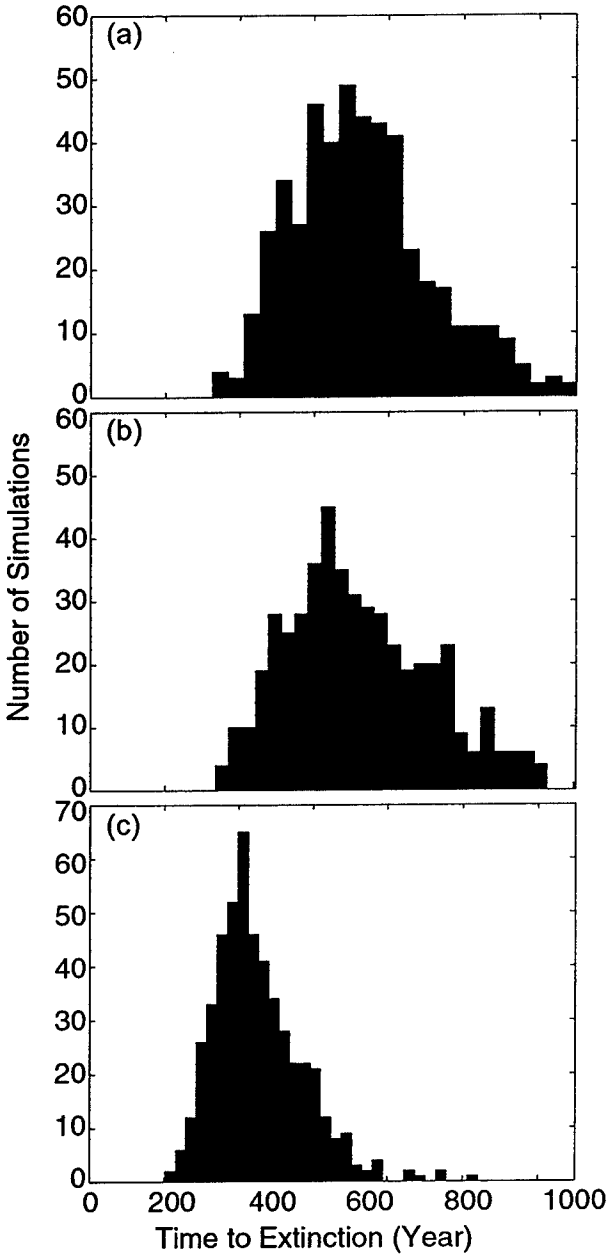

Figure 6.10: Distribution of quasi-extinction time showing the effect of both environmental and demographic stochasticity under M_1 (a), M_2 (b), and M_3 (c). The simulation does not assume the correlation between transition into the mother stage and fertility.

effect as the other correlation and reduce the time to extinction.

6.3.7 More simulations

We used three different analytical methods to calculate expected time to extinction (i.e. deterministic, diffusion approximation, and branching process); however, the comparisons of the results are not trivial. For example, the deterministic and diffusion approximation methods calculate the time to quasi-extinction, but the branching process method calculates the time to actual extinction. Furthermore, the three methods may have different implicit assumptions or use approximations that may be sensitive to different factors. Theoretical studies of these methods are beyond a scope of this study. Nevertheless, it would be nice if we could compare the results based on the same method. Fortunately, the simulation method used in the previous section also allows us to analyze environmental or demographic stochasticity alone.

For the analysis of the demographic stochasticity alone, we used the method in the previous section but only using the average matrix alone. Here we assumed no correlation between the reproduction and the transition from mature to mother stage to be consistent with the branching process calculation. Using this method, we calculated actual and quasi-extinction time.

For the analysis of the environmental stochasticity alone, we randomly selected one of the 17 matrices in the previous section for each year. However, instead of using the multinomial distribution to project the population in the following year, we multiplied the projection matrix to a vector containing number of individuals in each stage (equation (6.2)). For the initial population, we used 150 individuals distributed according to the stable stage distribution of the average matrix. We repeated this process until the sum of the total population size becomes 1. We noted this year as a quasi-extinction time. This process was repeated 500 times for each model.

Table 6.3.7 summarizes all the extinction time calculations made in this paper. The result shows that the analytical calculations using diffusion approximation and branching

Table 6.2: Results of extinction time calculations

Method	Type of Extinction	Factors Analyzed	Median Years to Extinction		
			M_1	M_2	M_3
Deterministic	Quasi		447	438	248
Diffusion Process	Quasi	ES	438	429	245
Branching Process	Actual	DS	359	355	219
Simulation	Quasi	ES	437	430	250
Simulation	Actual	DS	359	357	224
Simulation	Quasi	DS	313	318	199
Simulation	Quasi	DS+ES	338	333	201
Simulation	Actual	DS+ES	380	377	229
Simulation	Quasi	DS+ES+CR	317	315	194
Simulation	Actual	DS+ES+CR	355	352	217

DS: demographic stochasticity.
ED: environmental stochasticity.
CR: correlation between reproduction and transition into mother stage.

process methods agree very well with the simulations. The comparisons of actual and quasi-extinction times for the demographic stochasticity alone indicate that there is about 20 to 40 years difference between them.

6.4 Discussion

We analyzed the North Atlantic right whale data using 64 models that differ in hypotheses on how reproductive rate and survival probability of calves and mothers changed over time. Based on AIC, we selected the three statistical models that were supported by the data best. According to these models, the survival probability of mothers has declined over time and the reproductive rate of mature females has been correlated with the climate index. The three models disagree on whether the survival probability of mothers has been correlated with the climate index and also disagree on how the survival probability of calves has changed over time. However, throughout the series of the population viability analyses in this paper, results based on the three models did not give qualitatively different answers.

Based on the three models, we analyzed the uncertainties in parameter estimates using a

parametric bootstrap method. For this purpose, we used an asymptotic population growth rate (λ) as an index. According to the analysis, all three models agree on a 80% chance of extinction ($\lambda < 1$) provided that climatic conditions are maintained at the mean level between 1980 and 1997 and that other environmental conditions are maintained at the 1997 level in future years.

Using the estimates based on the three models, we analyzed the effects of environmental and demographic stochasticity on the viability of the population. We used four different methods to calculate the quasi-extinction and actual extinction times (Table 6.3.7). The results reveal that there is little effect of environmental stochasticity on the median time to quasi-extinction. The environmental stochasticity appears only to increase the range of quasi-extinction time projections. Considering that North Atlantic right whales are long-lived animals, and we are only adding noise at a small time-scale, this result is reasonable. On the other hand, demographic stochasticity has much larger effects on population viability. Simulation results suggest that there is an 80 to 90% chance that demographic stochasticity reduces the time to quasi-extinction, and there is a 20 to 30% reduction in median time to quasi-extinction.

The North Atlantic right whale is seriously endangered not only because of its small population size, but also because of the trend in the population growth rate (Caswell et al., 1999, Chapter 5). Previous studies suggested that the population is now slowly declining. In the current study, we analyzed the data on this population taking additional factors into consideration. Those additional factors are model selection uncertainty, the effect of environmental stochasticity, and some heterogeneity in the capture probability of mature females. With all these factors considered, the results do not suggest a bright future for this population.

Recently a few major management actions have been implemented. They include a disentanglement network system, a mandatory ship reporting system, and a temporary closure of areas from fishing activities (Waring et al., 1999). These management actions were implemented in the mid to late 1990's, and their effects will not be detectable for a

few more years. Saving only a few whales will protect the population (Chapter 5). We hope that these management actions are effective and that, in the future, we will be reporting the effects of successful management on the viability of the North Atlantic right whales.

Chapter 7

Conclusion

The main chapters (Chapters 2-6) were written for possible publications in journals, and they contain conclusions of their own. Therefore, I present a brief overview of this thesis in this chapter.

In this thesis, I presented new methods to analyze mark-recapture data (Chapters 2, 3, and 4) and applications of the methods to actual data (Chapters 5 and 6). These methods link mark-recapture data and existing population models that allow modern demographic analyses (e.g. Caswell, 2001). I presented selected demographic analyses such as sensitivity, branching process, and environmental stochasticity analyses based on the estimated parameters of the right whale models in Chapter 5 and 6. The study of the right whale population presented in Chapter 5 revealed some interesting facts about the status of the population. One of the most interesting findings is that the declining survival probability found by Caswell et al. (1999) appears to be caused by the increased mortality rate of females that are nursing their offspring. I believe that this and other results in the two chapters demonstrate the usefulness of the mark-recapture methods presented in the earlier chapters.

As marking techniques improve, individual mark-recapture data are becoming very common. Such data are already available for wandering albatross (*Diomedia exulans*) and Amsterdam albatross (*D. amsterdamensis*) (Weimerskirch et al., 1997), Atlantic humpback whales (Buckland, 1990), kittiwake gull (*Rissa tridactyla*) (Aebischer & Coulson, 1990),

Canada geese (*Branta canadensis*) (Hestbeck et al., 1991), tundra swan (*Cygnus columbinus*) (Nichols et al., 1992a), roseate tern (*Sterna dougallii*) (Spendelow et al., 1995), black-headed gull (*Larus ridibundus*) (Prevot-Julliard et al., 1998), Florida manatee (*Trichechus manatus latirostris*) (Langtimm et al., 1998), pig frog (*Rana grylio*) (Wood et al., 1998), Weddell seal (*Leptonychotes weddellii*) (Hastings & Testa, 1998), grizzly bear (*Ursus arctos*) (Pease & Mattson, 1999), grey seal (*Halichoerus grypus*) (Schwarz & Stobo, 2000), and northern spotted owl (*Strix occidentalis caurina*) (Franklin et al., 2000) to name some examples. The methods I presented allow reanalysis of these existing data taking full advantage of the demographic analyses and also allow planning of future sampling.

I here show that mark-recapture data contain a great deal of information. They are one of the best data to collect when studying a population. I was able to find a change in survival probability in only one life stage of individuals in a population that consists of about 300 individuals. This discovery would not have been possible if there were not the mark-recapture data and the appropriate analysis method presented in this thesis. However, mark-recapture data are not always available. One obvious limitation of the method is that individuals must be uniquely marked. When individuals cannot be marked, an alternative type of data is count data, which record how many individuals in each stage were observed at each sampling occasion. Recently, Zeng et al. (1998) and DeValpine & Hastings (2002) developed a method to estimate population parameters by fitting state-space models to count data. Because count data are easier to collect and more available than mark-recapture data, I suspect their method will become very important in ecological studies. However, I am not sure which type of data are superior given the same amount of sampling effort. I think the answer will depend on the size of a population and detectability of individuals (i.e. capture probability). It is also conceivable to collect both mark-recapture and count data on the same population. Then a single likelihood function for both data can be expressed to estimate parameters. Under such circumstance, I am interested to find what is the best allocation of effort between the two types of data.

Collecting data in a population study, whether they are mark-recapture data or count

data, is often an expensive process. The cost of the collecting data should warrant the most sophisticated analyses available. Once data are collected, they should be analyzed to a full extent. Unfortunately, ecological data are often under-utilized. In my opinion, this comes from the lack of emphasis in studies that try to link data and models. This is the area in which I am hoping to make contributions as an ecologist/biological oceanographer. This thesis is the first of such contributions.

Bibliography

AEBISCHER, N. J. & COULSON, J. C. (1990). Survival of the kittiwake in relation to sex, year, breeding experience and position in the colony. *Journal of Animal Ecology* **59**, 1063–1071.

AKAIKE, H. (1973). Information theory and an extension of the maximum likelihood principles. In *International Symposium on Information Theory*, B. Petran & F. Csaki, eds. Tsahkadsor, 1971: Akademiai Kiadi, Budapest, Hungary.

ARNASON, A. (1972). Parameter estimates from mark-recaptture experiments on two populations subject to migration and death. *Researches on Population Ecology* **13**, 97–113.

ARNASON, A. M. (1973). The estimation of population size, migration rates, and survival in a stratified population. *Researches in Population Ecology* **15**, 1–8.

BROWNIE, C., HINES, J., NICHOLS, J., POLLOCK, K. & HESTBECK, J. (1993). Capture-recapture studies for multiple strata including non-Markovian transitions. *Biometrics* **49**, 1173–1187.

BUCKLAND, S. T. (1990). Estimation of survival rates from sightings of individually identifiable whales. In *Conference Symp. and Workshop on Individual Recognition and the Estimation of Cetacean Population Parameters*, P. S. Hammond, S. A. Mizroch & G. P. Donovan, eds., vol. Special Issue 12. La Jolla, CA (USA): International Whaling Commision.

BURNHAM, K. P. & ANDERSON, D. R. (1998). *Model Selection and Inference: A Practical Information-Theoretic Approach.* New York, NY: Springer-Verlag.

BURNHAM, K. P., ANDERSON, D. R., WHITE, G. C., BROWNIE, C. & POLLOCK, K. H. (1987). *Design and Analysis Methods for Fish Survival Experiments Based on Release-Recapture*, vol. Monograph 5. Bethesda, Maryland: American Fisheries Society.

CAREY, P. D. & WATKINSON, A. R. (1993). The dispersal and fates of seeds of the winter annual grass *Vulpia ciliata*. *Journal of Ecology* **81**, 759–767.

CASWELL, H. (1978). A general formula for the sensitivity of population growth rate to changes in life history parameters. *Theoretical Population Biology* **14**, 215–230.

CASWELL, H. (1989). *Matrix Population Models.* Sunderland, Massachusetts: Sinauer Associate Inc., 1st ed.

CASWELL, H. (2001). *Matrix Population Models: Construction, Analysis, and Interpretation.* Sunderland, MA: Sinauer Associates Inc., 2nd ed.

CASWELL, H., FUJIWARA, M. & BRAULT, S. (1999). Declining survival probability threatens the North Atlantic right whale. *Proceedings of the National Academy of Sciences, USA* **96**, 3308–3313.

CATCHPOLE, E. & MORGAN, B. (1997). Detecting parameter redundancy. *Biometrika* **84**, 187–196.

CLARK, J. S. (1998). Why trees migrate so fast: Confronting theory with dispersal biology and the paleorecord. *American Naturalist* **152**, 204–224.

CLARK, J. S., HORVATH, L. & LEWIS, M. (2001a). On the estimation of spread rate for a biological population. *Statistics and Probability Letters* **51**, 225–234.

CLARK, J. S., LEWIS, M. & HORVATH, L. (2001b). Invasion by extremes: Population spread with variation in dispersal and reproduction. *American Naturalist* **157**, 537–554.

CLOBERT, J., LEBRETON, J.-D., ALLLAINÉ, D. & GAILLARD, J. M. (1994). The estimation of age-specific breeding probabilities from recaptures or resightings in vertebrate populations: II. Longitudinal models. *Biometrics* **94**, 375–387.

CORMACK, R. (1964). Estimates of survival from the sighting of marked animals. *Biometrika* **51**, 429–438.

CORMACK, R. M. (1968). The statistics of capture-recapture methods. *Oceanography and Marine Biology* **6**, 455–506.

CRONE, M. & KRAUS, S. (1990). *Right whale (Eubalaena glacialis) in the Western North Atlantic: a catalog of identified individuals.* Boston, Massachusetts: New England Aquarium.

DENNIS, B., MUNHOLLAND, P. L. & SCOTT, J. M. (1991). Estimation of growth and extinction parameters for endangered species. *Ecological Monographs* **61**, 115–143.

DERISO, R. B., QUINN, T. J., I. & NEAL, P. R. (1985). Catch-age analysis with auxiliary information. *Canadian Journal of Fisheries and Aquatic Sciences* **42**, 815–824.

DEVALPINE, P. & HASTINGS, A. (2002). Fitting population models incorporating process noise and observation error. *ECOLOGICAL MONOGRAPHS* **72**, 57–76.

DOBZHNSKY, T. & WRIGHT, S. (1943). Genetics of natural populations, x. dispersion rates in drosophila pseudoobscura. *Genetics* **28**, 304–340.

FORSMAN, E., DESTEFANO, S., RAPHAEL, M. & GUTIÉRREZ, R., eds. (1996). *Demography of the Northern Spotted Owl*, vol. 17 of *Studies in Avian Biology.* Camarillo, CA: Cooper Ornithological Society.

FOURNIER, D. & ARCHIBALD, C. P. (1982). A general theory for analyzing catch at age data. *Canadian Journal of Fisheries and Aquatic Sciences* **39**, 1195–1207.

FRANKLIN, A. B., ANDERSON, D. R., GUTIERREZ, R. J. & BURNHAM, K. P. (2000). Climate, habitat quality, and fitness in northern spotted owl populations in Northwestern California. *Ecological Monographs* **70**, 539–590.

FUJIWARA, M. & CASWELL, H. (2001). Demography of the endangered North Atlantic right whale. *Nature* **414**, 537–541.

HASTINGS, K. K. & TESTA, J. W. (1998). Maternal and birth colony effects on survival of weddell seal offspring from McMurdo Sound, Antarctica. *Journal of Animal Ecology* **67**, 722–740.

HESTBECK, J. B., NICHOLS, J. D. & MALECKI, R. A. (1991). Estimates of movement and site fidelity using mark-resight data of wintering Canada geese. *Ecology* **72**, 523–533.

HILBORN, R. (1990). Determination of fish movement patterns from tag recoveries using maximum likelihood estimators. *Canadian Journal of Fisheries and Aquatic Sciences* **47**, 635–643.

HINES, J. (1994). MSSURVIV user's manual.

HOSMER, D. W. & LEMESHOW, S. (1989). *Applied logistic regression.* Wiley series in probability and mathematical statistics. Applied probability and statistics. New York: Wiley.

JACKSON, C. H. N. (1933). On the true density of tsetse flies. *Journal of Animal Ecology* **2**, 204–209.

JOLLY, G. (1965). Explicit estimates from capture-recapture data with both death and immigration-stochastic model. *Biometrika* **52**, 225–247.

KAREIVA, P. M. (1983). Local movement in herbivorous insects: Applying a passive diffusion model to mark-recapture field experiments. *Oecologia* **57**, 322–327.

KENDALL, W. L. (1999). Robustness of closed capture-recapture methods to violations of the closure assumption. *Ecology* **80**, 2517–2525.

KENDALL, W. L., NICHOLS, J. D. & HINES, J. E. (1997). Estimating temporary emigration using capture-recapture data with Pollock's robust design. *Ecology* **78**, 563–578.

KNOWLTON, A. R., KRAUS, S. D. & KENNEY, R. D. (1994). Reproduction in North Atlantic right whales (*Eubalaena glacialis*). *Canadian Journal of Zoology* **72**, 1297–1305.

KOT, M. (1989). Diffusion-driven period-doubling bifurcations. *BioSystems* **22**, 279–287.

KOT, M., LEWIS, M. A. & VAN DEN DRIESSCHE, P. (1996). Dispersal data and the spread of invading organisms. *Ecology* **77**, 2027–2042.

LANGTIMM, C. A., O'SHEA, T. J., PRADEL, R. & BECK, C. A. (1998). Estimates of annual survival probabilities for adult Florida manatees (*Trichechus manatus latirostris*). *Ecology* **79**, 981–997.

LEBRETON, J., ALMERAS, T. & PRADEL, R. (1999). Competing events, mixture of information and multistratum recapture models. *Bird Study* **46 (suppl.)**, 39–46.

LEBRETON, J.-D. (1995). The future of population dynamic studies using marked individuals: a statistician's perspective. *Journal of Applied Statistics* **22**, 1009–1030.

LEBRETON, J. D., BURNHAM, K. P., CLOBERT, J. & ANDERSON, D. R. (1992). Modeling survival and testing biological hypotheses using marked animals: A unified approach with case studies. *Ecological Monographs* **62**, 67–118.

LEWIS, M. A. & PACALA, S. (2000). Modeling and analysis of stochastic invasion processes. *Journal of Mathematical Biology* **41**, 387–429.

LINCOLN, F. C. (1930). Calculating waterfowl abundance on the basis of banding returns. Tech. rep., U.S. Department of Agriculture.

MCCULLAGH, P. & NELDER, J. A. (1989). *Generalized Linear Models.* Monographs on Statistics and Applied Probability 37. Boca Raton, Florida: CRC Predss, 2nd ed.

NEUBERT, M. G. & CASWELL, H. (2000). Demography and dispersal: Calculation and sensitivity analysis of invasion speed for structured populations. *Ecology* **81**, 1613–1628.

NEUBERT, M. G., KOT, M. & LEWIS, M. A. (1995). Dispersal and pattern formation in a discrete-time predator-prey model. *Theoretical Population Biology* **48**, 7–43.

NEUBERT, M. G., KOT, M. & LEWIS, M. A. (2000). Invasion speeds in fluctuating environments. *Proceedings of the Royal Society of London, Series B: Biological Sciences* **267**, 1603–1610.

NICHOLS, J. D., HINES, J. E., POLLOCK, K., HINZ, R. & LINK, W. (1994). Estimating breeding proportions and testing hypotheses about costs of reproduction with capture-recapture data. *Ecology* **75**, 2052–2065.

NICHOLS, J. D. & KENDALL, W. L. (1995). The use of multi-state capture-recapture models to address question in evolutionary ecology. *Journal of Applied Statistics* **22**, 835–846.

NICHOLS, J. D., LIMPERT, R. J., SLADEN, W. J. L. & HINES, J. E. (1992a). Annual survival rates of adult and immature eastern population tundra swans. *Journal of Wildlife Management* **56**, 485–494.

NICHOLS, J. D., SAUER, J. R., POLLOCK, K. H. & HESTBECK, J. B. (1992b). Estimating transition probabilities for stage-based population projection matrices using capture-recapture data. *Ecology* **73**, 306–312.

OKUBO, A. (1980). *Diffusion and ecological problems : mathematical models.* Berlin ; New York: Springer-Verlag.

PAYNE, R., ROWNTREE, V., PERKINS, J. S., COOKE, J. G., LANKESTER, K., HAMMOND, P. S. & MIZROCH, S. A. (1990). Population size, trends and reproductive parameters of right whales (*Eubalaena australis*) off Peninsula Valdes, Argentina. In *Conference Symposium and Workshop on Individual Recognition and the Estimation of Cetacean*

Population Parameters, G. P. Donovan, ed., REP. INT. WHALING COMM. (SPEC. ISSUE), no. 12. La Jolla, CA (USA): International Whaling Commision.

PEASE, C. M. & MATTSON, D. J. (1999). Demography of the Yellowstone grizzly bears. *Ecology* **80**, 957–975.

PERSHING, A. & GREENE, C. (2002). Impact of climate variability on the endangered North Atlantic right whale. *Nature* Submitted.

PETERSEN, C. G. J. (1896). The yearly immigration of young plaice in the Limfjord from the German Sea. *Report of Danish Biological Station 1895* **6**, 1–77.

POLLOCK, K. (1982). A capture-recapture design robust to unequal probability of capture. *Journal of Wildlife Management* **46**, 757–760.

PRADEL, R. & LEBRETON, J. (1999). Comparison of different approaches to the study of local recruitment of breeders. *Bird Study* **46 (suppl.)**, 74–81.

PREVOT-JULLIARD, A. C., LEBRETON, J. D. & PRADEL, R. (1998). Re-evaluation of adult survival of black-headed gulls (*Larus ridibundus*) in presence of recapture heterogeneity. *Auk* **115**, 85–95.

QUINN, T. J. & DERISO, R. B. (1999). *Quantitative fish dynamics.* Biological resource management series. New York: Oxford University Press.

SCHWARZ, C. J. & STOBO, W. T. (2000). Estimation of juvenile survival, adult survival, and age-specific pupping probabilities for the female grey seal (*Halichoerus grypus*) on Sable Island from capture-recapture data. *Canadian Journal of Fisheries and Aquatic Sciences* **57**, 247–253.

SEBER, G. A. F. (1965). A note on the multiplerecapture census. *Biometrika* **52**, 249–259.

SEBER, G. A. F. (1982). *The estimation of animal abundance and related parameters.* London: Charles Griffin, 2nd ed.

SHIGESADA, N. & KAWASAKI, K. (1997). *Biological invasions : theory and practice.* Oxford series in ecology and evolution. Oxford: Oxford University Press, 1st ed.

SPENDELOW, J. A., NICHOLS, J. D., NISBET, I. C. T., HAYS, H., CORMONS, G. D., BURGER, J., SAFINA, C., HINES, J. E. & GOCHFELD, M. (1995). Estimating annual survival and movement rates of adults within a metapopulation of roseate terns. *Ecology* **76**, 2415–2428.

TAYLOR, R. A. J. (1978). The relationship between density and distance of dispersing insects. *Ecological Entomology* **3**, 63–70.

TULJAPURKAR, S. (1990). *Population dynamics in variable environments.* Lecture notes in biomathematics ; 85. New York: Springer-Verlag.

TULJAPURKAR, S. & CASWELL, H., eds. (1997). *Structured-Population Models in Marine, Terrestrial, and Freshwater Systems*, vol. 18 of *Population and Community BIology Series.* New York, NY: Chapman & Hall.

TURCHIN, P. & THOENY, W. T. (1993). Quantifying dispersal of southern pine beetles with mark-recapture experiments and a diffusion model. *Ecological Applications* **3**, 187–198.

VAN KIRK, R. W. & LEVIS, M. A. (1996). Dispersal data and the spread of invading organisms. *Bulletin of Mathematical Biology* **59**, 107–137.

VAN KIRK, R. W. & LEWIS, M. A. (1999). Edge permeability and population persistence in isolated habitat patches. *Natural Resource Modeling* **12**.

WARING, G. T., PALKA, D. L., CLAPHAM, P. J., SWARTZ, S., ROSSMAN, M. C., COLE, T. V., BISACK, K. D. & HANSEN, L. J. (1999). *U.S. Atlantic Marine Mammal Stock Assessments -1999.* Woods Hole, MA: NOAA Technical Memorandum NMFS-NE-153.

WEIMERSKIRCH, H., BROTHERS, N. & JOUVENTIN, P. (1997). Population dynamics of wandering albatross *Diomedea exulans* and Amsterdam albatross *D. amsterdamensis* in

the Indian ocean and their relationships with long-line fisheries: Conservation implications. *Biological Conservation* **79**, 257–270.

WERNER, P. (1975). A seed trap for determining patterns of seed deposition in terrestrial plants. *Canadian Journal of Botany* **53**, 810–813.

WHITE, G. & BURNHAM, K. (1999). Program MARK: Survival estimation from populations of marked animals. *Bird Study* **46 (suppl.)**, 120–138.

WHITE, G. C. (1983). Numerical estimation of survival rates from band recovery and biotelemetry data. *Journal of Wildlife Management* **47**, 716–728.

WOOD, K. V., NICHOLS, J. D., PERCIVAL, H. F. & HINES, J. E. (1998). Size-sex variation in survival rates and abundance of pig frogs, *Rana grylio*, in northern Florida wetlands. *Journal of Herpatology* **32**, 527–535.

ZENG, Z., NOWIERSKI, R. M., TAPER, M. L., DENNIS, B. & KEMP, W. P. (1998). Complex population dynamics in the real world: Modeling the influence of time-varying parameters and time lags. *Ecology* **79**, 2193–2209.

Document Library

Distribution List for Technical Report Exchange—November 1999

University of California, San Diego
SIO Library 0175C
9500 Gilman Drive
La Jolla, CA 92093-0175

Hancock Library of Biology & Oceanography
Alan Hancock Laboratory
University of Southern California
University Park
Los Angeles, CA 90089-0371

Gifts & Exchanges
Library
Bedford Institute of Oceanography
P.O. Box 1006
Dartmouth, NS B2Y 4 A2
CANADA

NOAA/EDIS Miami Library Center
4301 Rickenbacker Causeway
Miami, FL 33149

Research Library
U.S. Army Corps of Engineers
Waterways Experiment Station
3909 Halls Ferry Road
Vicksburg, MS 39180-6199

Institute of Geophysics
University of Hawaii
Library Room 252
2525 Correa Road
Honolulu, HI 96822

Marine Resources Information Center
Building E38-320
MIT
Cambridge, MA 02139

Library
Lamont-Doherty Geological Observatory
Columbia University
Palisades, NY 10964

Library
Serials Department
Oregon State University
Corvallis, OR 97331

Pell Marine Science Library
University of Rhode Island
Narragansett Bay Campus
Narragansett, RI 02882

Working Collection
Texas A&M University
Dept. of Oceanography
College Station, TX 77843

Fisheries-Oceanography Library
151 Oceanography Teaching Bldg.
University of Washington
Seattle, WA 98195

Library
R.S.M.A.S.
University of Miami
4600 Rickenbacker Causeway
Miami, FL 33149

Maury Oceanographic Library
Naval Oceanographic Office
Building 1003 South
1002 Balch Blvd.
Stennis Space Center, MS 39522-5001

Library
Institute of Ocean Sciences
P.O. Box 6000
Sidney, B.C. V8L 4B2
CANADA

National Oceanographic Library
Southampton Oceanography Centre
European Way
Southampton SO14 3ZH
UK

The Librarian
CSIRO Marine Laboratories
G.P.O. Box 1538
Hobart, Tasmania
AUSTRALIA 7001

Library
Proudman Oceanographic Laboratory
Bidston Observatory
Birkenhead
Merseyside L43 7 RA
UK

IFREMER
Centre de Brest
Service Documentation–Publications
BP 70 29280 PLOUZANE
FRANCE

50272-101

REPORT DOCUMENTATION PAGE	1. REPORT NO. MIT/WHOI 2002-08	2.	3. Recipient's Accession No.
4. Title and Subtitle Mark-Recapture Statistics and Demographic Analysis			5. Report Date June 2002 6.
7. Author(s) Masami Fujiwara			8. Performing Organization Rept. No.
9. Performing Organization Name and Address MIT/WHOI Joint Program in Oceanography/Applied Ocean Science & Engineering			10. Project/Task/Work Unit No. MIT/WHOI 2002-08 11. Contract(C) or Grant(G) No. (C) NA86RG0075 (G)
12. Sponsoring Organization Name and Address David and Lucile Packard Foundation Rinehart Coastal Research Center Sea Grant			13. Type of Report & Period Covered Ph.D. Thesis 14.

15. Supplementary Notes

This thesis should be cited as: Masami Fujiwara, 2002. Mark-Recapture Statistics and Demographic Analysis. Ph.D. Thesis. MIT/WHOI, 2002-08.

16. Abstract (Limit: 200 words)

Mark-recapture analyses of populations are an important tool in population biology. In this thesis, I extend mark-recapture analyses to provide a link between mark-recapture data and demographic models such as matrix population models and integrodifference equation models. I resolve some issues that are commonly encountered during sampling, such as the fact that the sex or life-stage of some individuals is unknown during some sampling occasions and that individuals become unobservable during some life stages. I introduce a stage structure that permits simple conversion of estimated transition probabilities into a matrix population model. I describe a simple algorithm to simplify programming for parameter estimation. I also introduce a method to estimate the distribution of dispersal displacements (dispersal kernel) from mark-recapture data. I use some of the above methods to estimate the vital rates of the North Atlantic right whale (*Eubalaena glacialis*). To the estimated vital rates, I apply demographic analyses including population viability analyses and sensitivity analysis. Finally, I compare effects of environmental and demographic stochasticities on the viability of the population.

17. Document Analysis a. Descriptors

Mark-recapture statistics
demographic analysis
matrix population models

b. Identifiers/Open-Ended Terms

c. COSATI Field/Group

18. Availability Statement	19. Security Class (This Report)	21. No. of Pages
Approved for publication; distribution unlimited.	UNCLASSIFIED	138
	20. Security Class (This Page)	22. Price

(See ANSI-Z39.18) *See Instructions on Reverse* OPTIONAL FORM 272 (4-77)
(Formerly NTIS-35)
Department of Commerce